

DEPARTMENT OF MECHANICAL ENGINEERING INDIAN INSTITUTE OF TECHNOLOGY MADRAS CHENNAI – 600036

Spray and Thermal Behavior of Atomized Nozzles for Electronic Cooling Applications





A Thesis

Submitted by

MONU KUMAR

*ME*22*S*032

For the award of the degree

Of

MASTER OF SCIENCE

July 2025



DEPARTMENT OF MECHANICAL ENGINEERING INDIAN INSTITUTE OF TECHNOLOGY MADRAS CHENNAI – 600036

Spray and Thermal Behavior of Atomized Nozzles for Electronic Cooling Applications





A Thesis

Submitted by

MONU KUMAR

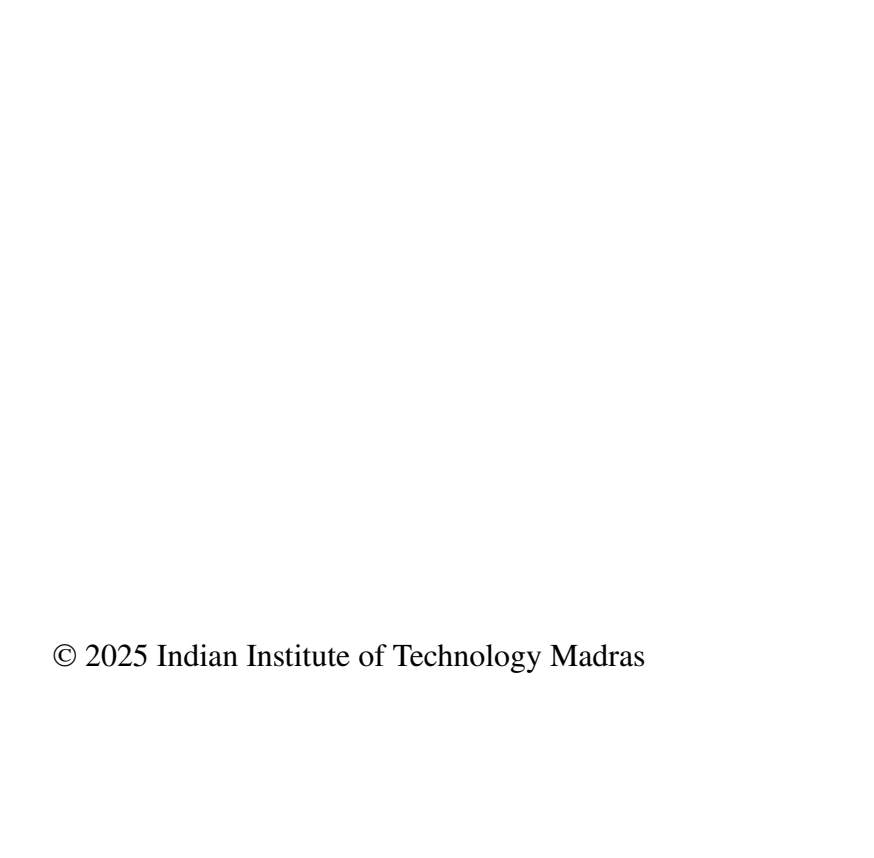
*ME*22*S*032

For the award of the degree

Of

MASTER OF SCIENCE

July 2025



"If your best effort isn't yielding results, take a step back. Think, evaluate, and then choose—improve your method or try a different path. Real progress comes from clear thinking, not just relentless effort."

- Monu Kumar

"To my parents, mentors, and everyone who supported me on this journey."

THESIS CERTIFICATE

This is to undertake that the Thesis titled SPRAY AND THERMAL BEHAVIOR

OF ATOMIZED NOZZLES FOR ELECTRONIC COOLING APPLICATIONS,

submitted by me to the Indian Institute of Technology Madras, for the award of Master

of Science, is a bonafide record of the research work done by me under the supervision

of Dr.Arvind Pattamatta and Prof.Marco Marengo. The contents of this Thesis, in

full or in parts, have not been submitted to any other Institute or University for the award

of degree.

Chennai 600036

MONU KUMAR

Date: July 2025

ME22S032

Dr.Arvind Pattamatta

Research advisor

Professor Department of Mechanical Engineering

IIT Madras

Prof. Marco Marengo

Research co-advisor

Professor of Thermal Sciences

Department of Civil Engineering and Architecture

University of Pavia

© 2025 Indian Institute of Technology Madras

LIST OF PUBLICATIONS

I. PRESENTATIONS IN CONFERENCE

Title: Spray and Thermal Analysis of Pressure and Air Atomized Nozzles for Electronic Cooling. Conference: 11th International Conference on Heat Transfer and Fluid Flow (HTFF 2024)| August 22–24, 2024 | Barcelona, Spain

II. PUBLICATIONS IN CONFERENCE PROCEEDINGS

Kumar *et al.*(2024)"Spray and Thermal Analysis of Pressure and Air Atomized Nozzles for Electronic Cooling".Proceedings of the 10th World Congress on Mechanical, Chemical, and Material Engineering (MCM'24).DOI: 10.11159/htff24.268

ACKNOWLEDGEMENTS

I would like to express my heartfelt gratitude to **Dr. Arvind Pattamatta** and **Prof. Marco Marengo** for their invaluable guidance, insightful suggestions, and constant encouragement throughout the course of this research. Their mentorship played a pivotal role in shaping the direction and quality of this work.

I am fortunate to have worked alongside inspiring research colleagues, including **Dr.** Laxman Malla, **Dr.** Ananda Prasanna, **Dr.** Praveen Dhanalakota, Mr. Hemanth D, Mr. Motiur Rahaman, Mr. Davis, Mr. Viraj Dusane, Mr.Sandeep Kumar and Ms. Kavitha Gummalla.

I extend my sincere thanks to all members of the Multi-scale Thermal Transport Research Lab (MT2RL) and the Multi-scale Multiphysics Lab (MML) for providing a collaborative and supportive research environment that greatly contributed to the progress of this work.

I am deeply appreciative of my labmates for their cooperative spirit and helpful discussions during the experimental phases of this study. Special thanks are due to **Mr.Surendran** for his invaluable technical support, and to **Mr.Sagaya Rajesh** and **Mr.Prabhakaran** from the HTTP Lab Workshop for their assistance in setting up and executing the experiments efficiently. I gratefully acknowledge the financial support from **Pravartak**, IIT Madras, and the **S. Ramakrishnan Centre** (**ISRO–IITM**), without which this research would not have been possible.

Lastly, I sincerely thank **Inventec Performance Chemicals, France**, for generously providing the **Thermasolv IM6** dielectric fluid used in my experiments.

Monu Kumar

ABSTRACT

KEYWORDS

Spray cooling, Electronics cooling, Infrared thermography and Temperature field distribution, pressure atomized nozzles (PAN), air atomized nozzles (AAN), PDPA, Low GWP Dielectric

Spray cooling is an advanced thermal management technique that leverages both convective and evaporative heat transfer mechanisms through the impingement of atomized liquid droplets on heated surfaces. This thesis presents a detailed experimental investigation into the spray cooling performance of two working fluids—deionized (DI) water and Thermasolv IM6, a low global warming potential (GWP) dielectric fluid—using Pressure Atomized Nozzles (PAN) and Air-Assisted Atomized Nozzles (AAN).

Experiments were conducted over a range of flow rates (0.1–0.2 L/min), fluid inlet temperatures (25–35°C), and surface heat fluxes (5.3–14.7W/cm²). Infrared thermography was employed to capture surface temperature distributions, while droplet dynamics were characterized using Phase Doppler Particle Anemometry (PDPA) and high-speed imaging.

Results reveal that although both PAN and AAN configurations generate comparable droplet sizes with Thermasolv, the AAN setup produces significantly higher droplet velocities, resulting in enhanced momentum transfer and improved surface wetting. This intensified interaction leads to vigorous evaporation and greater thermal uniformity. Notably, at a heat flux of 14.7W/cm² and an inlet temperature of 25°C, the AAN-Thermasolv configuration achieved a substantial reduction in surface temperature to 18.4°C—significantly lower than the 43.6°C observed with PAN under the same conditions.

While DI water offers superior sensible heat absorption due to its high specific heat, its high surface tension and non-dielectric nature limit its applicability in electronic cooling environments. In contrast, Thermasolv IM6 demonstrated superior latent heat utilization,

especially at higher inlet temperatures and lower flow rates, where a greater proportion of the fluid underwent phase change. The AAN configuration further promoted vapor removal and film rewetting, contributing to consistent and effective thermal performance.

Overall, the study confirms that the combination of AAN atomization and the favorable thermophysical properties of Thermasolv IM6 enables efficient, uniform, and low-temperature spray cooling. This synergy positions AAN with Thermasolv as a robust and promising strategy for managing high heat fluxes in compact electronic devices

CONTENTS

		Pa	age
ACKNO	WLEDGI	EMENTS	i
ABSTRA	ACT		iii
LIST OF	F TABLES	S	vii
LIST OF	F FIGURI	ES	ix
ABBRE	VIATION	S	xi
NOTAT	ION		xiii
СНАРТ	ER 1	INTRODUCTION	1
1.1 1.2 1.3 1.4	Performa Thermal	nnd	8
CHAPT	ER 2	LITERATURE SURVEY	15
2.1 2.2 2.3	Research	e Review on Spray Cooling	15 23 23
СНАРТ	ER 3	EXPERIMENTAL FACILITY AND PROCEDURE	25
3.1 3.2 3.3 3.3.1 3.3.2 3.3.3 3.4 3.5	Uncertain Spray An Thermop Laser-Ba High Spe Droplet M	ental Layout and Component Description	25 31 32 32 34 39 41 45
СНАРТ	ER 4	RESULTS: SPRAY CHARACTERIZATION	51
4.14.2	Assisted Spray C	aracterization of DI Water using Pressure(PAN) and Air(AAN) Nozzle	51
4.3	Compara	I) Assisted Nozzle	60

CHAP	I EK 3	PRESSURE ATOMIZED NOZZLE(PAN)	71
5.1 5.2		Temperature Distribution for DI Water and Thermasolv mperature Behavior and Uniformity Analysis with Varying Fluid	. 71
		mperatures	. 74
5.3	Evaluat	ion of Thermasolv Evaporation Using PAN	. 85
5.3.1	Equatio	ns	. 85
CHAP	TER 6	RESULTS: HEAT TRANSFER ANALYSIS USING AIR ATOMIZED NOZZLE(AAN)	89
6.1		Temperature Distribution for DI Water and Thermasolv	. 89
6.2		mperature Behavior and Uniformity Analysis with Varying Fluid mperatures	. 92
6.3		Cooling Behavior based on Non-Dimensional Numbers	
CHAP	ΓER 7	CONCLUSIONS AND FUTURE SCOPE	105
7.1 7.2		Scope	
APPEN	DIX A	GENERAL NOTES	111
Append	ix A: Equ	ipment and Materials Utilized for the Experiments	. 111
APPEN	DIX B	CALIBRATION OF INFRARED CAMERA	113
Append	ix B: Cali	bration Procedure of Infrared Camera	. 113
REFE	RENCES		115
CURR	ICULUM	VITAE	121
GENEI	RAL TES	T COMMITTEE	123

LIST OF TABLES

Table	Caption	Page
3.1	Comparison of PAN and AAN nozzle specifications	. 28
3.2	Detailed description of parts used in the heating section	. 29
3.3	Thermophysical properties Comparison of DI Water and Thermasolv	
	IM6 for electronic cooling	. 33
3.4	Thermo-physical properties of SS-304 heater foil used in the current stud	y. 47
A.1	Equipment and materials utilized for the experiments	. 111

LIST OF FIGURES

Figure	Caption P	age
1.1 1.2	Various spray cooling applications in different industries	2
1.0	Robinson (2025)]	4
1.3	Comparison of different heat transfer method[Xu et al. (2021a)]	6
1.4	Various regimes in Spray cooling[Schmidt et al. (2023)]	8
3.1	Schematic Diagram of Experimental Set-up	26
3.2	Photograph of Experimental Set-up	27
3.3	Photograph of Nozzles(Company-Spraying Systems)	28
3.4	CAD schematic of the spray cooling heater assembly	30
3.5	PDPA setup in NCCRD, IIT MADRAS	37
3.6	Spray Angle Measurement with HSI(PAN)	41
3.7	Spray Angle Measurement with HSI(AAN)	41 43
3.8 3.9	HSI Image processing for Diameter with MATLAB	43
3.10	· · · · · · · · · · · · · · · · · · ·	45
3.10	Illustration of energy balance at a pixel element for heat flux field	46
3.11	mustration of energy balance at a pixer element for heat max field	70
4.1	PDPA measurement planes for droplet characterization at 10 mm, 20 mm, and 30 mm from nozzle outlet	52
4.2	Diameter Distribution of DI Water spray at $\dot{V} = 0.2$ L/min at 20 mm plane	
4.3	Velocity Distribution of DI Water spray at $\dot{V} = 0.2$ L/min at 20 mm Plane	55
4.4	Variation of SMD with flow rate at N-SD = 10, 20, and 30 mm for DI water	57
4.5	Variation of average droplet velocity with flow rate at N-SD = 10, 20, and 30 mm for DI water	59
4.6	Droplet Diameter Distribution of Thermasolv spray at $\dot{V} = 0.2$ L/min at	39
7.0	20 mm Plane	61
4.7	Velocity distribution of Thermasolv spray at a $\dot{V} = 0.2$ L/min at 20mm	01
,	Plane	62
4.8	Variation of SMD with flow rate at N-SD = 10, 20, and 30 mm for	-
	Thermasolv	65
4.9	Variation of average droplet velocity with flow rate at $N-SD = 10, 20$,	
	and 30 mm for Thermasolv	67
4.10	Validation of HSI against PDPA for droplet velocity for DI water	69
5.1	Steady Foil Temperature Distribution with IR Camera for PAN The	
3.1	accompanying scale bar indicates surface temperature in °C	73
5.2	Steady foil temperature and uniformity comparison for DI Water and	, 5
2.2	Thermasolv at $\dot{V} = 0.1$ L/min (PAN, 25°C)	76
5.3	Heat Transfer Coefficient Comparison at $\dot{V} = 0.1$ L/min for PAN at 25°C.	77
5.4	Steady foil temperature and uniformity comparison for DI Water and	
	Thermasolv at $\dot{V} = 0.1$ L/min (PAN, 35°C)	79

5.5 5.6	Heat Transfer Coefficient Comparison at $\dot{V} = 0.1$ L/min for PAN at 25°C. Steady foil temperature and uniformity comparison for DI Water and	80
	Thermasolv at $\dot{V} = 0.2$ L/min (PAN, 25°C)	82
5.7 5.8	Heat Transfer Coefficient Comparison at $\dot{V} = 0.2$ L/min for PAN at 25°C. Steady foil temperature and uniformity comparison for DI Water and	83
	Thermasolv at $\dot{V} = 0.2$ L/min (PAN, 35°C)	84
5.9	Thermasolv mass evaporation (%) on PAN at $\dot{V}=0.1$ and 0.2 L/min	87
6.1	Steady Foil Temperature Distribution with IR Camera for AAN The accompanying scale bar indicates surface temperature in °C	91
6.2	Steady foil temperature and uniformity comparison for DI Water and	71
o 	Thermasolv at $\dot{V} = 0.1$ L/min (AAN, 25°C)	93
6.3	foil temperature and uniformity comparison for DI Water and Thermasolv	, ,
	at $\dot{V} = 0.1$ L/min (AAN, 35°C)	95
6.4	foil temperature and uniformity comparison for DI Water and Thermasolv	-
	at $\dot{V} = 0.2$ L/min (AAN, 25°C)	97
6.5	foil temperature and uniformity comparison for DI Water and Thermasolv	
	at $\dot{V} = 0.2 \text{ L/min (AAN, 35°C)}$	99
6.6	Average Nusselt number for DI water with PAN and AAN	102
6.7	Average Nusselt number for Thermosolv with PAN and AAN	
7.1	Foil temperature variation with PAN and AAN at $\dot{V} = 0.1$ and 0.2 L/min, and $T_{\text{f,inlet}} = 25^{\circ}\text{C}$ and 35°C .	106
B1	Curve fitting for converting intensity to temperature	114

ABBREVIATIONS

AAN Air Atomized Nozzle.

DI Deionized.

GWP Global Warming Potential.

HSI High Speed Imaging.

IITM IIT Madras.

IR Camera Infrared Camera.

MWIR Mid-wave Infrared.

NSD Nozzle to Surface Distance.

PAN Pressure Atomized Nozzle.

PDPA Phase Doppler Particle Analyser.

SMD Sauter Mean Diameter.

NOTATION

ṁ	Mass flow rate, kg/s
\dot{V}	Volumetric flow rate, L/min
Φ	Non-dimensional temperature difference
\boldsymbol{A}	Area, m^2
c_p	Specific heat capacity, $kJ/kg.K$
Ca	Capillary number
D	Diameter, μ m
e	Energy, J
F	Force,N
f	Frequency,Hz
g	Gravitational acceleration, m/s^2
h	Heat transfer coefficient, W/m^2 . K
h_{fg}	Latent heat of vaporization, kJ/kg
I	Current, amps
k	Thermal conductivity, $W/m.K$
m	Mass,kg
Nu	Nusselt number
P	Pressure, N/m^2
q''	Heat flux, W/cm^2

 Q_{cond} Heat conducted through the foil

 Q_{conv} Heat lost due to natural convection

 $Q_{\rm fluid}$ Heat removed by the fluid

 q_{fluid} Heat flux removed by the fluid

 $Q_{\rm gen}$ Heat generated by Joule heating

 $Q_{\rm rad}$ Heat lost due to radiation

 Q_{stored} Energy stored in the foil

R Thermal resistance,K/W

We Weber number

CHAPTER 1

INTRODUCTION

1.1 BACKGROUND

The rapid advancement of high-power electronics, energy systems, and propulsion systems has led to a significant increase in the demand for efficient thermal management solutions. As devices become smaller and operate at higher power densities, their performance is increasingly limited by their ability to dissipate heat effectively. Currently, the heat flux generated by electronic chips can reach levels between 10 and 100 W/cm². In emerging power electronic systems, the average heat flux can surpass 1000W/cm², with localized hotspots potentially ranging from 1500 to 5000W/cm², as reported by (Sadique *et al.* (2022)). If these extreme thermal loads are not managed effectively, they can result in elevated surface temperatures and significant temperature gradients, leading to performance degradation, reduced lifespan, or even catastrophic failure of the system. Intel's founder, Gordon Moore, gave a trend known as Moore's Law. He said that the number of transistors on a microchip doubles roughly every two years, while the cost goes down. But along with power, there is a challenge of heat that comes at the time of operation. And as electronics get smaller and more powerful with a huge number of transistors, they produce even more heat in very small spaces.

The exponential growth of the nuclear industry, diode lasers, and electronic components has led to increased heat density. Also, the rapid miniaturization and integration of electronic components used in industry have increased the power density sharply. As such, dissipating large heat fluxes safely is considered one of the greatest challenges in thermal management. The performance, reliability, and lifetime of electronic devices depend highly upon their surface temperature. To meet the demands of the electronics industry, several advanced cooling strategies have been integrated into thermal management systems, replacing conventional air cooling with more efficient and compact solutions

(Kheirabadi and Groulx (2016)).

Figure 1.1 illustrates that spray cooling is applied over a wide temperature range, serving critical functions in diverse industrial sectors. In low-temperature applications—such as computing, electric vehicles, LEDs, and power systems—the primary objective is to keep surface temperatures below safety limits for electronic components. Deionized water is often used in these scenarios due to its high thermal conductivity and stability in single-phase cooling. However, its electrical conductivity requires the use of sealed systems. To address this issue, dielectric fluids like HFC134a and FC-72 are employed, allowing direct contact with components. These fluids take advantage of nucleate boiling to significantly improve heat dissipation through the release of latent heat. Nevertheless, this two-phase cooling introduces challenges as pressure and volume fluctuations occur during the phase change.

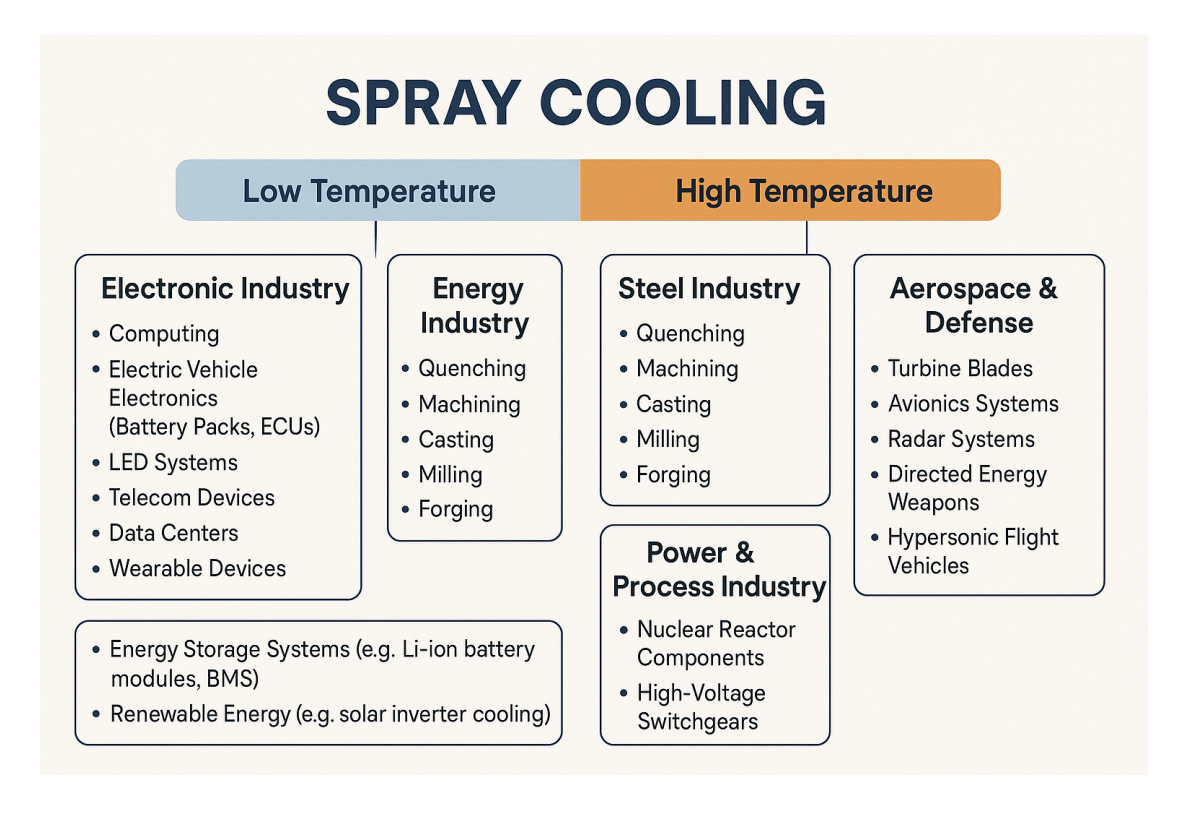


Figure 1.1: Various spray cooling applications in different industries

In contrast, high-temperature applications, such as those found in metallurgy, involve the rapid cooling of surfaces that exceed 900°C. In these cases, spray cooling transitions

from a film boiling regime—where vapor blankets limit heat transfer—to more effective nucleate and single-phase cooling as temperatures decrease. Enhancing heat removal during the film boiling stage is crucial, as it affects the material microstructure and mechanical properties during processes like quenching and casting. These various applications highlight the versatility and significance of spray cooling in addressing thermal challenges across a wide range of temperatures by (GaneshKumar *et al.* (2024)). Xu *et al.* (2021b) present a comparative analysis of various cooling techniques in Figure 1.3, highlighting their respective heat flux capacities and heat transfer coefficients (HTCs). In the bottom left region, natural convection (air and liquid) and forced convection (air) are shown to operate at low heat flux levels (typically below 1 W/cm²) and low HTCs, making them suitable for low-power thermal management scenarios.

Figure 1.2 presents a historical progression of processor heat flux demands, highlighting a dramatic escalation from the mid-1980s to the present. Earlier generation CPUs, such as the 8086DX, A86DX, and initial versions of the Celeron series, operated at relatively modest heat flux levels—typically below 20W/cm²—which allowed for simple air-based or passive cooling solutions.

However, over the past two decades, this landscape has shifted significantly. The introduction of high-performance microprocessors like the Ryzen 7000 series, Core Ultra 1300, and most notably the Ryzen AI Max, demonstrates heat fluxes surpassing 180W/cm². This steep rise is directly attributed to advances in semiconductor technology, including increased transistor density, higher clock speeds, and the integration of multiple computational cores and AI accelerators within a single chip package.

Figure 1.2 also visually emphasizes a clear trend of escalating thermal demand, marked by the upward trajectory and widening performance gap between legacy and contemporary processors. This trend poses substantial challenges to traditional thermal management techniques. Air cooling and even standard liquid-cooled systems are approaching their operational limits in terms of thermal resistance and spatial constraints.

Consequently, the data reinforces the urgency for next-generation cooling technologies, such as spray cooling, which offer significantly higher critical heat flux (CHF) capabilities and improved heat transfer coefficients (HTC). These systems are particularly well-suited for high-power-density applications, where localized hotspots and overall thermal loads must be managed efficiently to ensure device reliability and performance stability.

In summary, Figure 1.2 not only reflects the rapid evolution of processor technology but also underscores the growing necessity for advanced thermal solutions that can keep pace with the ever-increasing power densities in modern electronic devices.

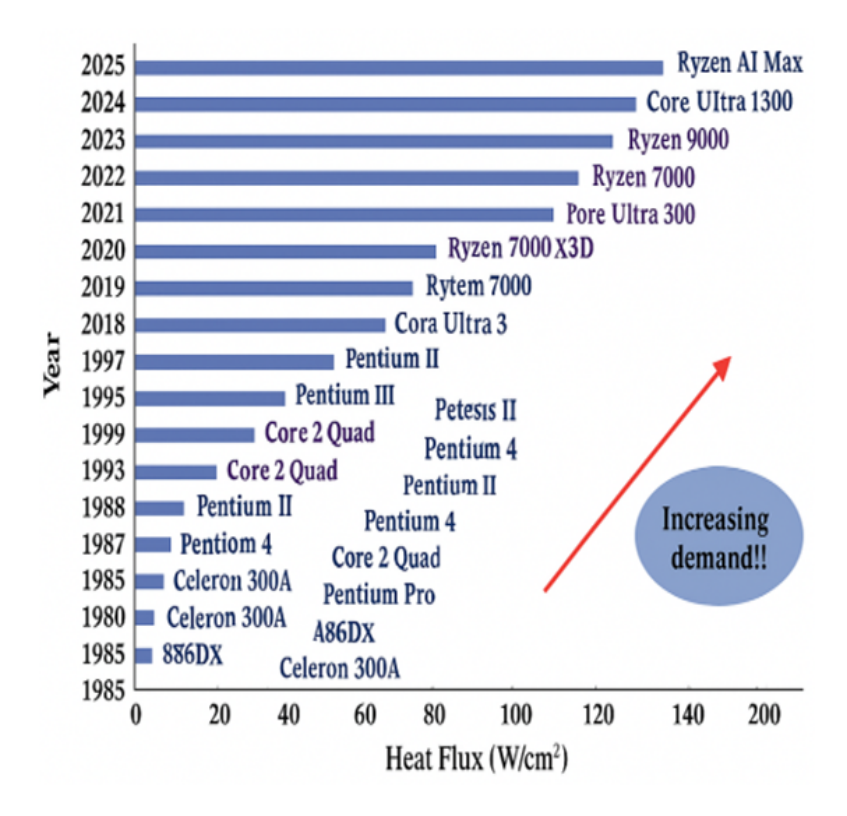


Figure 1.2: Chronological evolution of heat emitted by Intel processors[Elliott and Robinson (2025)]

This trend is a reflection of rising transistor density and performance, which consequently requires advanced cooling methods. Traditional cooling solutions are no longer adequate, highlighting the necessity for high-efficiency systems, such as spray cooling, to manage the increasing thermal loads in next-generation electronics.

As wall temperature increases, the spray cooling process transitions into the nucleate boiling regime. In this phase, surface imperfections act as nucleation sites for vigorous bubble formation, enhancing heat transfer through the latent heat of vaporization. While this regime may provide higher heat flux removal, it also introduces instability and the potential for hot spots, making it less favorable for tightly controlled electronic devices. Following nucleate boiling, the system enters the transitional boiling regime, which is characterized by unstable bubble dynamics and intermittent vapor blanketing, resulting in a heat transfer process that is highly sensitive to surface conditions. This regime marks the transition to film boiling and identifies the critical heat flux (CHF) point, an upper limit beyond which surface temperatures rise rapidly, and cooling efficiency declines. At even higher wall temperatures, vapor channels dominate the interface in the film boiling regime. In this stage, droplets cannot directly contact the surface due to a stable vapor layer (known as the Leidenfrost effect), significantly reducing heat transfer efficiency and posing a risk of thermal damage. While this regime may be beneficial in advanced applications like quenching or metal treatment, it is undesirable for electronics cooling. Therefore, to achieve reliable and effective thermal management in electronic systems, the convection and evaporation regime with its balance of stable operation, moderate heat flux capacity, and controllable cooling represents the most practical and safe operating zone, which serves as the core focus of this experimental study.

1.2 PERFORMANCE COMPARISON OF CONVENTIONAL AND ADVANCED COOLING METHODS

At the top right corner of the graph, spray cooling emerges as the most efficient technique, providing very high heat flux dissipation (up to approximately 1000 W/cm²) and high HTC values (approaching 100 W/cm²·K). This efficiency is attributed to the

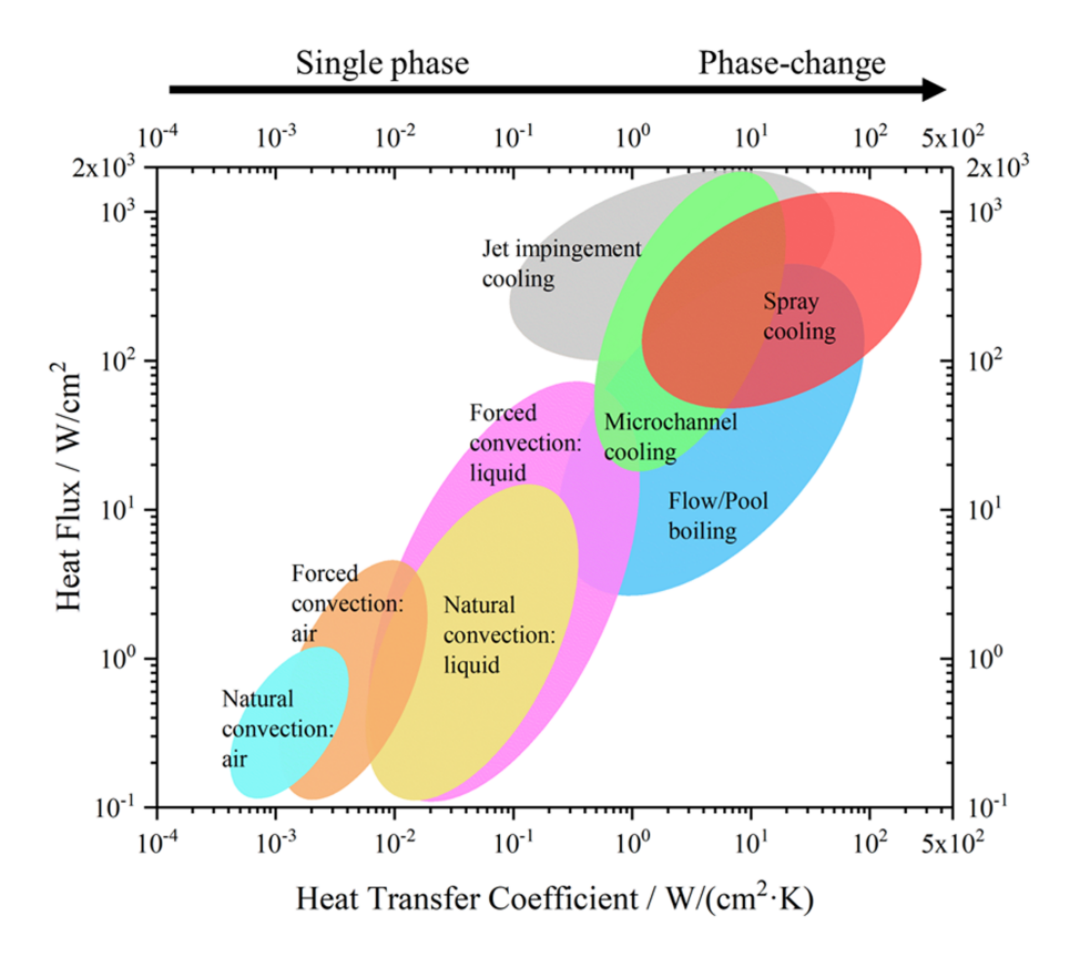


Figure 1.3: Comparison of different heat transfer method[Xu et al. (2021a)]

combined effects of convection and evaporation. Overall, this chart highlights the superiority of spray cooling for high-performance applications that require compact, uniform, and reliable thermal control.

Effective thermal management is essential for ensuring the reliability, performance, and longevity of modern electronic and high-power systems. Devices such as computer chips, solid-state lasers, insulated gate bipolar transistors (IGBTs), hypersonic vehicles, and phased-array radar systems are becoming increasingly compact and powerful. This miniaturization leads to high heat fluxes that often exceed several hundred watts per square centimeter (W/cm²) and must be dissipated efficiently to prevent performance degradation and system failure. In diode laser chips, it may reach as high as 1000 W/cm². Research shows that even a temperature rise of 75°C can significantly increase the failure rate of electronic components, with nearly 50% of integrated circuit failures

attributed to thermal issues. This highlights the urgent need for advanced thermal management techniques that can maintain low temperature and pressure conditions while ensuring operational efficiency and reliability by (He *et al.* (2021)).

To ensure the stable and reliable operation of high-power systems, cooling solutions must provide precise and uniform temperature control, a rapid response to dynamic thermal loads, and long-term operational stability. Additionally, these solutions must adhere to constraints related to cost, efficiency, compactness, and weight.

Conventional cooling technologies, which primarily rely on single-phase air or liquid convection, have reached their performance limits due to increasing demands. Consequently, phase-change cooling techniques that utilize the latent heat of vaporization have garnered significant interest. Among these techniques, spray cooling has emerged as one of the most promising solutions because of its high heat removal capacity, uniform temperature distribution, effective fluid utilization, and adaptability. Spray cooling demonstrates a significantly higher critical heat flux (CHF) compared to conventional water cooling under the same operating conditions, allowing for superior heat dissipation. In open surface scenarios, the CHF of spray cooling can reach up to 1000 W/cm² by (Zhang *et al.* (2022*b*)). This exceptional performance is primarily due to the effect of spray droplets on the heated surface, which creates strong disturbances in the liquid film and enhances both convective and phase-change heat transfer. Additionally, spray cooling effectively prevents the depletion of liquid from the surface during intense boiling, ensuring consistent thermal performance.

Zhang et al. (2022a) are investigating spray cooling as a method to mitigate thermal runaway in power batteries for EVs. Key advantages of this technique include minimal surface temperature gradients, low consumption of cooling medium, and low surface superheat. These favorable characteristics make spray cooling a key area of research in modern thermal management technologies.

1.3 THERMAL REGIMES IN SPRAY COOLING SYSTEM

Figure 1.4 illustrating the relationship between spray cooling heat flux and wall temperature reveals distinct thermodynamic regimes, each contributing uniquely to heat transfer performance. This study primarily focuses on the convection and evaporation regime, which is particularly relevant for electronic cooling applications. In this regime, fine atomized droplets impact the heated surface, forming thin liquid films that facilitate heat removal through sensible heating and partial evaporation. This mechanism ensures efficient and stable cooling without aggressive boiling, maintaining controlled sub-ambient surface temperatures that are ideal for sensitive electronic components. By operating below the onset of nucleate boiling, the system avoids risks such as dry-out and temperature overshoots, thereby ensuring long-term reliability and thermal uniformity.

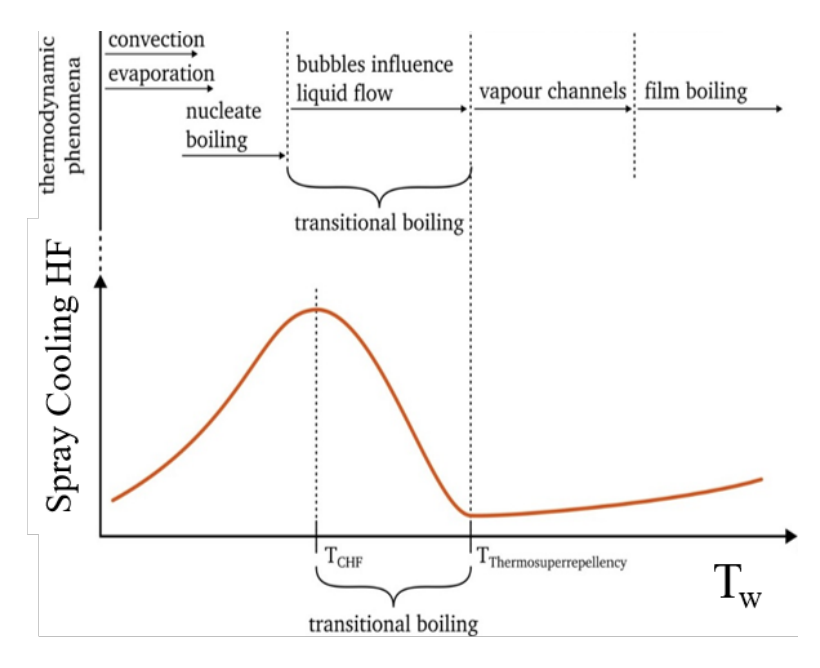


Figure 1.4: Various regimes in Spray cooling[Schmidt *et al.* (2023)]

Spray cooling offers several advantages, but it is a complex process influenced by various factors, including flow rate, type of working fluid, system pressure, injection velocity and angle, as well as surface properties. Optimizing these parameters or integrating advanced techniques can significantly enhance thermal performance.

Lin et al. (2019) reported that at a surface temperature below 30 °C, the heat transfer coefficient (HTC) at a spray distance of 25 mm was approximately 60% higher than that at a distance of 100 mm. Similarly, Salman et al. (2019) demonstrated an 80% improvement in heat transfer enhancement by modifying a flat surface and using deionized water with a temperature differential of 20 K. These findings underscore the considerable potential for further development and refinement of spray cooling systems. A thorough understanding of spray cooling mechanisms is crucial for advancing this technology. Researchers are increasingly exploring its applications in various high-impact fields, including electronics cooling, aerospace systems, medical treatments, and battery thermal management.

In a spray cooling system, a mist of fine droplets, generated by either pressure atomized or gas-atomized nozzles, is directed toward a heated surface. When these droplets impact the surface, they form a thin liquid film that evaporates rapidly, aided by the low thermal resistance of the film and efficient bubble dynamics. The incoming droplets enhance convection and promote bubble breakup, while the resulting vapor is effectively removed by the spray flow. This process reduces vapor back-pressure, further improving evaporation. Together, these factors enable spray cooling to achieve heat fluxes exceeding 1000 W/cm² and heat transfer coefficients (HTC) as high as 60 W/cm²·K, particularly when operated near the critical heat flux (CHF) limit studied by (Benther *et al.* (2021)). Traditional cooling methods like air cooling and water-cooled cold plates are increasingly inadequate for managing the thermal loads of high-power electronic components.

Liquid cooling offers a promising alternative due to the superior thermal properties of fluids. Indirect liquid cooling methods, where a cold plate transfers heat away from the source, are commonly used, particularly with water for high thermal performance. However, this approach requires careful fluid management to prevent leaks and often involves complex circulation systems. On the other hand, direct liquid cooling methods, including immersion cooling with dielectric fluids, eliminate thermal contact resistance

and further enhance cooling efficiency, especially in compact, high-power environments.

Although air cooling systems are the simplest and most affordable cooling method, they require a large surface area, and have a limited cooling capacity due to the poor thermo-physical properties of air explored by (Smakulski and Pietrowicz (2016)).

The maximum heat transfer coefficient of a standard air fan is 150 W/m2.K; thus, it is appropriate for low heat flux applications. To resolve this issue, thermal engineers have proposed liquid cooling techniques for thermal management systems as a sustainable and reliable solution in terms of cooling energy by (Kheirabadi and Groulx (2016)).

This heat can damage the electronics or limit how well they work. So now, one of the biggest challenges in the electronics world is figuring out how to cool these devices properly, i.e, thermal management of electronic devices. If we don't solve the heat problem, we can't fully utilize the power of these systems in the long run. In this study, we focus on the low-temperature range of spray cooling, where most of the heat is removed through convection and evaporation. Unlike very high temperatures where boiling becomes unstable and vapor hinders the liquid from touching the heated surface, we worked in a more stable region. This helps us clearly understand how the droplets interact and cool the surface without too much interference from boiling. By working in this range, we studied the cooling performance more accurately and found out how well the spray works for electronic devices.

For instance, air cooling has a limited heat flux capacity of around 37 W/cm² and suffers from low thermal conductivity. While improvements such as Computer Room Air Conditioning (CRAC) systems have been implemented in data centers, these consume nearly 40% of the facility's total energy input, significantly impacting overall energy efficiency. In 2020, the total energy demand for global data centers was estimated to be between 200 and 250 TWh, accounting for about 1% of the world's electricity consumption. As a result, there is a growing interest in more efficient and environmentally friendly cooling technologies.

Among emerging cooling technologies, two-phase spray cooling has garnered significant

attention. This technique involves atomizing a fluid into fine droplets using pressurized nozzles, which then strike the heated surface. The combination of heat transfer mechanisms, which include droplet impact, surface boiling, and thin film evaporation, enables extraordinarily high heat transfer coefficients (HTCs) and critical heat flux (CHF) levels. For example, studies have shown HTCs exceeding 500,000 W/m²·K and CHFs over 1000 W/cm² when using fluids such as water and ammonia by (Hu *et al.* (2025)).

Additionally, dielectric fluids, although offering slightly lower performance, provide the advantage of electrical insulation, making them suitable for direct contact cooling applications. Spray cooling systems also deliver relatively uniform surface temperatures, compact designs, and energy-efficient operation, making them highly desirable for aerospace, defense, and high-performance computing sectors.

The versatility of spray cooling extends to aerospace and near-space vehicles (NSVs), where thermal management poses unique challenges. Vehicles like hypersonic planes and reusable two-stage orbit systems endure varying atmospheric conditions and extreme aerodynamic heating. During near space cruise, typically between 20 km and 100 km in altitude, the atmospheric density decreases significantly while the incoming air temperature rises dramatically due to compression. Traditional air-assisted cooling fails under these conditions, necessitating innovative thermal management solutions like spray cooling, which can effectively operate under low ambient pressure and high heat flux situations.

As we move upward and to the right, both forced liquid convection and pool/flow boiling demonstrate improved thermal performance due to enhanced fluid movement and phase-change mechanisms. Microchannel cooling achieves higher HTCs and moderate to high heat flux capabilities by utilizing confined boiling. Jet impingement cooling performs even better, particularly at high HTCs, due to its ability to extract heat through localized momentum-driven processes.

Recent developments have also explored the application of spray cooling in sustainable

energy systems. For instance, researchers have proposed using the water produced as a byproduct of fuel cells for radiator spray cooling in electric vehicles. This approach not only enhances thermal performance but also improves water reuse efficiency, making it an eco-friendly and integrated solution for energy and thermal management.

Spray cooling performance is influenced by a complex combination of fluid properties, system geometry, and environmental conditions. Key factors include the thermal conductivity, specific heat, viscosity, and latent heat of the coolant, all of which determine its ability to absorb and dissipate heat. The characteristics of the spray nozzle—such as orifice diameter, geometry, and orientation—also play a crucial role, as they define the spray angle, droplet distribution, and coverage uniformity.

Droplet dynamics, including size and velocity at impact, significantly affect heat transfer by influencing film formation, wetting behavior, and the initiation of phase change. Additionally, the surface temperature and texture influence local boiling behavior and fluid interactions, while external conditions like ambient pressure and temperature can change evaporation rates and vapor removal efficiency. To improve the effectiveness of spray cooling, recent advancements aim to optimize these parameters through experimental techniques, surface engineering, and numerical simulations. This multiparameter approach is essential for maximizing heat dissipation and ensuring reliable operation in demanding thermal environments, such as in high-power electronics and compact energy systems.

1.4 MOTIVATION

In light of this background, the present thesis aims to experimentally investigate the spray cooling performance of both water and dielectric fluids for electronic thermal management. The study emphasizes the role of spray parameters, flow regimes, and surface fluid behaviors in determining overall heat transfer effectiveness. Through this research, we seek to contribute to the development of high-performance, sustainable,

and compact thermal management systems for advanced applications in electronics, aerospace, and renewable energy technologies.

The main goal of this study is to use advanced cooling techniques to help electronics perform better and last longer. If we can keep things cool, we can push technology to do even more safely and reliably. Spray cooling systems are generally categorized into two main types based on how droplets are created: pressure sprays and air-atomized sprays. In pressure sprays, liquid is forced at high pressure through a narrow nozzle to form droplets, whereas in air-atomized sprays, a high-speed gas such as air or nitrogen is used to break the liquid into fine droplets.

In this study, both spray system was selected for the study to determine the impact of thermal management. Specifically, a UniJet full cone nozzle, TG0.3-a pressure Atomized nozzle, and SU22B-Air Atomized nozzle (Spraying Systems Co.) with a circular impact pattern were used to provide even droplet distribution over the target area. When the droplets strike a heated surface with sufficient force, they form a thin liquid film that spreads across the surface. Within this film, several heat transfer processes can occur, mainly convection and evaporation. The dominant mechanism depends on factors like the surface temperature, droplet velocity, and the pressure conditions inside the cooling chamber.

CHAPTER 2

LITERATURE SURVEY

2.1 LITERATURE REVIEW ON SPRAY COOLING

Ghodbane and Holman (1991) investigated how various spray parameters, such as mass flux, droplet speed, droplet size, and distance between the nozzle and the surface, affect cooling performance. They used a closed-loop spray cooling system with Freon-113 as the working fluid, delivering a continuous heat flux to a vertically heated surface. Two types of nozzles were tested: a complete cone circular nozzle and a hydraulic square nozzle. The flow rates ranged from 50.47 to 126.18 cm³/s. The nozzle-to-surface distance was set at 18.42, 27.3, and 34.92 cm, and the sub-cooling temperature ranged between 5°C and 10°C. Their findings indicated that larger mass flux facilitated heat transfer.

Labergue *et al.* (2015); Mudawar *et al.* (2009); Visaria and Mudawar (2009); Mudawar (2013); Liang and Mudawar (2017*b,a*) explored how droplet size (measured as Sauter Mean Diameter or SMD), nozzle orientation (facing upward or downward), and volumetric flux affect spray cooling with fluids such as PF-5052, FC-72, and FC-87. Their experiments revealed that the nozzle's direction (up or down) had no significant impact on cooling performance. Instead, the spray's volumetric flux and droplet size (SMD) were the two most important elements influencing heat transmission.

Chen *et al.* (2004, 2002) investigated how average droplet size, flux, and speed influenced critical heat flux (CHF) in spray cooling. Their findings indicated that droplet velocity had the greatest influence on both CHF and the heat transfer coefficient. The quantity of droplets (droplet flux) showed a considerable effect, though not as much as velocity. Surprisingly, the average droplet size (Sauter mean diameter, D_{32}) showed less impact on CHF. Overall, increasing droplet velocity improved cooling performance by increasing both CHF and the heat transfer rate.

Pautsch and Shedd (2005) studied the droplet formation method. Spray cooling systems are generally categorized into two types: pressure sprays and Air-atomized sprays. In pressure sprays, the liquid alone is pushed through a narrow orifice at high pressure, naturally breaking into small droplets. On the other hand, Air atomized sprays use a stream of high-pressure gas, such as air or an inert gas, to assist in breaking up the liquid into fine droplets.

Kim (2007) explored that spray cooling takes place when a high-pressure liquid is forced through a small nozzle, causing the liquid to break apart into fine droplets with high velocity and increased surface area.

Yan et al. (2010) investigated the impingement spray cooling using R134a was experimentally investigated for the thermal management of a high-power 1 kW 6U electronic board, represented by a copper plate of equivalent dimensions. The study confirmed that effective cooling could be achieved, keeping the average surface temperature below 25°C with minimal temperature variation (approximately 2°C). This was accomplished by carefully adjusting operating parameters such as coolant mass flow rate, nozzle inlet pressure, and chamber pressure. Increased nozzle inlet and chamber pressures resulted in improved heat transfer effectiveness and better uniformity of surface temperatures. However, the study also noted potential liquid accumulation on the large heated surface, likely caused by spray interactions and limited drainage of the coolant. This observation underscores the necessity for optimized fluid runoff and drainage design in large-area impingement cooling systems to ensure consistent performance and prevent localized overheating. Overall, the findings highlight the potential of impingement spray cooling for high-density electronic systems while indicating areas for key design improvements for practical implementation.

Cheng *et al.* (2011) experimentally explored the effects of the spray characteristics on the thermal performance of a spray cooling system, utilizing distilled water as a working fluid.

Huai and Tao et al. (2011) also investigated the effect of the volumetric flow rate of

liquid, the nozzle to surface height, and the fluid inlet temperature on the spray cooling heat transfer performance in the single-phase region. The experiments were performed in an open-loop test system working with deionized water as a working medium. The results indicated that increasing the volumetric flow rate or reducing the coolant inlet temperature improves the heat transfer performance.

Mudawar (2013), studied the effectiveness of spray cooling depends primarily on the fluid stream breakup into droplets. The droplet break-up process, which consists of three stages: formation of liquid sheets, then dispersion into ligaments, and eventually break-up into fine droplets, as graphically explained.

Xie *et al.* (2014) employed Particle Image Velocimetry (PIV) and Phase Doppler Interferometry (PDI) to study how heat influences the geometry of a water spray cone, which is critical for spray cooling efficiency. They investigated with different nozzle inlet pressures and surface temperatures to determine how they affected the spray cone's behavior. Their results demonstrated that surface temperature has a significant impact; at higher temperatures, the spray cone widens. This broader cone can result in uneven surface temperatures and reduced heat transfer efficiency.

Zhou *et al.* (2017) conducted studies to determine how different spray parameters, such as spray height, heat flux, input pressure, and spray angle, affect spray cooling efficiency. Their investigation sought to determine which component had the most impact. The results showed that the mass flow rate had the biggest effect: greater flow rates resulted in enhanced heat transfer. They also observed that the cooling performance was highest when the spray angle relative to gravity was between 30° and 120°, and the poorest when it was 180°.

Gao and Li (2017) carried out experiments to find out how the height and orientation of the spray nozzle affect cooling performance in a spray cooling system. They applied a complete cone nozzle to spray water over a heated surface. Their studies showed that the best cooling was achieved when the nozzle was positioned closer than the required height to cover the entire heated area. They additionally observed that when the spray flow rate

increased, the optimal nozzle height decreased. When they varied the nozzle's tilt angle while keeping the spray impact length equal to the surface length, they discovered that nozzle height had minimal effect at small angles but substantially more at greater angles. Salman and Khan (2017) investigated how various spray parameters affect the cooling efficacy of a spray cooling system. Their experiments used deionized water in a closed-loop system, with the nozzle 10 mm above the heated surface, and it operated at various inlet pressures. The findings demonstrated that increasing the nozzle inlet pressure had the biggest impact on cooling performance for both types of surfaces. This improvement was primarily owing to the greater momentum of the droplets at higher pressures.

Another study by Salman *et al.* (2018) investigated how the distance between the nozzle and the hot surface influences spray cooling efficiency. They investigated nozzle-to-surface lengths from 10 to 16 mm, maintaining a constant mass flux of 15.5 kg/s·m². The study found that reducing this gap significantly improved thermal performance. This enhancement can be attributed to a larger ratio between the sprayed and liquid film areas, as well as increased surface instability and a higher Weber number, which all boost heat transfer-particularly inside the thin liquid film created on the surface.

Wang *et al.* (2018) address the thermal management challenges of electro-driven systems in near-space environments, a Low-Pressure Large-Space Spray Cooling System (LLSCS) was developed to cool an array of Permanent Magnet Synchronous Motors (PMSMs) used in hypersonic vehicles. The system was experimentally tested under simulated near-space conditions in a vacuum chamber, focusing on the effects of environmental pressure, spray parameters, and heat load. Notably, phenomena such as flash boiling, including droplet and film boiling, were found to enhance cooling in low-pressure environments. An empirical correlation was proposed to predict the thermal behavior in the flash boiling regime, providing a foundation for future large-scale system design and optimization in low-pressure aerospace applications.

Zhou *et al.* (2019) is the study of the impact of surface structuring on the performance of a closed-loop flash evaporation spray cooling system was experimentally analyzed using both macro-structured and nano-porous surfaces. The study found that macro fins, particularly rough pyramid fins, significantly enhanced the critical heat flux (CHF) and heat transfer coefficient. This improvement was attributed to the increased surface area and capillary-driven rewetting, achieving CHF values of up to 330 W/cm².

On the other hand, while nano-porous coatings enhanced wettability and increased the density of nucleation sites, resulting in an 85% improvement in CHF, they exhibited lower heat transfer performance compared to macro-structured surfaces because of the additional thermal resistance. The research also introduced a transition model that connects pore size to CHF behavior, offering valuable insights for surface design in high-performance thermal management systems.

Wang et al. (2019) address the rising thermal demands of onboard electronics in next-generation aircraft, a closed-loop gas-atomized spray cooling system (GSCS) was developed and experimentally validated. This system utilizes high-pressure air to atomize the coolant and incorporates a gas-driven ejector for efficient droplet collection and recycling. Performance evaluation revealed that optimal air and water pressures significantly enhance heat flux removal and heat transfer coefficients. The system achieved a peak heat flux of 885.4W/cm² at a safe surface temperature, demonstrating its potential for high-performance electronic cooling applications in aviation environments. Sijs et al. (2021) is a comparative study of droplet sizing techniques, including image analysis (VisiSizer and stroboscopic imaging), Phase Doppler Particle Analysis (PDPA), and laser diffraction, highlighting how discrepancies between methods increase with coarser sprays. While image analysis and PDPA show good agreement for droplets up to 400 µm, their accuracy diverges for larger, non-spherical, or inhomogeneous droplets, where PDPA tends to underestimate sizes. Laser diffraction, although fast and easy to use, can misrepresent distributions due to assumptions in its fitting algorithms and the influence of droplet velocity on sampling concentration. The study emphasizes

the importance of selecting appropriate measurement techniques based on droplet characteristics and application needs.

Variable and intermittent spray cooling strategies were experimentally evaluated to

determine their effectiveness in managing dynamic thermal loads using a pressureatomized nozzle and HFE-7100 as the working fluid. The study compared smooth surfaces to microporous surfaces, finding that microporous structures significantly improved the heat transfer coefficient and critical heat flux under steady conditions. Liu et al. (2021) is to improve the thermal and energy efficiency of spray cooling systems, a specialized experimental setup was created to analyze the effects of key parameters, including spray height, inlet pressure, effective flow rate, and heat flux. The results indicated that increasing the inlet pressure enhances both the atomization quality and the heat transfer coefficient; however, this also leads to a corresponding increase in power consumption. Notably, even with a low inlet pressure of 0.1 bar, the system achieved a heat transfer coefficient greater than 1.8 W/cm²·K, significantly surpassing the performance of conventional convective water cooling. Additionally, the study identified an optimal spray height associated with maximum thermal performance, which also corresponded to the highest system efficiency based on a performance evaluation criterion. These findings highlight the importance of optimizing geometric and flow parameters to achieve effective heat dissipation with minimal energy consumption, making the system ideal for applications that require compact and energy-efficient cooling solutions.

Liu *et al.* (2023) is to enhance the cooling efficiency and energy performance of data centers, a new spray-cooled rack system was developed and tested under various dynamic thermal conditions. A thermal model was created to evaluate how environmental factors affect system performance. The study found that ambient temperature is the primary influence on chamber pressure and cooling performance, while changes in dry tower fan power and water flow rate have little effect. Additionally, the thermal inertia of the dry tower significantly mitigated external temperature fluctuations, allowing for a quick response to changes in cooling water temperature. The validated thermal model

closely matched the experimental results and provided a solid foundation for future work on predictive control strategies aimed at improving operational efficiency and system adaptability.

Bostanci *et al.* (2021) is the study of variable flow; the system was able to maintain effective cooling at levels up to 150 W/cm² while also reducing coolant usage and pumping power. In contrast, intermittent flow resulted in higher surface temperatures and a substantial decrease in critical heat flux, revealing limitations in high heat flux scenarios. Overall, variable flow cooling emerged as a promising method for energy-efficient thermal management in applications with fluctuating heat loads.

Zhao *et al.* (2024) studied in-depth experimental analysis was conducted to understand the spray cooling behavior at a height of 15 cm, focusing on the relationship between surface fluid dynamics and heat transfer performance. The study identified four distinct surface fluid regimes: liquid film, stream flow, droplet flow, and misty flow, each associated with unique heat transfer characteristics. Among these, the droplet flow regime proved to be the most effective, offering the highest heat transfer coefficient (HTC). It was observed that increasing the spray pressure significantly enhanced droplet atomization and initial velocity, resulting in denser and finer droplets, which led to up to a 34% improvement in HTC. Additionally, increasing the spray flow rate substantially boosted the critical heat flux (CHF), with nearly a 60% increase observed when the flow rate was raised from 20 to 35 mL/min.

Zeng *et al.* (2025) is a novel approach to thermal management that has been proposed that utilizes the water generated from fuel cells for radiator spray cooling, with its effectiveness evaluated under New European Driving Cycle (NEDC) conditions. The study systematically analyzed strategies for water production, collection, and application, while also experimentally investigating spray parameters such as pressure, distance, and angle. The results indicate that an optimal spray pressure of 0.4 MPa achieved efficient droplet formation and minimized water loss. Additionally, a spray distance of 400 mm and an angle of 0° provided the best coverage for the radiator. Compared to traditional

cooling methods, the spray-cooled system enhanced the heat dissipation coefficient by up to three times and reduced fluctuations in fuel cell temperature by 45.6%. Despite challenges related to water availability, a control strategy focused on high heat-load periods increased overall heat dissipation power by 43%. This demonstrates the potential of water recycling for high-efficiency thermal management in fuel cell systems.

These findings emphasize the importance of operating within the droplet flow regime for optimal cooling performance. They also highlight the potential of combining experimental and numerical approaches in future studies to refine predictive models and system designs for spray cooling applications. In conclusion, past research has shown that spray cooling is a highly complex process driven by a variety of parameters, including droplet size, droplet flux, volumetric flow rate, and nozzle-to-surface distance. While several studies have consistently identified volumetric flow rate as a critical driver of thermal performance, the effect of nozzle distance and other spray variables is less clear and frequently system-specific. Furthermore, despite substantial studies on conventional fluids such as water and common dielectric liquids, little is known about newer, low GWP dielectric fluids such as Thermasolv, particularly under a variety of nozzle configurations and precise spray characterisation.

This gap provides an opportunity to improve our understanding of spray cooling mechanisms by examining fluid characteristics, droplet dynamics, and thermal behavior with IR thermography, which is a non-invasive technique that gives us insights into the temperature field and heat flux distribution. This study aims to bridge the existing knowledge gap by evaluating the spray cooling performance of Thermasolv using both pressure and air atomizing nozzles. Additionally, it investigates the correlation between spray hydrodynamics—characterized through Phase Doppler Particle Anemometry (PDPA) and high-speed imaging—and the resulting heat transfer performance. The findings contribute valuable insights toward the development of sustainable and efficient thermal management strategies for next-generation electronic devices.

2.2 RESEARCH OBJECTIVES

- 1. To investigate the spray cooling performance of Thermasolv (Company-Inventec Performance Chemicals), a dielectric fluid with Low Global Warming Potential(GWP) for electronic cooling applications.
- 2. To compare the Heat transfer performance of Thermasolv and water using two nozzle types: Pressure Atomizing Nozzle (PAN) and Air Atomizing Nozzle (AAN).
- 3. To perform spray characterization of both fluids using the Phase Doppler Particle Analyzer (PDPA) and high-speed imaging.
- 4. To evaluate the effect of flow rate and inlet fluid temperature on spray cooling effectiveness.

This research investigates the spray cooling performance of Thermasolv—a low global warming potential (GWP) dielectric fluid developed by Inventec Performance Chemicals—in comparison with water, using both pressure and air-atomizing nozzles. Water is utilized as the thermal benchmark due to its superior specific heat capacity and thermal conductivity, while Thermasolv is examined for its viability in direct-contact cooling of electronic components. The study incorporates spray characterization techniques, including Phase Doppler Particle Anemometry (PDPA) and high-speed imaging, complemented by a parametric evaluation of flow rate and inlet temperature. It examines the influence of droplet behavior and thermal properties on heat transfer effectiveness. The primary goal is to determine the most efficient and environmentally sustainable combinations of fluid and nozzle configurations for thermal management in compact, high-power electronic devices.

2.3 NOVELTY

◆ First-time use of Thermasolv with low-GWP dielectric fluid specifically evaluated for high heat flux spray cooling of electronic components.

- ◆ Simultaneous comparison of PAN and AAN to compare atomization and spray cooling across two fundamentally different nozzle types.
- ◆ Combined heat transfer with spray cooling to correlate droplet characteristics with thermal performance.
- ◆ Employed non-invasive IR thermography for real-time, high-resolution mapping of temperature and heat flux in spray cooling.

This study presents significant advancements in the domain of electronic spray cooling by introducing several key innovations. It is the first experimental investigation to assess Thermasolv—a dielectric fluid with low global warming potential (GWP)—for moderate heat flux applications in spray cooling systems, offering novel insights into its thermal reliability and hydrodynamic performance. The research involves a comparative evaluation of pressure atomizing nozzles (PAN) and air atomizing nozzles (AAN), using both Thermasolv and water as working fluids. This comparison underscores the influence of nozzle type on droplet formation and cooling effectiveness. Through the combined application of Phase Doppler Particle Anemometry (PDPA) and high-speed imaging, the study establishes a direct correlation between droplet properties and heat transfer behavior. Furthermore, the integration of infrared thermography—a non-intrusive technique for temperature measurement—enables whole-field, real-time thermal mapping, thereby providing a comprehensive understanding of temperature distribution and spatial uniformity throughout the cooling process.

CHAPTER 3

EXPERIMENTAL FACILITY AND PROCEDURE

3.1 EXPERIMENTAL LAYOUT AND COMPONENT DESCRIPTION

The experimental setup, consisting of a foil heater powered by a DC supply, spray nozzle, spray chamber, and data acquisition system, is illustrated schematically in Figure 3.1 and shown photographically in Figure 3.2. A positive displacement gear pump (SHENCHEN, labGM) is used in the system to move working fluid that is kept in a reservoir. A filter (Swagelok) is placed between the reservoir and the pump to ensure no contaminants enter the flow loop, and a Coriolis flow meter is used to measure the coolant volumetric flow. Spray nozzles play a crucial role in the efficiency of spray cooling systems, as their design affects droplet size, distribution, and overall cooling performance. The most common nozzle types include full cone, hollow cone, and flat fan, each providing different spray patterns: full cone nozzles deliver uniform area coverage, hollow cone nozzles focus on edge spraying, and flat fan nozzles offer linear coverage.

Nozzles are generally classified as single-fluid or two-fluid. Single-fluid nozzles, such as plain orifice and swirl nozzles, use only the coolant fluid, with swirl nozzles improving atomization via induced vortex motion. In contrast, two-fluid nozzles, including internal and external mixing designs, incorporate compressed air to aid in atomization, allowing for finer and more controlled droplet generation. Additionally, advanced nozzle types like impinging jet, ultrasonic, and piezoelectric nozzles provide high-precision cooling through their unique atomization mechanisms.

This study investigates the spray cooling performance of deionized water and Thermasolv IM6 using two full-cone spray nozzles: the TG-0.3, a pressure-atomizing nozzle, and the SU22B, an air-atomizing nozzle. The TG-0.3 nozzle operates solely on liquid pressure to

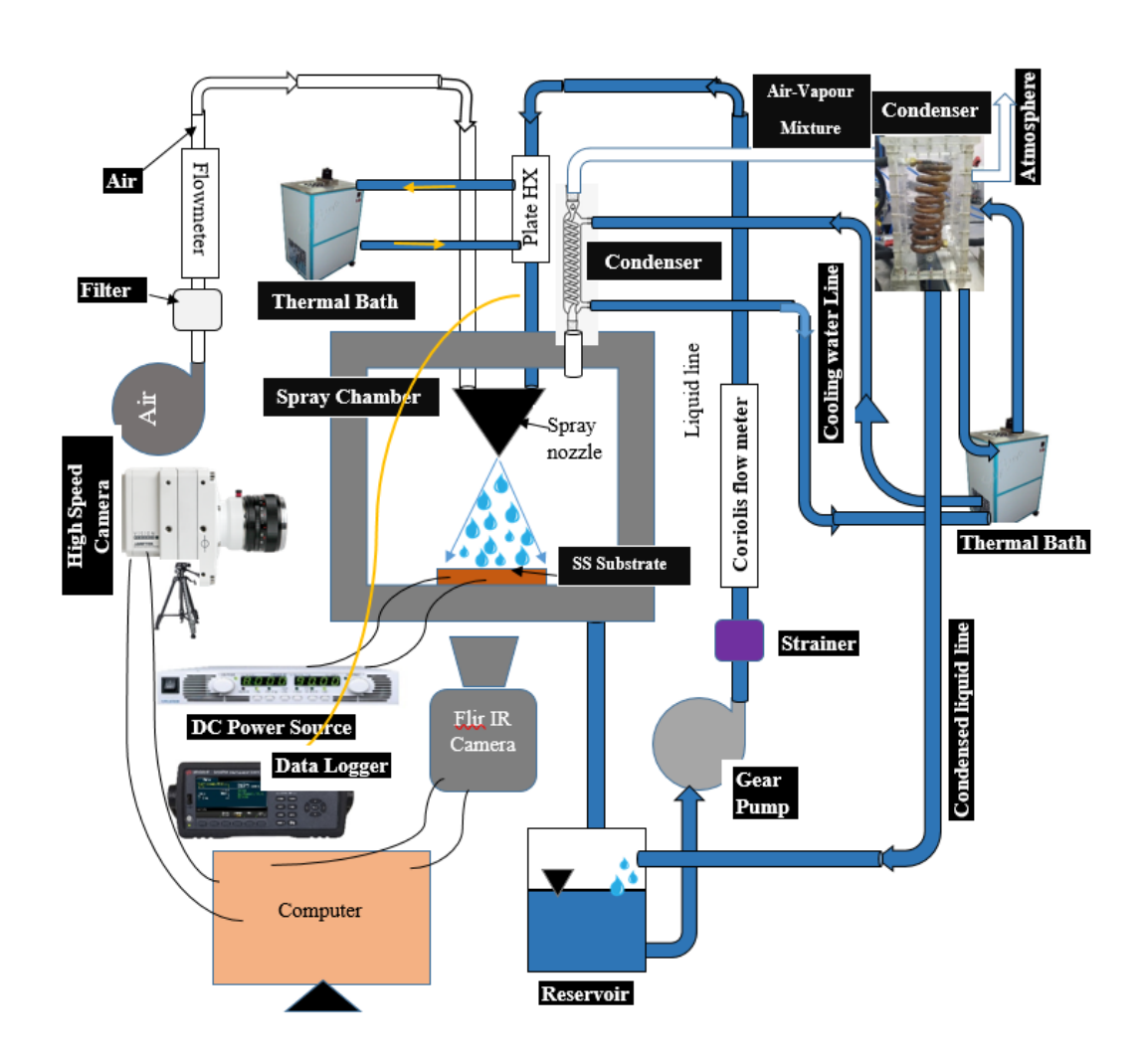


Figure 3.1: Schematic Diagram of Experimental Set-up.

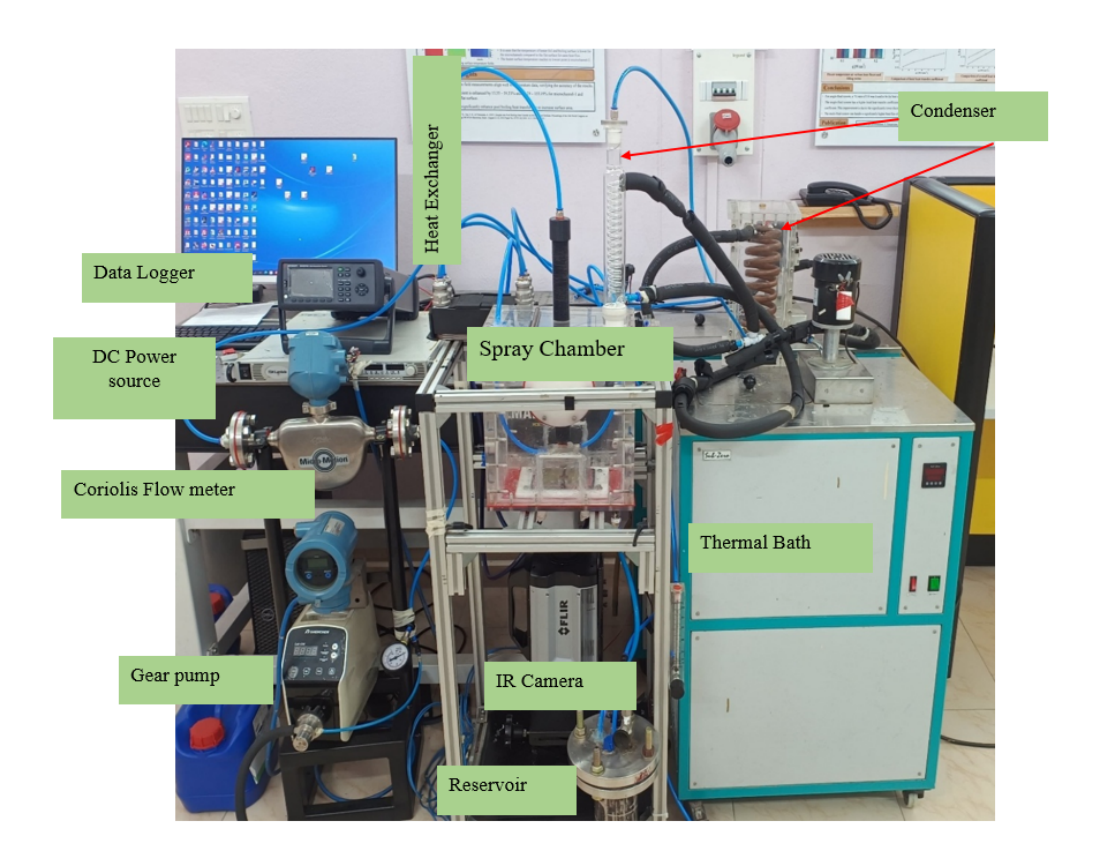


Figure 3.2: Photograph of Experimental Set-up.

create droplets, resulting in a uniform spray with moderate droplet sizes that are effective for steady cooling. In contrast, the SU22B nozzle uses compressed air to help break the liquid into much finer droplets. This improved atomization enhances evaporation and increases heat transfer efficiency, making it particularly advantageous for electronic cooling applications with moderate heat flux. Figure.3.3 illustrates the use of full cone nozzles—TG 0.3 (pressure atomizing nozzle, PAN) and SU22B (air atomizing nozzle, AAN)—manufactured by Spraying Systems Co., for droplet generation.

For the heat transfer and PDPA experiments using PAN and AAN, we supplied fluid at rates of 0.1 and 0.2 L/min at room temperature, maintaining a nozzle-to-surface distance of 20 mm. The substrate is 40x80 mm² and is made of SS foil with a thickness of 100 microns. The SS foil used is SS-304, known for its high hardness, shine, wear resistance, and rustproof properties.

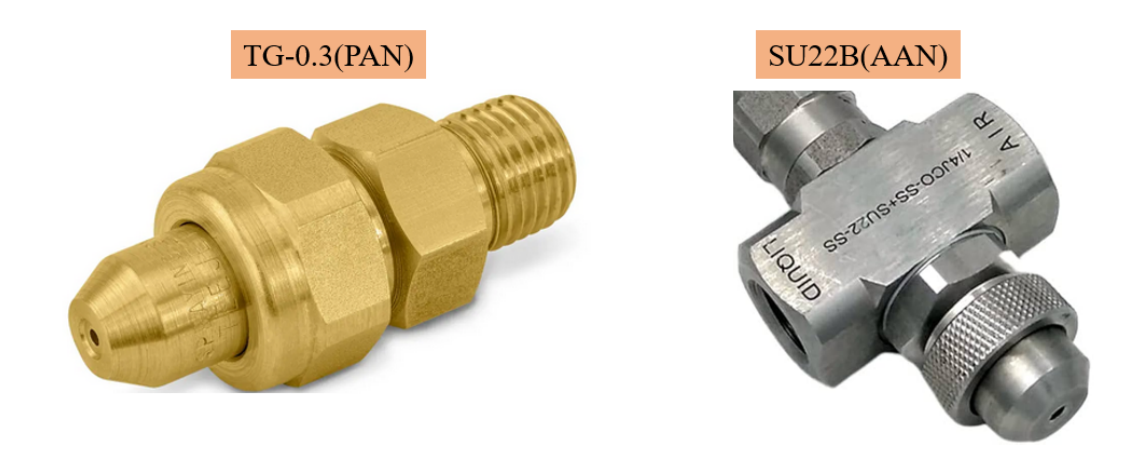


Figure 3.3: Photograph of Nozzles(Company-Spraying Systems)

Detailed specifications of the nozzle configurations are presented in Table3.1.

Table 3.1: Comparison of PAN and AAN nozzle specifications

Parameter	PAN (TG-0.3)	AAN (SU22B)	
Orifice Diameter	0.51 mm	_	
Spray Angle Description	Hollow Cone	Full Cone	
Spray Angle Image	52°	20°	
Operating Pressure	3 bar	4 bar	

Figure 3.4 and Table 3.2 show the heating setup, which includes a copper bus bar, Teflon plate, Bakelite plate, silicon gaskets, hylam plate, and 100 µm thick SS foil. The electricity is supplied by using a constant current DC power source through the foil,

which is attached to copper bus bars. There are two bus bar openings on the Teflon plate. A 100 μ m-thick SS foil is sandwiched between the two silicon gaskets. The bus bars heat the foil as the DC power source sets the necessary current. A Hylam cover plate is placed above the gasket. A 20x20 mm² portion of the foil is exposed at the top for spraying, and the bottom surface of the SS heater foil is painted matte black using high-temperature-resistant black paint to increase the emissivity and minimize reflection and glare. The emissivity, thickness, and thermal conductivity of the black paint are 0.92, 10 μ m, and 1.45 W/mK, respectively. The thermal images are captured at a frame rate of 1000 Hz.

Table 3.2: Detailed description of parts used in the heating section

Component	Dimensions / Thickness	Purpose / Description
Spray Area	$20 \times 20 \text{ mm}^2$	Region where the liquid is sprayed; primary area for heat extraction during cooling.
Hylam Plate	3 mm thick	Serves as a thermal insulator; restricts heat conduction to surroundings.
Gasket	2 mm thick	Prevents liquid leakage from the spray area to the infrared (IR) camera below.
SS Foil (Stainless Steel)	$100~\mu\mathrm{m}$ thick	Represents the heated surface of an electronic device; undergoes Joule heating.
Bakelite Plate	2 mm thick	Withstands high temperatures and acts as a sealing layer to prevent liquid leakage.
Bus Bars	$20 \times 40 \text{ mm}^2$	Provides soldered electrical connection between the stainless steel foil and high current DC power supply.
Teflon Plate	214 × 122 × 12 mm ³	Acts as a base support for the heating assembly, offering thermal insulation and mechanical strength.

Joule heating is powered by an input power supply (TDK-Lambda) with a high current DC power source. Thermocouples and pressure transducers measure the temperature and pressure in the fluid flow loop through a data acquisition system (HIOKI LR8500). A high-speed infrared camera (FLIR X6900sc MWIR), along with a macroscopic lens, is used to acquire the temperature field of the heater foil's bottom surface. We are employing a macroscopic lens in an FLIR IR camera to analyse a 20x20 mm² area. With

- 1. 20x20 mm² Spray Area
- 2. Hylam Plate(3mm)
- 3. Gasket(2mm)
- 4. SS Foil(100µm)
- 5. Bakelite plate(2mm)
- 6. Bus Bars(20x40 mm²)
- 7. Teflon Plate(214x122x12mm³)

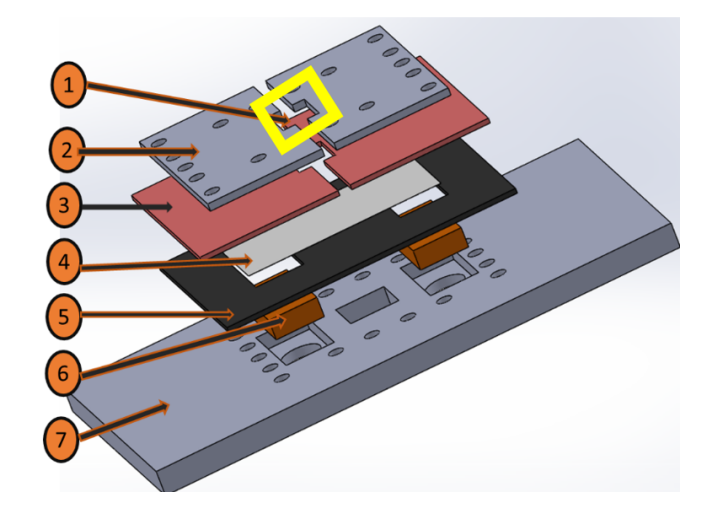


Figure 3.4: CAD schematic of the spray cooling heater assembly

this specific lens, 1 pixel is equivalent to 0.0408 mm for field measurement.

The TG-0.3 is a brass-bodied, single-fluid nozzle that relies completely on hydraulic pressure to atomize the liquid. When pressurized fluid is forced through a narrow orifice, it experiences a sudden drop in pressure and velocity, breaking the liquid into fine droplets. The internal geometry is designed to promote swirl and turbulence, aiding in the atomization process. This nozzle is compact, mechanically simple, and well-suited for applications where consistent spray at a fixed pressure is required. It generates relatively larger droplets compared to air-assisted designs, which makes it more reliant on fluid flow rate and pressure for effective cooling.

The SU22B nozzle features a stainless-steel construction and operates on a two-fluid atomization principle, where pressurized air is used to shear and break up the liquid jet at the nozzle exit. This results in much finer droplets and better dispersion. The nozzle has separate inlets for air and liquid, allowing independent control over both parameters. This type of nozzle is especially effective at low liquid flow rates, where the presence of air helps to enhance spray uniformity and surface coverage. In this study, the air pressure was maintained constant across tests to isolate the effect of fluid properties and flow rate. The SU22B nozzle is particularly useful in applications requiring fine atomization and uniform cooling over a larger area.

A temperature control bath manufactured by Sub-Zero was employed to maintain the desired fluid inlet temperature for the spray system. The bath operates over a broad temperature range of -25°C to +200°C, making it suitable for both sub-ambient and elevated temperature experiments. It is equipped with a circulation pump that delivers a consistent flow rate of 8 litres per minute, ensuring uniform temperature distribution throughout the fluid path. The system offers temperature stability within ±0.5°C, which is critical for minimizing thermal fluctuations during spray cooling experiments. Precise thermal regulation is achieved through an integrated PID (Proportional-Integral-Derivative) control system, allowing for accurate and stable temperature control throughout the duration of the tests.

3.2 UNCERTAINTY ANALYSIS

An Emerson Micro Motion F-Series Coriolis mass flowmeter was employed for precise measurement of fluid mass flow rates. Renowned for its accuracy and reliability, the F-Series provides liquid flow measurement accuracy up to $\pm 0.10\%$. To ensure experimental repeatability and statistical confidence, each test case was conducted three times.

Temperature measurements were obtained using calibrated thermocouples with an estimated uncertainty of $\pm 1^{\circ}$ C. The heat flux field estimation, derived from infrared thermal mapping, exhibited a maximum uncertainty of approximately $\pm 7.05\%$, accounting for both IR camera calibration and emissivity correction.

For droplet sizing and velocity, a Phase Doppler Particle Analyzer (PDPA) by Artium Inc. was utilized. The droplet diameter measurement uncertainty is $\pm 0.5 \mu m$ or $\pm 0.5 \%$ of the full range (whichever is greater), and the size resolution falls within the same bounds. Velocity measurements using PDPA are accurate to $\pm 0.1\%$ of the measured value.

The high-speed shadowgraphy system, used for visualizing droplet morphology and spray cone characteristics, introduces uncertainties primarily from image resolution and frame

timing. Based on system calibration and lighting consistency, the estimated uncertainty in droplet diameter measurement from image post-processing is around $\pm 2-3\%$, while velocity estimation (derived from displacement-time analysis) carries an uncertainty of $\pm 5\%$.

For infrared thermography, an IR camera with known spectral sensitivity and calibration was used. Considering factors such as surface emissivity, ambient reflections, and camera resolution, the uncertainty in temperature profiling is estimated at $\pm 2\%$, and the derived heat flux estimation maintains uncertainty within $\pm 7-8\%$.

3.3 SPRAY ANALYSIS AND THERMAL IMAGING METHODOLOGY

3.3.1 Thermophysical Comparison of Cooling Fluids

Table 3.3 gives insights about comparative analysis of deionized (DI) water and Thermasolv IM6, focusing on their thermophysical properties and suitability for electronic spray cooling applications, revealing the strengths and trade-offs of each fluid. DI water exhibits excellent thermal properties, including a high specific heat capacity (4182 J/kg·K), high thermal conductivity (0.6 W/m·K), and an exceptionally high latent heat of vaporization (2260 kJ/kg). These characteristics make it highly effective for both single-phase and phase-change cooling. However, its primary limitations for electronic applications arise from its electrical conductivity, which poses a risk of short-circuiting in the event of leakage. Additionally, its high surface tension (72 mN/m) and greater viscosity (1.002 mPa·s) hinder its wettability and atomization quality, particularly in fine spray applications.

In contrast, Thermasolv IM6 is a specially engineered dielectric fluid designed for the immersion and spray cooling of electronic components. Although it has a boiling point of 47 °C, low latent heat (93 kJ/kg), and lower specific heat capacity (1044 J/kg·K), which might initially make it seem thermally inferior to water, it has several advantageous properties. Its high liquid density (1600 kg/m³), low surface tension (11.4)

Table 3.3: Thermophysical properties Comparison of DI Water and Thermasolv IM6 for electronic cooling.

Property	DI Water	Thermasolv IM6	Relevance in Electronic Cooling
Dielectric Strength	Very low (conductive)	>35 kV/mm	Thermasolv allows direct contact with electronics; DI water cannot.
Global Warming Potential (GWP)	0	<20	Thermasolv is environmentally safe due to ultra-low GWP.
Boiling Point (°C)	~100	~47	Lower boiling point enables rapid phase change for IM6.
Specific Heat Capacity (J/g·K)	~4.18	~1.044	DI water stores more sensible heat per gram.
Latent Heat of Vaporization (kJ/kg)	~2260	~93	Water absorbs more energy during evaporation.
Thermal Conductivity (W/m·K)	~0.6	~0.110	Water provides better heat spreading on the surface.
Viscosity at 25°C (mPa·s)	~0.89	~0.59	Lower viscosity of IM6 improves spray atomization.
Density (kg/m³)	~997	~1600	IM6 is denser; may impact droplet dynamics and momentum.
Electrical Conductivity	High	Very low	IM6 avoids the risk of short-circuiting in electronic systems.
Surface Tension (mN/m)	~72.8	~11.4	Lower surface tension of IM6 aids in spreading over surfaces.

mN/m), and significantly lower dynamic viscosity (0.576 mPa·s) enhance atomization, film spreading, and surface interaction. These features, combined with its high dielectric strength (79 kV) and very low global warming potential (GWP = 20), make Thermasolv a safer and more sustainable option for direct spray or immersion cooling in high-density electronic systems. Its low vapor pressure (35 kPa @ 20 °C) also promotes explosive evaporation and improved cooling near its boiling point, especially under pulsed or

intermittent spray conditions.

In summary, while DI water is more efficient in terms of raw thermal capacity, Thermasolv IM6 offers distinct advantages for electronic cooling, including safe dielectric behavior, reliable two-phase performance, compatibility with sensitive components, and environmentally friendly properties. These qualities make Thermasolv an ideal working fluid for modern thermal management in compact, high-power electronics where direct contact cooling is essential.

3.3.2 Laser-Based Droplet Characterization Using PDPA

The characteristics of droplets, such as diameter, velocity, and flux, depend mainly on the pressure difference across a nozzle, the thermophysical properties of the working fluid, and the nozzle characteristics, such as orifice diameter and spray angle, atomizing mechanism. The characteristics of droplets are explained as follows: The Sauter Mean Diameter (SMD), abbreviated as D_{32} , refers to the average droplet size in spray. It refers to the diameter of a droplet with the same volume-to-surface area ratio as the entire spray. The mathematical definition is as follows:

$$SMD = \frac{\sum n_i d_i^3}{\sum n_i d_i^2}$$
 (3.1)

In this equation, d_i represents the diameter of each droplet and n_i represents the number of droplets of that size. SMD is particularly effective in spray cooling, as heat transfer is determined not only by droplet size but also by the surface area accessible for evaporation and convection. Smaller droplets with a higher surface area-to-volume ratio can improve heat transfer. The Phase Doppler Particle Analyzer (PDPA) is a laser-based, non-intrusive tool used to measure droplet size and velocity in sprays. Spray cooling heat transfer performance is heavily influenced by droplet velocity, an important physical characteristic. The quantity of energy exchange between the target surface and the working fluid is determined mostly by droplet motion and properties. Droplet velocity is significantly dependent on nozzle differential pressure, nozzle features, and the coolant's

thermophysical parameters. In spray cooling, higher droplet velocity generally means more momentum, which enhances the droplet's ability to reach the hot surface, penetrate the boundary layer, and spread effectively. This improves convective and evaporative heat transfer. The velocity is influenced by: Nozzle differential pressure means that higher pressure results in higher velocity. Nozzle geometry (orifice size, internal structure), Coolant thermos-physical properties (density, viscosity, surface tension).

The PDPA system determines droplet velocity based on the Doppler shift of scattered laser light. As a droplet moves through the measurement volume (where two laser beams intersect), it scatters light that shifts in frequency due to its motion.

$$V = \frac{\Delta x}{\Delta t} = \frac{\lambda}{2\sin\left(\frac{\theta}{2}\right)} \cdot f_D \tag{3.2}$$

V is the droplet velocity component in the direction perpendicular to the interference fringes, where:

- *v* is the particle velocity,
- λ is the laser wavelength,
- θ is the angle between the laser beams,
- f_D is the Doppler frequency shift.

The PDPA typically gives velocity components in three orthogonal directions (1D, 2D, or 3D, depending on system setup), which can then be resolved into resultant velocities. By combining droplet size (e.g., SMD) and velocity data from PDPA with IR Thermography, we gained an understanding of spray behavior and how it impacts spray cooling effectiveness. Droplets encounter a variety of forces before reaching the heated surface, including drag, buoyancy, and gravity, which impact their velocity. These forces have a substantial impact on droplet velocity, which in turn affects spray cooling performance. The extent to which each force acts is determined by characteristics such as the droplet's size, starting velocity, distance covered (droplet path length), and the surrounding environment within the spray chamber. Understanding how these forces

Interact is critical for estimating droplet behaviour and optimizing spray cooling efficiency. The spray characterization in this study was carried out using a three-dimensional Phase Doppler Particle Analyzer (PDPA) system from Artium Technologies, USA, shown in Fig.3.5. This system comprises two laser transmitters and a receiver unit. The transmitters emit three pairs of laser beams, which intersect at a common region known as the probe volume, creating an interference pattern. One of the transmitters includes two channels with different laser wavelengths (561 nm and 532 nm), used to measure droplet size and axial velocity components in the Z–R plane. The receiver unit captures the scattered light from droplets passing through the probe volume. The droplet size is calculated from the phase difference between Doppler burst signals received by adjacent detectors, while droplet velocity is obtained by multiplying the fringe spacing by the burst frequency of the scattered signal. Since the transmitter is positioned at a 30° angle relative to the receiver, a coordinate transformation is applied to convert the measured data into cylindrical components of velocity (Z, R, θ).

The nozzle is mounted on a threaded rod to adjust its height, and the PDPA system is fixed on a three-dimensional traverse stage, enabling precise movement across axial and radial locations.

To thoroughly understand the spray characteristics, such as droplet diameter and velocity across the atomized region, a detailed and spatially distributed measurement approach was employed. Measurements were performed using a Phase Doppler Particle Analyzer (PDPA) system, with the intersecting laser beams positioned at axial distances of 10 mm, 20 mm, and 30 mm downstream from the nozzle exit. At each of these vertical cross-sections, three strategically selected measurement points were used to capture a comprehensive profile of the spray characteristics. These included one point along the central axis of the spray cone and two additional points located symmetrically near the periphery of the spray envelope.

This tri-point sampling strategy was designed to accurately represent both the core and

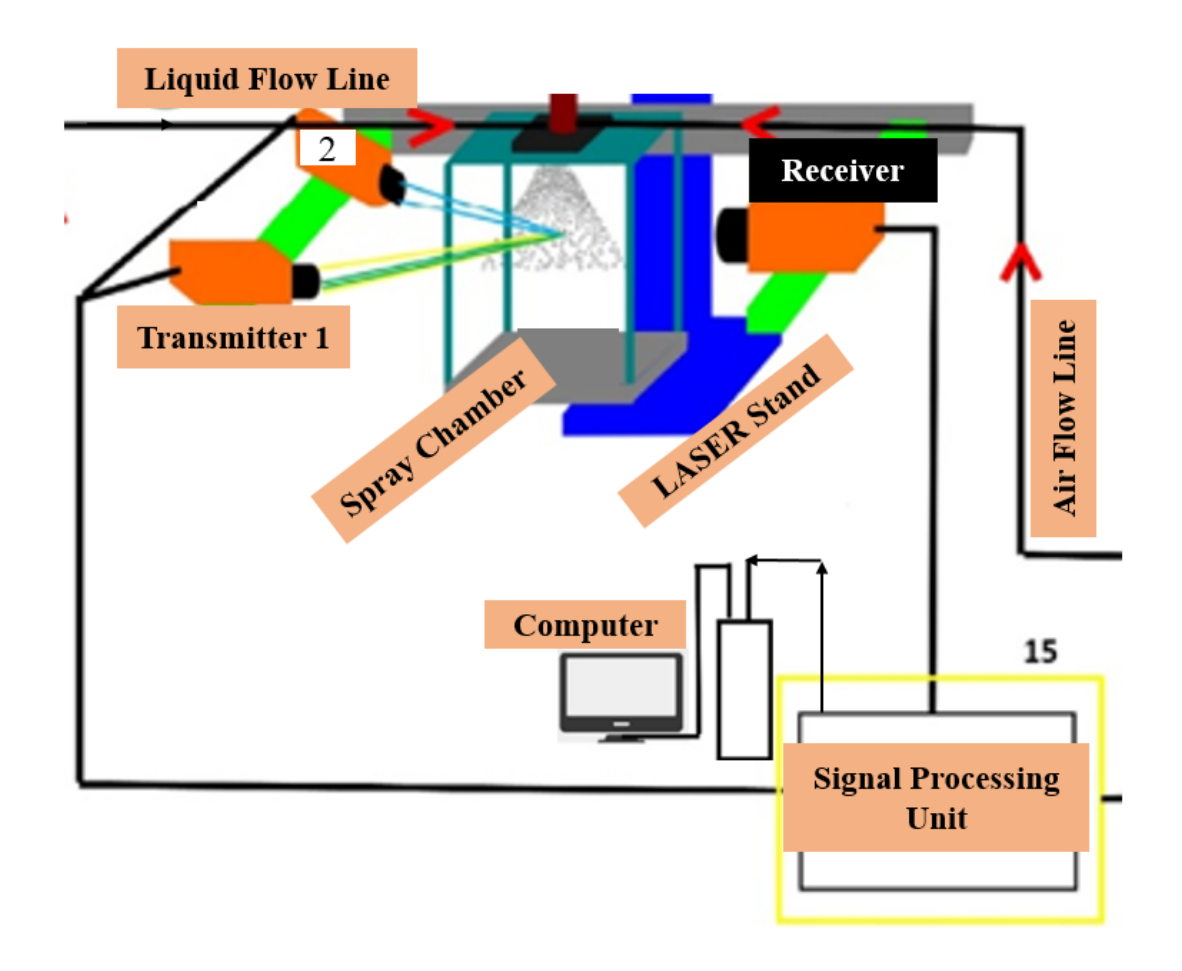


Figure 3.5: PDPA setup in NCCRD, IIT MADRAS

peripheral regions of the spray field. The central axis region, typically characterized by higher droplet velocities and more uniform size distributions, reflects the primary trajectory of atomized fluid, where breakup mechanisms are more stable and consistent. In contrast, the outer edge regions experience enhanced turbulence, secondary breakup, and droplet coalescence phenomena, particularly pronounced in Air-Assisted Nozzle (AAN) configurations due to higher shear forces and mixing instabilities.

By including both axial and radial positions in the data acquisition, this approach enables a detailed spatial resolution of spray dynamics, offering critical insights into the influence of nozzle type and operating parameters on droplet behavior and overall spray uniformity—key factors that directly affect heat transfer efficiency in spray cooling

applications.

By repeating this measurement configuration at different heights (10 mm, 20 mm, and 30 mm from the nozzle), a comprehensive view of the axial evolution of spray characteristics was obtained. This allowed for a clear understanding of how droplet dynamics change as the spray propagates downstream. For instance, at closer distances (e.g.10 mm), larger primary droplets and higher velocities were typically observed due to the initial momentum and minimal air interaction. At farther planes (20 mm and 30 mm), droplets showed reduced velocity and size variations as a result of air drag, evaporation, and secondary atomization.

This multi-point, multi-plane measurement approach enabled the generation of droplet size and velocity distribution profiles, which are critical for assessing the effectiveness of the spray cooling system. It also helped differentiate between the behaviors of Pressure Atomized (PAN) and Air-Assisted (AAN) sprays, revealing how nozzle design and operating conditions influence spatial uniformity, droplet breakup, and ultimately, the heat transfer efficiency on the target surface.

By repeating this measurement configuration at different heights (10 mm, 20 mm, and 30 mm from the nozzle), a comprehensive view of the axial evolution of spray characteristics was obtained. This allowed for a clear understanding of how droplet dynamics change as the spray propagates downstream. For instance, at closer distances (e.g.10mm), larger primary droplets and higher velocities were typically observed due to the initial momentum and minimal air interaction. At farther planes (20 mm and 30 mm), droplets showed reduced velocity and size variations as a result of air drag, evaporation, and secondary atomization.

This multi-point, multi-plane measurement approach enabled the generation of droplet size and velocity distribution profiles, which are critical for assessing the effectiveness of the spray cooling system. It also helped differentiate between the behaviors of Pressure

Atomized (PAN) and Air-Assisted (AAN) sprays, revealing how nozzle design and operating conditions influence spatial uniformity, droplet breakup, and ultimately, the heat transfer efficiency on the target surface.

At most locations, around 40,000 droplets were recorded with over 90% validation, whereas in sparse regions near the nozzle centerline, around 21,000 droplets were captured to ensure statistical convergence. This detailed mapping provides a comprehensive understanding of the spray dynamics and their influence on spray cooling performance.

3.3.3 High Speed Imaging(HSI) Shadowgraphy-Based Assessment for Spray Nozzle Cone Angle Assessment

High-speed imaging (HSI) was utilized to capture the rapid evolution of spray dynamics with high temporal and spatial accuracy. The experimental setup incorporated a Phantom VEO340 high-speed camera paired with a Navitar Zoom 6000 lens, enabling variable magnification and precise focusing on the spray region. The camera was operated at a resolution of 640×480 pixels with a frame rate of 8400 frames per second (fps), which proved sufficient to resolve fast transient events such as droplet formation, ligament stretching, secondary breakup, and droplet motion.

To achieve high-contrast visualization using the shadowgraphy technique, a uniform and continuous light source was essential. A 150-watt Wipro LED was employed to illuminate the area of interest. This high-intensity LED was selected for its capability to deliver a bright and collimated light beam suitable for capturing sharp droplet silhouettes against the background. Importantly, the LED was connected to a direct current (DC) power supply, which provided stable and uninterrupted illumination. This configuration was deliberately chosen to eliminate the flickering and intensity fluctuations typically associated with alternating current (AC) power sources. The use of DC power ensures constant light output, thereby enhancing image clarity and reducing motion blur or artifacts caused by inconsistent lighting. As a result, the shadowgraphy images exhibited improved contrast and detail, facilitating accurate qualitative and quantitative analysis of the spray behavior.

Shadowgraphy imaging was employed to visualize the spray structure generated by the PAN (Pressure Atomized Nozzle), revealing an expanded full-cone pattern with increased surface coverage as the flow rate of deionized (DI) water increased. This enhanced spray uniformity and density are beneficial for thermal management applications. Additionally, shadowgraphy was used to estimate Sauter Mean Diameter (SMD) and droplet velocity, and these measurements closely matched those obtained from Phase Doppler Particle Analyzer (PDPA), validating the effectiveness of the shadowgraphy technique for droplet characterization.

From figure 3.6, increasing the flow rate of deionized (DI) water significantly affects the spray behavior of both the Plain Atomizing Nozzle (PAN) and the Air Atomizing Nozzle (AAN). For the PAN nozzle, raising the flow rate leads to a notable increase in the spray angle, which moves from approximately 45° at lower flow rates to about 54° at higher flow rates. This widening of the spray angle results in a larger coverage area of the full-cone spray pattern, indicating that more fluid is being distributed over a broader surface. Similarly, from figure 3.7, the AAN nozzle shows a comparable response; its spray angle increases from around 14° to 21° as the flow rate is elevated to 0.2 liters per minute (L/min). This expansion in the spray angle suggests that atomization quality improves with the increased fluid supply, allowing for better dispersion of droplets.

Overall, the trends observed for both nozzle types highlight the direct impact of flow rate on spray characteristics, which is crucial for optimizing cooling performance and ensuring uniformity in thermal management applications.

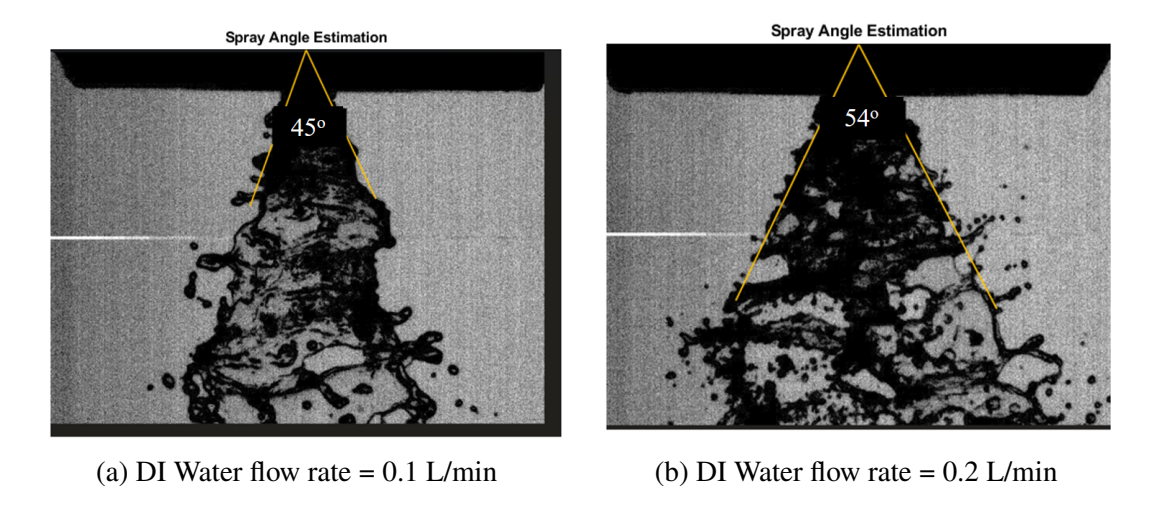


Figure 3.6: Spray Angle Measurement with HSI(PAN)

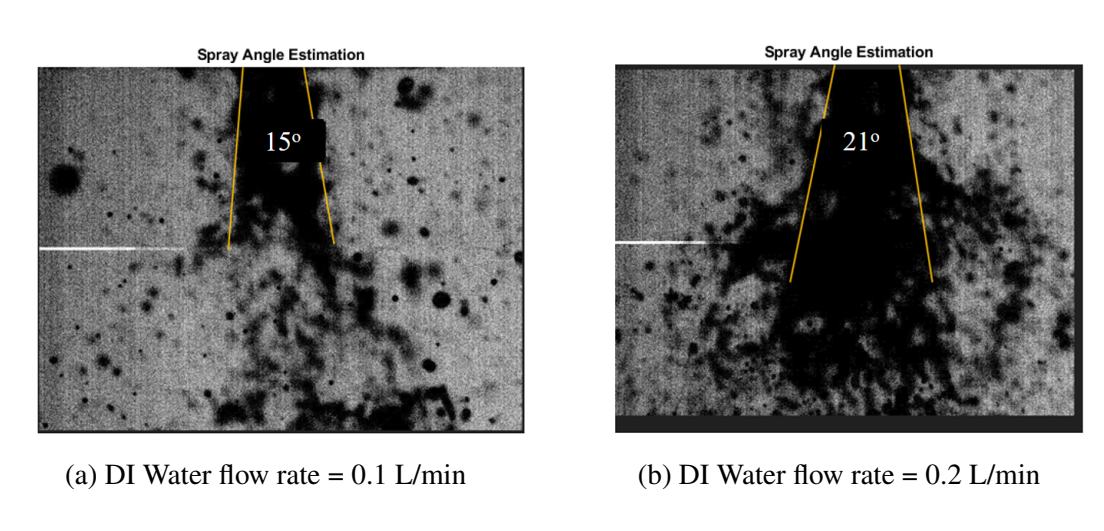


Figure 3.7: Spray Angle Measurement with HSI(AAN)

3.4 DROPLET MORPHOLOGY AND MOTION ASSESSMENT BY SHADOWGRAPHY

Figure 3.8 illustrates the methodology employed to extract accurate droplet size and velocity data using high-speed imaging (HSI). A comprehensive, multi-stage image processing framework was developed and implemented in MATLAB to ensure reliable droplet characterization. The workflow initiates with pre-processing, where each raw frame is subjected to a 3×3 median filter to suppress high-frequency noise and enhance the definition of droplet edges without blurring critical features.

Following noise reduction, the images undergo binarization through adaptive thresholding, which dynamically adjusts the threshold value across localized regions. This method proves significantly more robust than global thresholding, particularly under conditions of spatially varying illumination—a common challenge at downstream imaging planes due to light attenuation or angle-induced gradients. Adaptive thresholding thus ensures consistent and accurate delineation of droplet boundaries across the entire frame.

Subsequently, a morphological closing operation is applied to the binary images to bridge small gaps between segmented regions and eliminate minor voids within droplet projections. This step enhances droplet contour integrity, enabling more accurate size estimation. The refined binary images then serve as the basis for droplet feature extraction, including centroid tracking and equivalent diameter computation, which are essential for velocity estimation when paired with inter-frame displacement analysis. Once pre-processed, the binary images are analyzed using MATLAB's bwboundaries function, which identifies and outlines each connected object. To isolate true droplets, components are filtered based on geometric properties. Specifically, features with an area exceeding 600 µm are discarded as they likely represent ligaments or overlapping artifacts. Similarly, elements with high eccentricity and aspect ratios, indicative of elongated shapes, are removed to avoid misclassifications. For near-nozzle regions, where overlapping artifacts are more frequent, a child contour removal algorithm is incorporated to eliminate nested or falsely identified elements.

To quantify droplet size, only droplets detected in the final one-fifth portion of the image frame are considered, as this region minimizes the influence of partial or merging droplets. Their diameters are extracted to create distribution histograms for each flow rate and imaging plane. In the final step, droplet velocity is determined by tracking the displacement of droplets across successive frames using two computational methods. A comparative assessment of these methods validates the consistency of the approach. This methodology not only enables estimation of Sauter Mean Diameter (SMD) and average velocity but also provides detailed insights into the droplet field characteristics

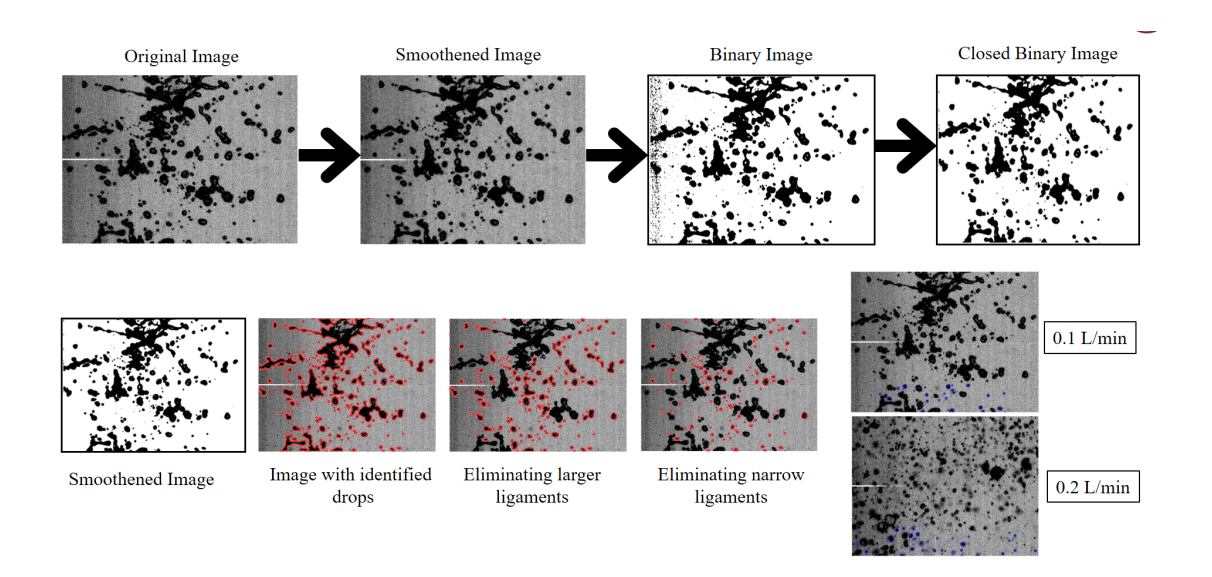


Figure 3.8: HSI Image processing for Diameter with MATLAB

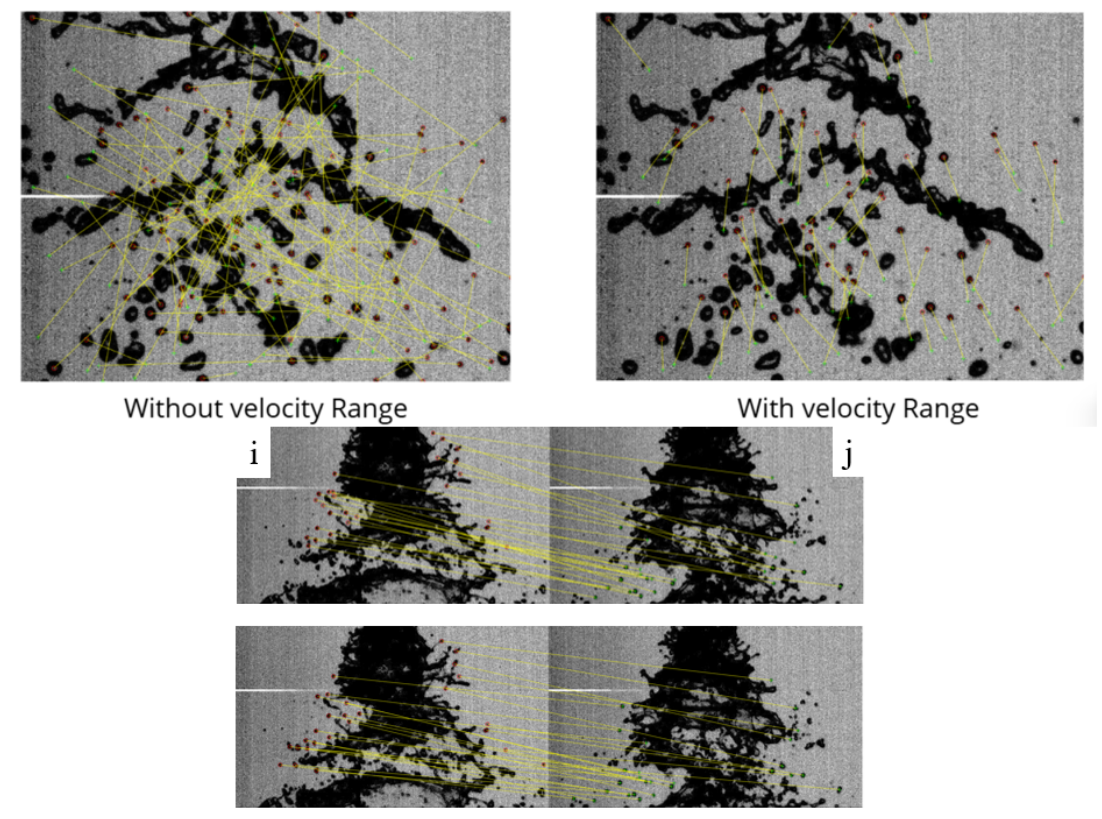
necessary for evaluating spray cooling effectiveness.

In Fig.3.9, to accurately calculate the velocity of droplets in spray flow, a robust tracking method was implemented using droplet area-based matching across consecutive image frames. The foundation of this technique lies in the use of a similarity metric that quantifies how closely two droplets match based on their projected area.

Specifically, the similarity between a droplet in frame 1 and a droplet in frame 2 is computed using an exponential decay function of their absolute area difference. This results in a similarity score ranging from 0 to 1, where 1 represents a perfect match and values closer to 0 reflect poor matches. These scores populate a similarity matrix, with each element indicating the strength of the match between a droplet pair across the two frames. i.e similarity matrix is then constructed, where each element (i, j) represents the similarity between droplet i in frame 1 and droplet j in frame 2. To ensure robust and accurate matching, a mutual best-match criterion is applied. A droplet i in frame 1 is matched with droplet j in frame 2 only if:

- Droplet j is the best match for droplet i
- Droplet i is also the best match for droplet j.

To enhance accuracy, a mutual best-match criterion is applied. This means a droplet in



Mutual best match condition ensures accurate droplet pairing between consecutive frames

Figure 3.9: HSI Image processing for Velocity with MaTlaB

the first frame is only considered a valid match with a droplet in the second frame if both droplets are each other's best possible match based on the similarity matrix. This reciprocal validation helps to eliminate ambiguous or incorrect matches, particularly in dense sprays where many droplets may have similar areas.

Additionally, to prevent mismatches due to noise or extreme movement, a velocity filter is introduced. This filter only allows matches that result in displacement vectors within a physically reasonable range for both x and y directions. The inclusion of this velocity constraint is especially important at higher flow rates, where droplets move faster and the risk of false positives increases. However, a careful balance is needed, allowing too broad a velocity window may compromise accuracy, while a narrow one might exclude valid matches. By combining mutual best area similarity with velocity-based filtering, this method provides a reliable framework for droplet tracking and velocity estimation in

high-speed spray imaging.

3.5 IR CAMERA-BASED TEMPERATURE AND HEAT FLUX ESTIMATION

The first step is to calibrate the infrared camera at the required integration time (0.5 sec) and frame rate (1000 frames/s). The temperature data recorded from the infrared camera is smoothed to remove noise. The second step is to extract the heat flux field by performing pixel-wise energy balance on the heater foil temperature field. The illustration of energy balance at a pixel element for heat flux field is illustrated in Fig.3.10.

The second step is to extract the heat flux field by performing pixel-wise energy balance on the heater foil temperature field. The illustration of energy balance at a pixel element for the heat flux field is illustrated in Figure 3.11a and 3.11b. The application of energy balance to the pixel element gives Eq.3.3.

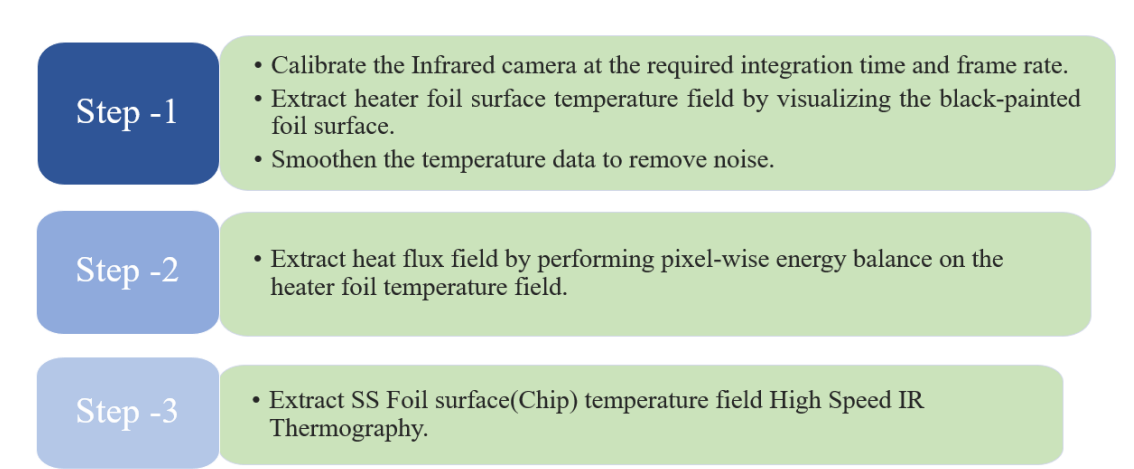
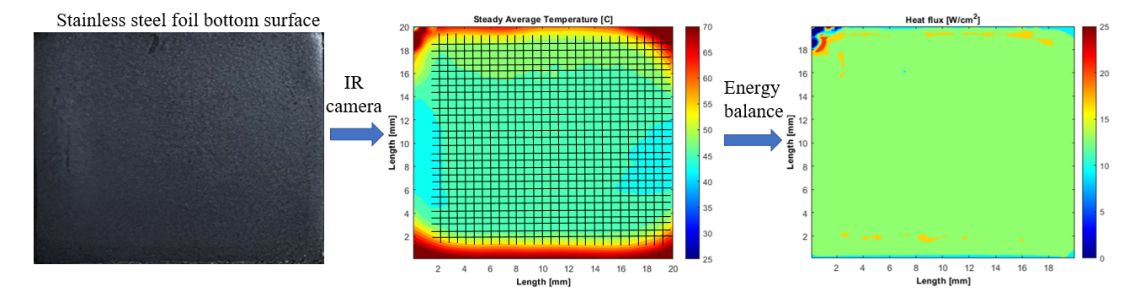


Figure 3.10: Outline of the experimental methodology for field measurements

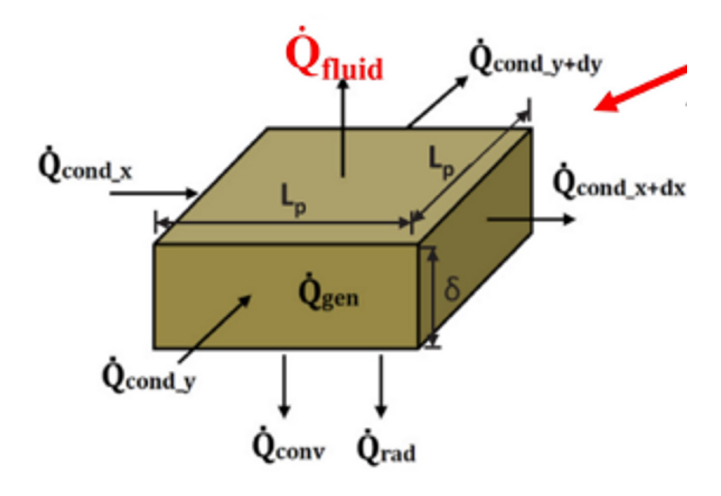
$$Q_{\text{stored}} = Q_{\text{gen}} + Q_{\text{cond}} - Q_{\text{rad}} - Q_{\text{conv}} - Q_{\text{fluid}}$$
(3.3)

where fluid heat transfer is represented as Q_{fluid} [W]. Thus,

$$Q_{\text{fluid}} = Q_{\text{gen}} + Q_{\text{cond}} - Q_{\text{rad}} - Q_{\text{conv}} - Q_{\text{stored}}$$
 (3.4)



(a) Foil Temperature and Heat Flux Extraction from IR Camera



(b) Pixel-wise Energy Balance on Foil

Figure 3.11: Illustration of energy balance at a pixel element for heat flux field.

The average fluid heat flux q_{fluid} is calculated using the pixel element's length L_p as given in Eq.3.5.

$$q_{\text{fluid}} = \frac{Q_{\text{fluid}}}{L_p^2} \tag{3.5}$$

The heat generated in the foil due to joule-heating, i.e., for passing the current through the foil, is given in Equ.3.6

$$Q_{\rm gen} = \frac{I^2 R V_p}{V_s} \tag{3.6}$$

where I is the current passing through the foil, V_p is the volume of the pixel element, V_s is the volume of the heater foil surface, and R is the resistance of the heater foil.

Table 3.4: Thermo-physical properties of SS-304 heater foil used in the current study.

Property	Value
Density	7900 kg/m^3
Thermal conductivity	16.3 W/mK
Electrical resistivity	2.5×10^{-6} Ohm-m
Specific heat capacity	500 kJ/kgK
Temperature coefficient of resistance	$17.8 \times 10^{-6} \text{ 1/K}$

The resistance of heater foil *R* is calculated using the Eq.3.7

$$R = \frac{\rho_s L_p \left(1 + \theta_s (T - T_\infty)\right)}{A_p} \tag{3.7}$$

where T is the temperature of pixel element, T_{∞} is the ambient temperature, L_p is the length of pixel element, $A_p = L_p \delta$ is the cross-sectional area of pixel element, ρ_s is the foil's electrical resistivity, and θ_s is the foil's temperature coefficient of resistance.

The properties of the heater foil are listed in Table 3.4. The effects of conduction perpendicular to the heater foil surface are minimal compared to the other directions because of the foil's negligible thickness (Schweizer (2010); Sielaff *et al.* (2014); Guggilla *et al.* (2020)).

Therefore, the heat transfer by conduction along the surface is considered and expressed as Eq.3.8.

$$Q_{\text{cond}} = (Q_{\text{cond}})_{\text{in}} - (Q_{\text{cond}})_{\text{out}}$$
(3.8)

Simplifying Eq.3.8 gives Eq.3.9

$$Q_{\text{cond}} = \frac{k_s A_p \left(T_{i+1,j} + T_{i-1,j} + T_{i,j+1} + T_{i,j-1} - 4T_{i,j} \right)}{L_p}$$
(3.9)

Where k_s is the foil's thermal conductivity. $T_{i,j}$ is the temperature of the element in consideration, and $T_{i-1,j}$, $T_{i+1,j}$, $T_{i,j-1}$, $T_{i,j+1}$ are the temperatures of adjacent pixel elements in corresponding directions. The bottom surface of the heater foil is painted black and subjected to high temperatures, so radiation heat transfer has to be considered.

The heat transfer due to radiation from the bottom surface of the heater foil is given by Equ. 3.10

$$Q_{\text{rad}} = \sigma \varepsilon L_p^2 \left(T_{i,j}^4 - T_{\infty}^4 \right) \tag{3.10}$$

where $\sigma(=5.67\times 10^{-8}\,\mathrm{W/m^2K^4})$ is the Stefan-Boltzmann constant, $\varepsilon=0.92$ is the emissivity of the black-painted heater foil surface, and T_∞ is the ambient temperature. The bottom surface of the heater foil is exposed to the ambient while visualized by the infrared camera. Therefore, natural convection currents are bound to develop eventually beneath the heater foil surface.

The heat transfer due to natural convection is given by Eq.3.11.

$$Q_{\text{conv}} = h_i L_p^2 \left(T_{i,j} - T_{\infty} \right) \tag{3.11}$$

where h_i is the heat transfer coefficient of natural convection and is given by Eq.3.12

$$h_i = \frac{0.27 \, Ra_i^{0.25}}{L} k_{\text{air}} \tag{3.12}$$

where Ra_i represents the Rayleigh number, with all properties evaluated at the film temperature, T_f .

$$T = \frac{T_{i,j} + T_{\infty}}{2} \tag{3.13}$$

The heat stored in the pixel element is given by Eq.3.14

$$Q_{\text{stored}} = \frac{m_s c(T_t - T_{t-1})}{\Delta t}$$
 (3.14)

where m_s is the pixel element's mass and c is the specific heat capacity. T_{t-1} and T_t are the pixel element's temperatures at the t-1 and t time intervals, respectively. At steady state, there is no significant change in temperature with time, so $T_{t-1} = T_t$ and

$$Q_{\text{stored}} = 0$$

A Matlab code is written to perform data processing and the energy balance on the temperature field of the heater foil surface that we get from the infrared camera. The energy balance on the heater foil's temperature gives the heat flux field. A MATLAB

code is written to perform data processing and the energy balance on the temperature field of the heater foil surface obtained from the infrared camera. The energy balance on the heater foil's temperature provides the heat flux field.

It is noted that $Q_{\rm stored}$ represents the change in energy of the surface due to cooling, and $Q_{\rm gen}$ is the heat generated by the DC power supply. Meanwhile, $Q_{\rm cond}$, $Q_{\rm rad}$, and $Q_{\rm con}$ correspond to the net conduction along the surface, radiation heat transfer, and convection heat transfer underneath the surface, respectively.

A MATLAB code is written to perform data processing and apply the energy balance to the temperature field of the heater foil surface obtained from the infrared camera.

CHAPTER 4

RESULTS: SPRAY CHARACTERIZATION

4.1 SPRAY CHARACTERIZATION OF DI WATER USING PRESSURE(PAN) AND AIR(AAN) ASSISTED NOZZLE

The droplet size distribution generated by spray nozzles plays a pivotal role in determining the overall efficiency of spray cooling systems. This is particularly evident when comparing the performance of Pressure Atomized Nozzles (PAN) and Air Atomized Nozzles (AAN), both operating with water at a flow rate of 0.2L/min.

In this study, droplet characterization using the Phase Doppler Particle Analyzer (PDPA) was conducted at multiple axial planes to assess spray behavior under different nozzle configurations—Pressure Atomizing Nozzle (PAN) and Air-Assisted Atomizing Nozzle (AAN). As illustrated in the figure 4.1, the measurement planes were strategically positioned at 10mm, 20mm, and 30mm below the nozzle exit to capture the spatial evolution of droplet size and velocity within the spray cone. These planes were selected to map the spray dynamics both near the nozzle and closer to the surface to analyze droplet breakup and velocity attenuation. By acquiring data along the central axis and at spray edges on each plane, a comprehensive three-point analysis was performed to evaluate the uniformity, atomization quality, and momentum distribution of the droplets. The final heat transfer experiments for both nozzle types were conducted with a fixed nozzle-to-surface distance(N-SD) of 20mm. This distance, marked as the target surface in the figure, represents the location of the heated foil where IR-based thermal mapping and surface cooling performance were assessed. Characterizing the spray behavior leading up to this surface helped establish a strong correlation between droplet dynamics and heat transfer outcomes. Figure 4.2a illustrates the Droplet Diameter distribution for PAN, where droplet sizes range broadly from 80µm to 360µm, with a mean value of 169.18µm. This wide distribution reflects a non-uniform spray field, which can lead

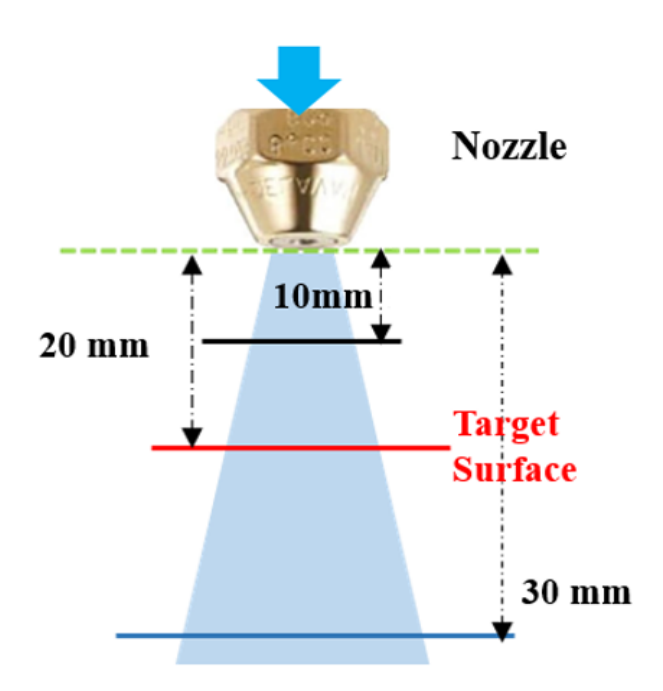


Figure 4.1: PDPA measurement planes for droplet characterization at 10 mm, 20 mm, and 30 mm from nozzle outlet.

to uneven surface wetting and localized cooling inefficiencies. In contrast, Figure 4.2b presents the Droplet diameter distribution for AAN under the same flow rate. Here, the droplets range from 20µm to 280µm with a notably lower SMD of 116.6µm. This indicates a finer and more homogeneous spray structure, which is advantageous for enhancing heat transfer performance.

The superior atomization observed in the AAN is primarily driven by the additional energy imparted by the assistive air stream. This air supply increases the relative velocity between the air and liquid phases, thereby inducing greater shear forces at the nozzle exit. As a result, the liquid jet breaks into much smaller and more uniformly distributed droplets. Smaller droplets possess a higher surface area-to-volume ratio, which facilitates more efficient heat removal through both convection and evaporation when they impinge on the heated surface. Moreover, a narrower droplet size distribution ensures more consistent surface coverage, contributing to improved thermal uniformity and overall cooling effectiveness.

In essence, the comparative analysis of these PDPA results underscores the advantage

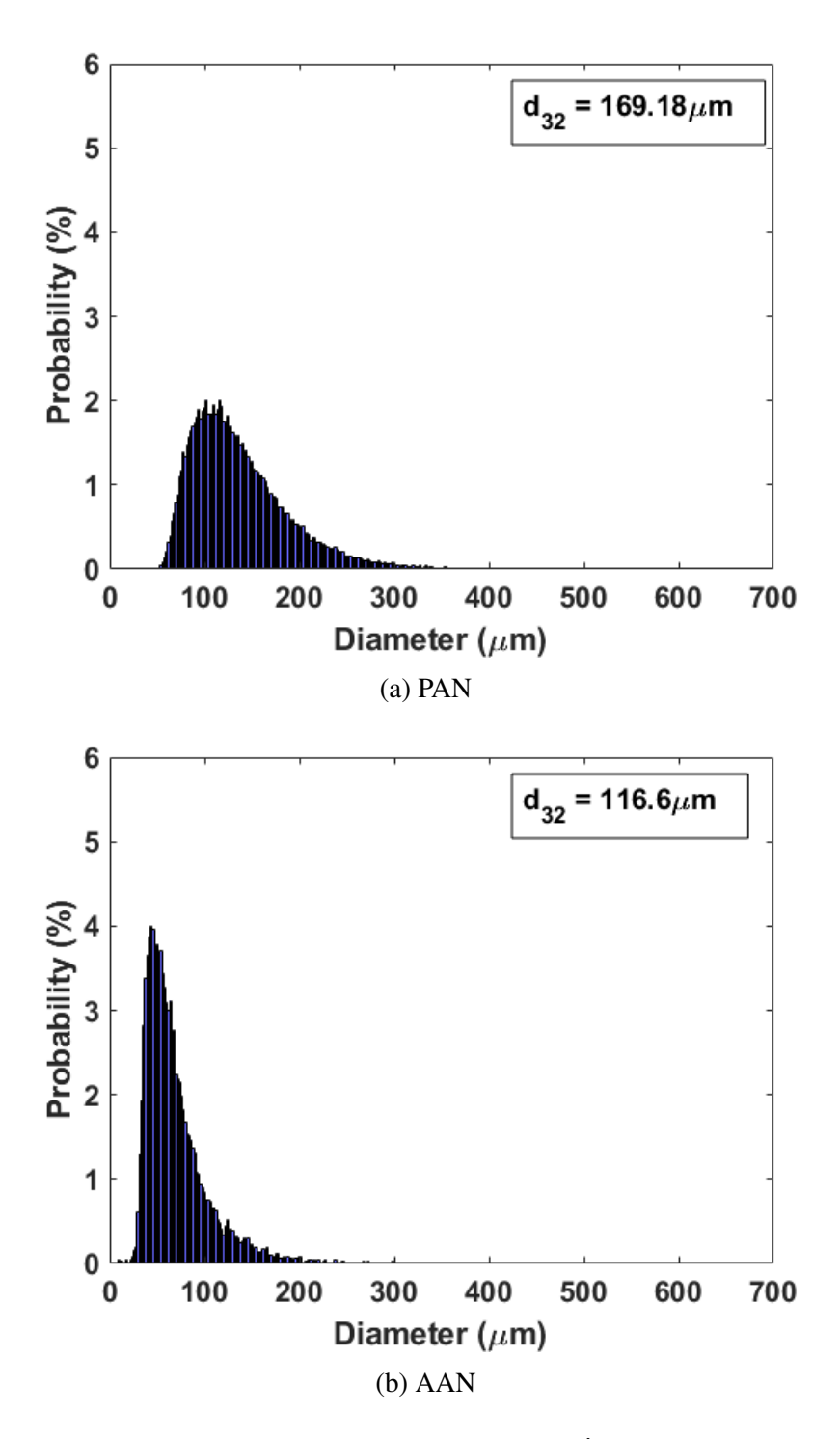


Figure 4.2: Diameter Distribution of DI Water spray at $\dot{V} = 0.2$ L/min at 20 mm plane

of using AAN over PAN in high heat flux spray cooling scenarios. The AAN's ability to produce finer, faster droplets not only promotes rapid surface wetting and energy transfer but also minimizes the risk of hot spots due to patchy spray distribution. Therefore,

the enhanced droplet breakup and resulting uniformity from air-assisted atomization make AAN a more suitable choice for applications demanding high-performance thermal management, such as in electronics cooling or power-intensive devices.

The velocity distribution of droplets is a critical parameter in spray cooling, as it directly influences the momentum transfer, surface wetting, and ultimately the efficiency of heat removal. Figures 4.3a and 4.3b depict the droplet velocity distribution measured using Phase Doppler Particle Anemometry (PDPA) at a volumetric flow rate of 0.2L/min and a nozzle-to-surface distance (NSD) of 20mm for the Pressure Atomized Nozzle (PAN) and the Air Atomized Nozzle (AAN), respectively. The velocity distribution for PAN is relatively narrow, ranging from 10 to 18m/s, with an average droplet velocity of 12m/s. This indicates limited velocity variability and lower overall droplet momentum, which could lead to less aggressive impingement on the surface and less effective penetration through the thermal boundary layer. As a result, cooling tends to be more localized, and the uniformity of heat removal may suffer under high heat flux conditions.

In contrast, the AAN exhibits a much broader velocity distribution, extending from 9 to 38m/s, and achieves a significantly higher average velocity of 18.97m/s. This pronounced difference can be attributed to the enhanced atomization mechanism in AAN, where a high-velocity assistive air stream is used to shear the liquid jet, resulting in finer droplets and imparting additional momentum. The presence of faster droplets allows for deeper penetration into the thermal boundary layer, stronger convective heat transfer, and more dynamic surface interactions such as splashing and spreading, which contribute to more uniform and efficient cooling. The broader velocity range also suggests a more heterogeneous droplet population, which can enhance surface rewetting and mitigate the formation of dry spots during high heat flux operation.

Overall, the superior velocity characteristics of AAN, including higher average speed and wider distribution, highlight its capability to deliver enhanced thermal performance in spray cooling applications. This makes AAN particularly suitable for electronic cooling systems requiring high heat flux removal with reliable temperature control and spatial

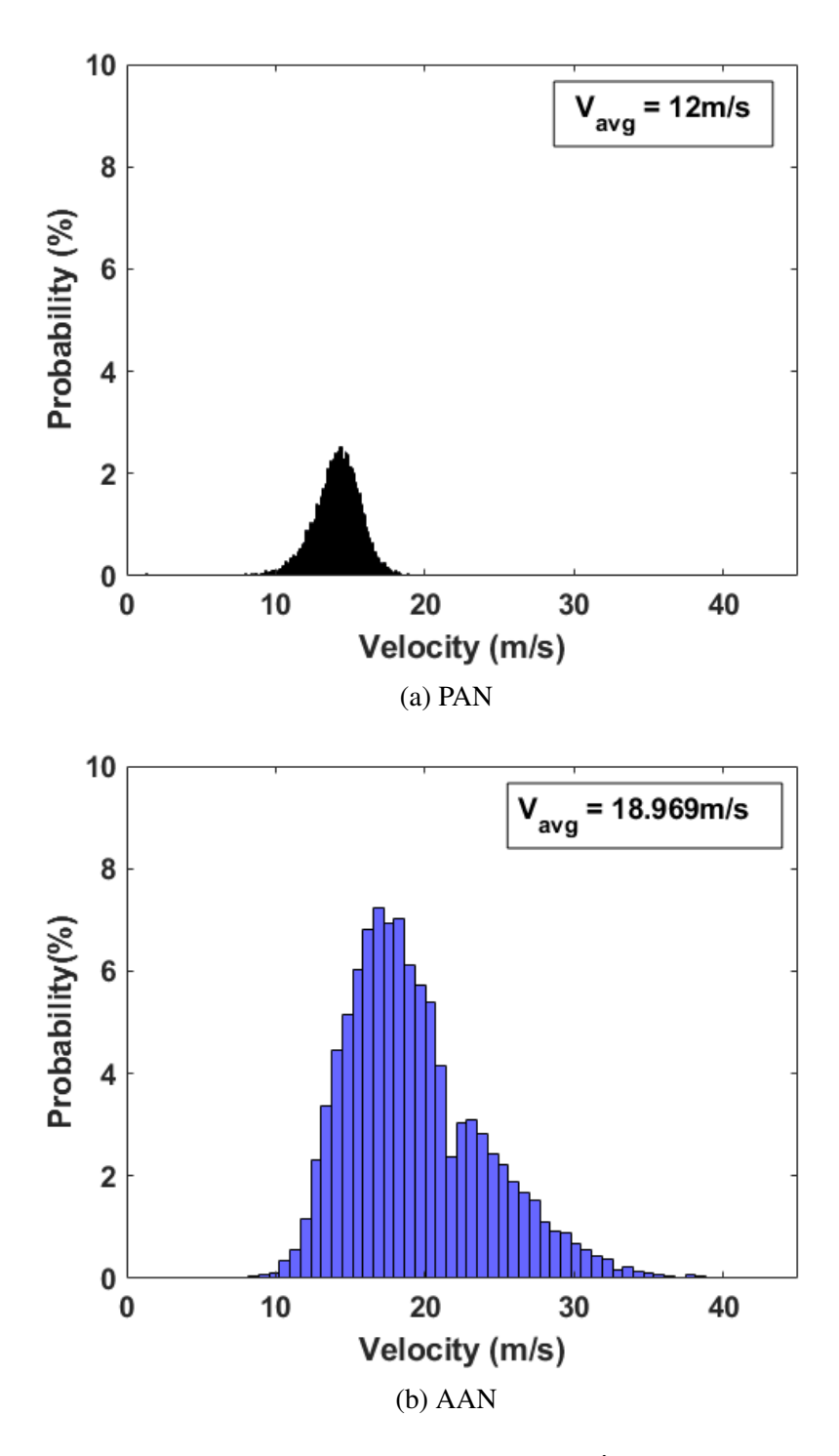


Figure 4.3: Velocity Distribution of DI Water spray at $\dot{V} = 0.2$ L/min at 20 mm Plane

uniformity. When compared under the same flow rate and experimental conditions, the AAN outperforms PAN by offering more aggressive and distributed droplet impingement, leading to better surface coverage and greater cooling effectiveness.

The Sauter Mean Diameter (SMD) of spray droplets plays a vital role in governing the overall heat transfer efficiency in spray cooling applications, as it directly affects surface wetting, evaporation rate, and uniformity of cooling.

Figure 4.4a illustrates the variation of SMD with respect to flow rate for a Pressure Atomized Nozzle (PAN) at two vertical planes, 10 mm and 20 mm from the nozzle exit. As seen, increasing the flow rate from 0.1 L/min to 0.2 L/min results in a consistent reduction in SMD at both measurement locations. Specifically, the SMD at the 10 mm plane drops from approximately 190 μm to 170 μm, while at the 20 mm plane, it reduces more significantly from 243 μm to around 185 μm. This downward trend signifies enhanced primary and secondary atomization processes at higher flow rates, which promote more efficient droplet breakup. The closer 10 mm plane, influenced by high shear regions due to turbulence and nozzle geometry, supports aggressive breakup into finer droplets. On the other hand, although the spray continues to evolve downstream, the 20 mm plane shows slightly larger droplets due to coalescence effects and reduced breakup energy further away from the nozzle.

In contrast, Figure 4.4b represents the SMD trends for Air Atomized Nozzles (AAN) under the same flow rate conditions. The AAN consistently produces finer droplets compared to PAN, with SMD decreasing from about 155 µm to 120 µm at the 10 mm and 20 mm planes as the flow rate increases. This finer droplet generation is a result of the increased atomization due to the helpful high-velocity air stream in AAN, which increases the shearing stresses at the liquid-air interface. Smaller droplets have a greater surface area-to-volume ratio, which increases the potential for convective heat transfer and evaporation when they impinge on a heated surface. The improved droplet uniformity and reduced diameter also contribute to better wetting characteristics and more uniform cooling, especially critical in high heat flux electronic applications.

In summary, higher flow rates enhance the spray atomization regardless of nozzle type, but AAN significantly outperforms PAN in generating finer droplets with lower SMD across both measurement planes. These findings reinforce the importance of nozzle

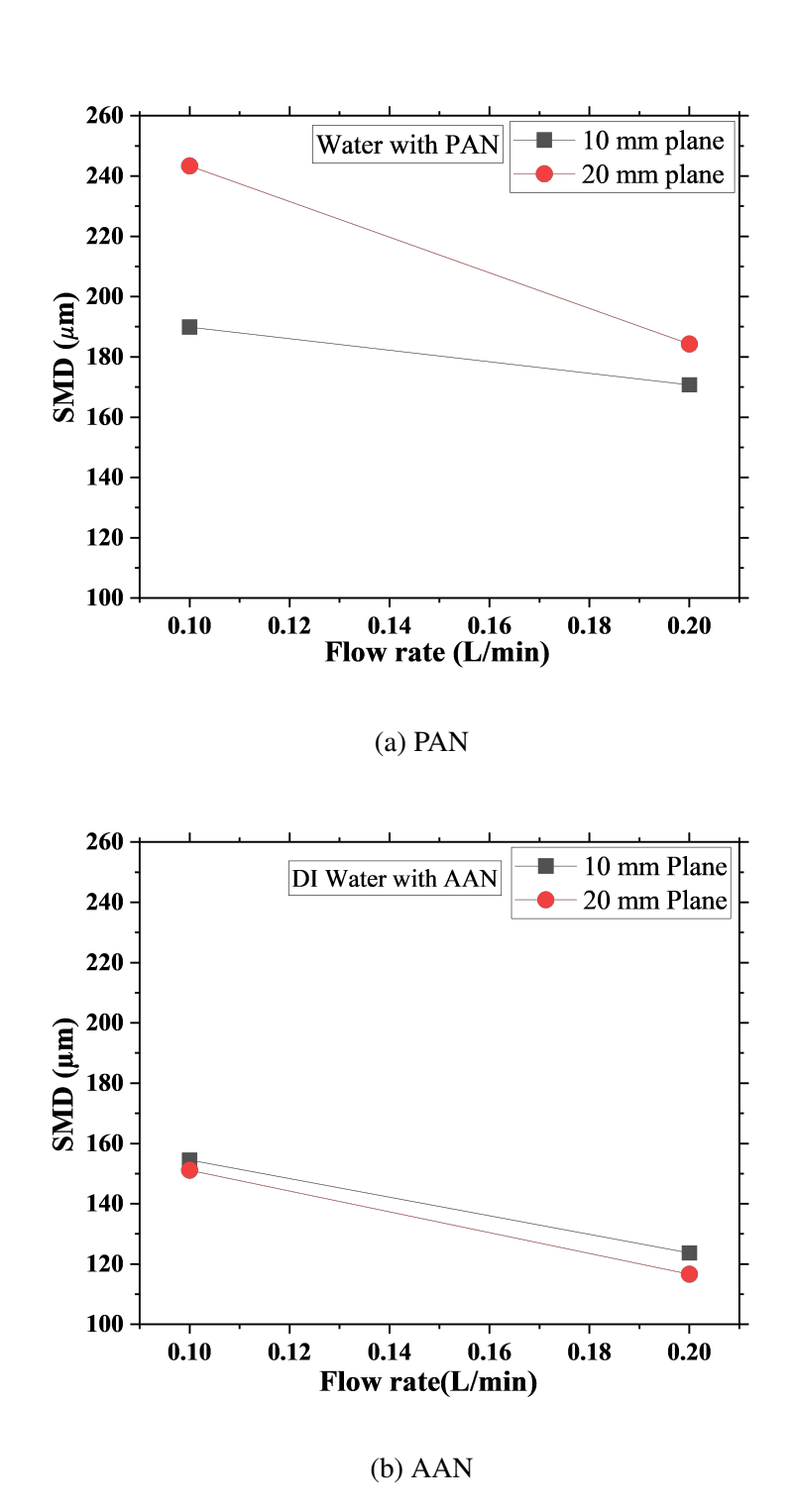


Figure 4.4: Variation of SMD with flow rate at N-SD = 10, 20, and 30 mm for DI water

selection and flow optimization in designing effective thermal management systems for next-generation electronic devices.

The average velocity of droplets plays a crucial role in determining the effectiveness of

spray cooling, as it directly influences the impingement momentum, liquid film dynamics, and surface wetting efficiency. Figure 4.5a presents the variation in average droplet velocity with respect to flow rate for a Pressure Atomized Nozzle (PAN) measured at two axial planes (10 mm and 20 mm). A consistent upward trend is observed, where velocity increases from approximately 7 m/s at 0.1 L/min to over 12 m/s at 0.2 L/min. This indicates that higher liquid flow rates enhance the spray's kinetic energy, thereby improving the impingement force on the heated surface. Stronger impingement promotes thinner liquid films and better surface wetting, which together contribute to increased convective heat transfer. The minimal difference in velocity between the two planes suggests that the spray momentum is well maintained with negligible dissipation over the short distance from the nozzle to the measurement plane.

In contrast, Figure 4.5b shows the average velocity variation for Air Atomized Nozzles (AAN) at the same conditions. As expected, AAN consistently delivers higher droplet velocities compared to PAN due to the added momentum from the assistive air stream. At a flow rate of 0.2 L/min, velocities reach up to 23.8 m/s at the 10 mm plane, highlighting the powerful atomization and acceleration enabled by the air assistance. The 10 mm plane, located in the spray core region, shows significant turbulence and droplet-air interactions that lead to high-velocity peaks, whereas the 20 mm plane experiences some velocity decay but still maintains strong momentum due to evenly distributed atomization. The elevated velocities in AAN sprays enable more effective surface impingement and enhanced shear-driven evaporation, all of which are beneficial for high heat flux removal in thermal management systems.

These trends emphasize the importance of nozzle type and flow rate in controlling droplet momentum, which is a key parameter in optimizing spray cooling performance. AAN systems, through the combination of high velocity and fine droplet generation, demonstrate superior thermal control capability, making them more suitable for compact, high-power electronic cooling applications. Including both velocity and droplet size behavior in the analysis allows for a comprehensive understanding of how spray characteristics impact

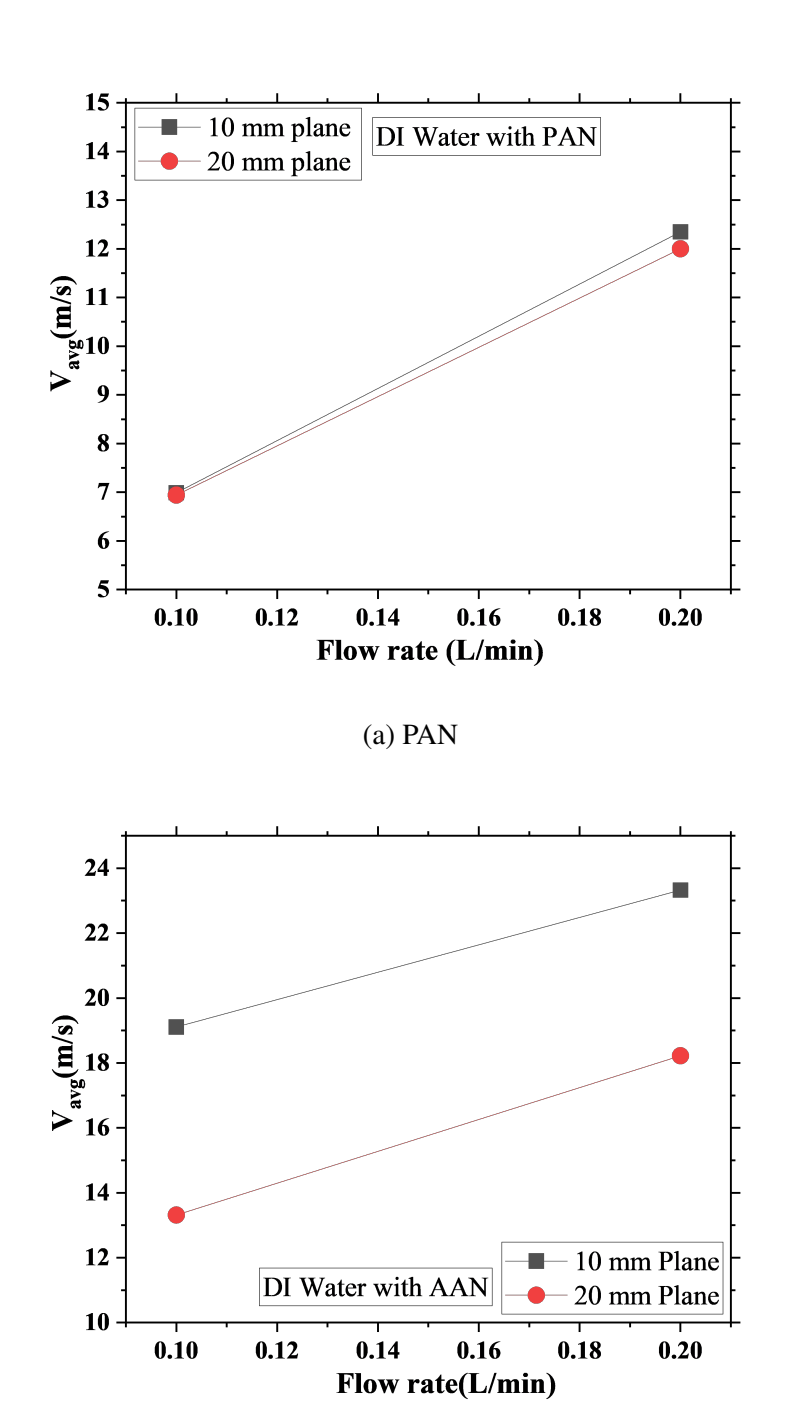


Figure 4.5: Variation of average droplet velocity with flow rate at N-SD = 10, 20, and 30 mm for DI water

(b) AAN

heat transfer at different spatial locations.

4.2 SPRAY CHARACTERIZATION OF THERMASOLV USING PRESSURE(PAN) AND AIR(AAN) ASSISTED NOZZLE

At a flow rate of 0.2L/min, the droplet diameter distribution for Thermasolv sprayed using both PAN and AAN nozzles reveals key differences in atomization behavior and its influence on cooling performance. In Figure 4.6a, the distribution for PAN shows a narrower spread of droplet sizes with an SMD of 142.1µm, suggesting a more uniform spray pattern. This is typical of pressure-based atomization, where the liquid is forced through a nozzle under high pressure, creating relatively consistent droplets. Such uniformity supports stable surface coverage, which is beneficial for achieving predictable and steady heat removal, particularly through convection and partial evaporation. In contrast, Figure 4.6b shows the droplet distribution for AAN, where Thermasolv is atomized with the aid of high-speed air. The result is a broader range of droplet sizes and a slightly higher SMD of 166.2µm. This wider distribution is due to the additional shearing forces introduced by the assistive air stream, which promotes more aggressive breakup of the liquid jet. The outcome is a mix of fine and larger droplets that can enhance both surface wetting and evaporation. Smaller droplets offer higher surface area, enabling faster heat absorption and quicker evaporation, while the larger ones contribute to sustained liquid film formation for continued convective cooling. When compared to deionized (DI) water under the same conditions, Thermasolv demonstrates a notably different droplet breakup behavior. Due to its higher surface tension and dynamic viscosity, water resists atomization, resulting in slightly larger droplets under similar flow conditions. However, water also has higher specific heat and thermal conductivity, making it effective for heat absorption, even though it evaporates more

In contrast, Thermasolv, with its lower surface tension and viscosity, breaks up more easily into finer droplets and creates a more stable spray profile, especially in air-assisted atomization (AAN) applications. Additionally, its higher density gives the droplets greater momentum, enhancing their ability to penetrate the spray field and effectively

quickly in high-temperature zones.

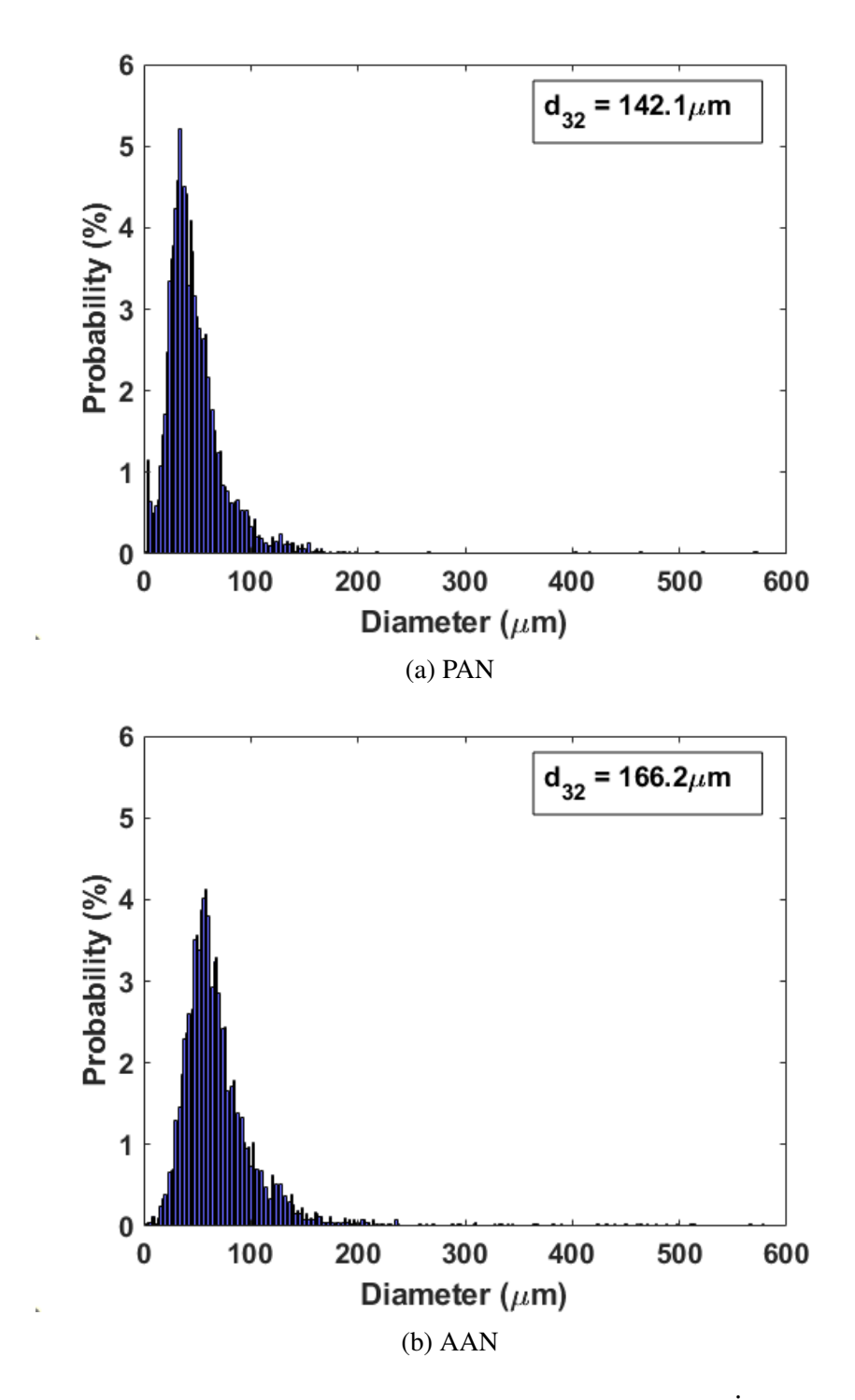


Figure 4.6: Droplet Diameter Distribution of Thermasolv spray at $\dot{V}=0.2$ L/min at 20 mm Plane

reach the heated surface, particularly in PAN sprays.

Figure 4.7a velocity distribution plots for Thermasolv sprayed through PAN and

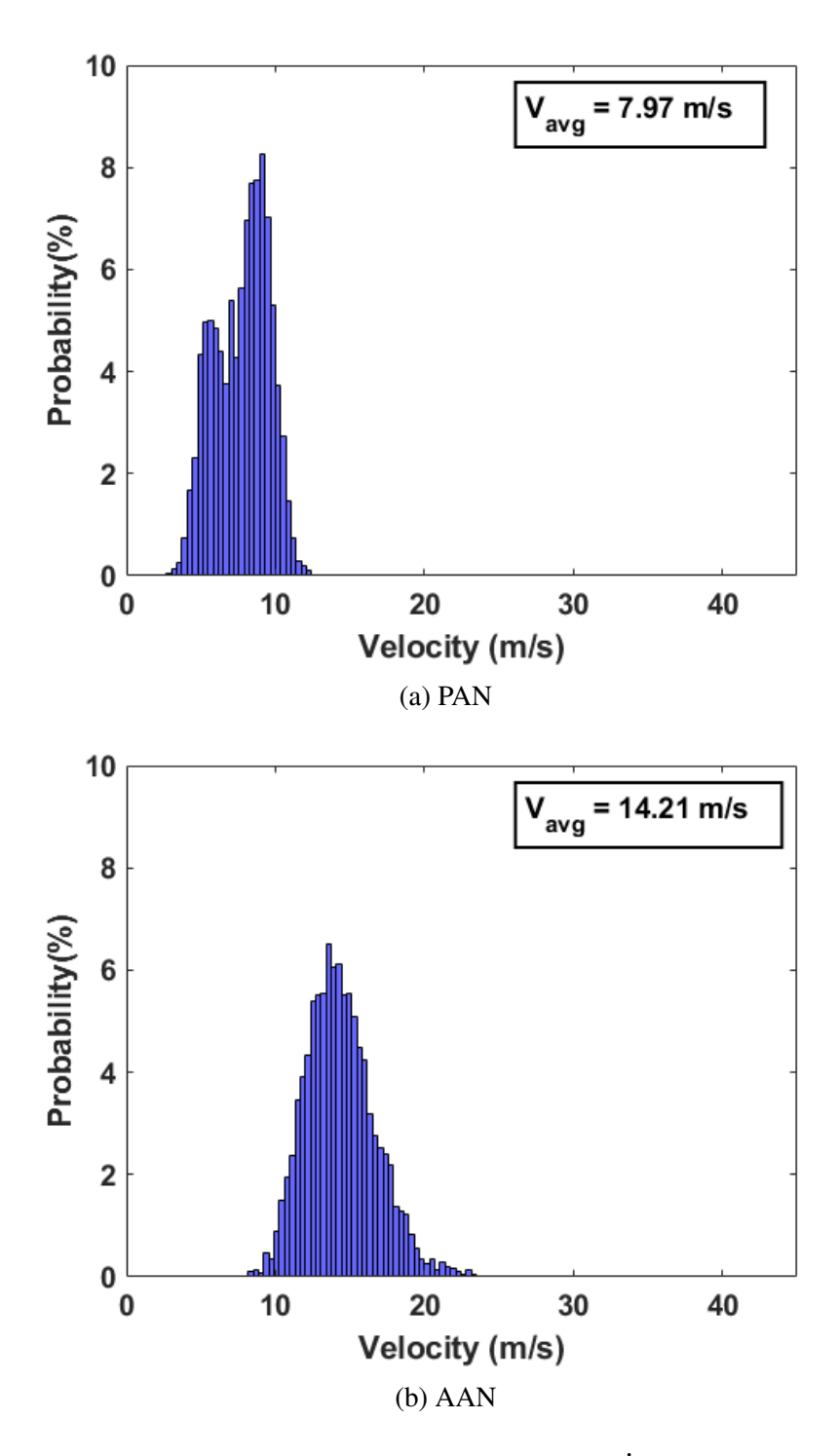


Figure 4.7: Velocity distribution of Thermasolv spray at a $\dot{V} = 0.2$ L/min at 20mm Plane

AAN at 0.2L/min reveal insightful differences in spray dynamics and their implications for heat transfer performance. In the left plot, PAN exhibits a narrower distribution centered around an average droplet velocity of 7.97m/s, with most droplets falling in the

3.2–12.4m/s range. This indicates a relatively uniform spray but with limited momentum, as the atomization relies solely on the internal liquid pressure. Lower droplet velocities can lead to weaker surface impingement, reducing the droplet spreading and lowering convective heat transfer efficiency.

In contrast, the right plot Figure 4.7b for AAN shows a much broader velocity spread from 9.7m/s to as high as 22.6m/s, with an average velocity of 14.21m/s. This wider and higher velocity distribution is due to the air-assist mechanism, where the high-speed air shears the liquid jet and significantly enhances droplet breakup and acceleration. The greater droplet momentum in AAN allows for more forceful impingement on the heated surface, improving surface wetting and liquid film formation. This, in turn, enhances both convective and evaporative heat transfer processes. Higher velocities also reduce the boundary layer resistance and enable better thermal penetration into the surface, making AAN particularly effective in handling high heat flux regions.

When compared to DI water under similar conditions, Thermasolv behaves slightly differently due to its higher density and lower viscosity. These properties contribute to higher inertia of the droplets, allowing them to maintain momentum over longer distances and enhancing cooling even at moderate velocities. In DI water, finer droplets tend to decelerate faster and may evaporate or deflect before reaching the surface, which can affect heat transfer consistency. Thermasolv droplets, driven by air in AAN, retain their energy better, contributing to more robust and sustained cooling across the surface.

Overall, the higher velocity and wider distribution of droplets with AAN and Thermasolv enable more intense and spatially uniform cooling, making this combination advantageous for applications requiring efficient thermal management of high-performance electronic components.

The variation in Sauter Mean Diameter (SMD) for Thermasolv at different axial planes, as shown in Figures 4.8a and 4.8b, provides important insights into spray behavior and its implications for heat transfer. In both PAN and AAN configurations, SMD increases

consistently with higher flow rates at all measured distances from the nozzle (10 mm, 20 mm, and 30 mm). This trend can be explained by the increased inertia of the liquid at higher flow rates, which resists aerodynamic shear and delays secondary breakup, especially in regions further downstream. As a result, larger droplets tend to persist longer before fragmenting into finer particles. This phenomenon is particularly evident in the AAN case, where the SMD increase at 30 mm is more prominent, likely due to coalescence effects and weakened atomization force with distance from the nozzle. From a heat transfer perspective, the presence of larger droplets at higher flow rates and longer distances can reduce the surface wetting efficiency and the rate of droplet evaporation. Finer droplets, typically formed closer to the nozzle or under stronger atomization conditions, provide higher surface area-to-volume ratios, which promote faster evaporation and more efficient convective heat transfer. Therefore, regions with lower SMD, especially near 20 mm in PAN and AAN cases, are expected to offer better thermal performance due to improved surface coverage and enhanced phase change activity.

Furthermore, Thermasolv's lower surface tension and viscosity compared to water play a critical role in achieving finer atomization, even under identical operational conditions. These properties lead to quicker destabilization of the liquid jet and facilitate droplet breakup into smaller sizes. Consequently, Thermasolv generally produces smaller droplets than water at all tested planes, which contributes to better thermal interaction with the heated surface and more effective heat dissipation. Overall, the observed SMD behavior with Thermasolv aligns with its superior cooling performance, especially when used with air-assist nozzles like AAN that support aggressive droplet breakup. This makes Thermasolv a favorable candidate for applications requiring uniform and efficient heat removal from high-performance electronic components.

The velocity behavior of Thermasolv droplets under varying flow rates and nozzle types, as depicted in Figure 4.9a and 4.9b, plays a crucial role in determining heat transfer efficiency during spray cooling. In the case of the pressure atomized nozzle (PAN), the

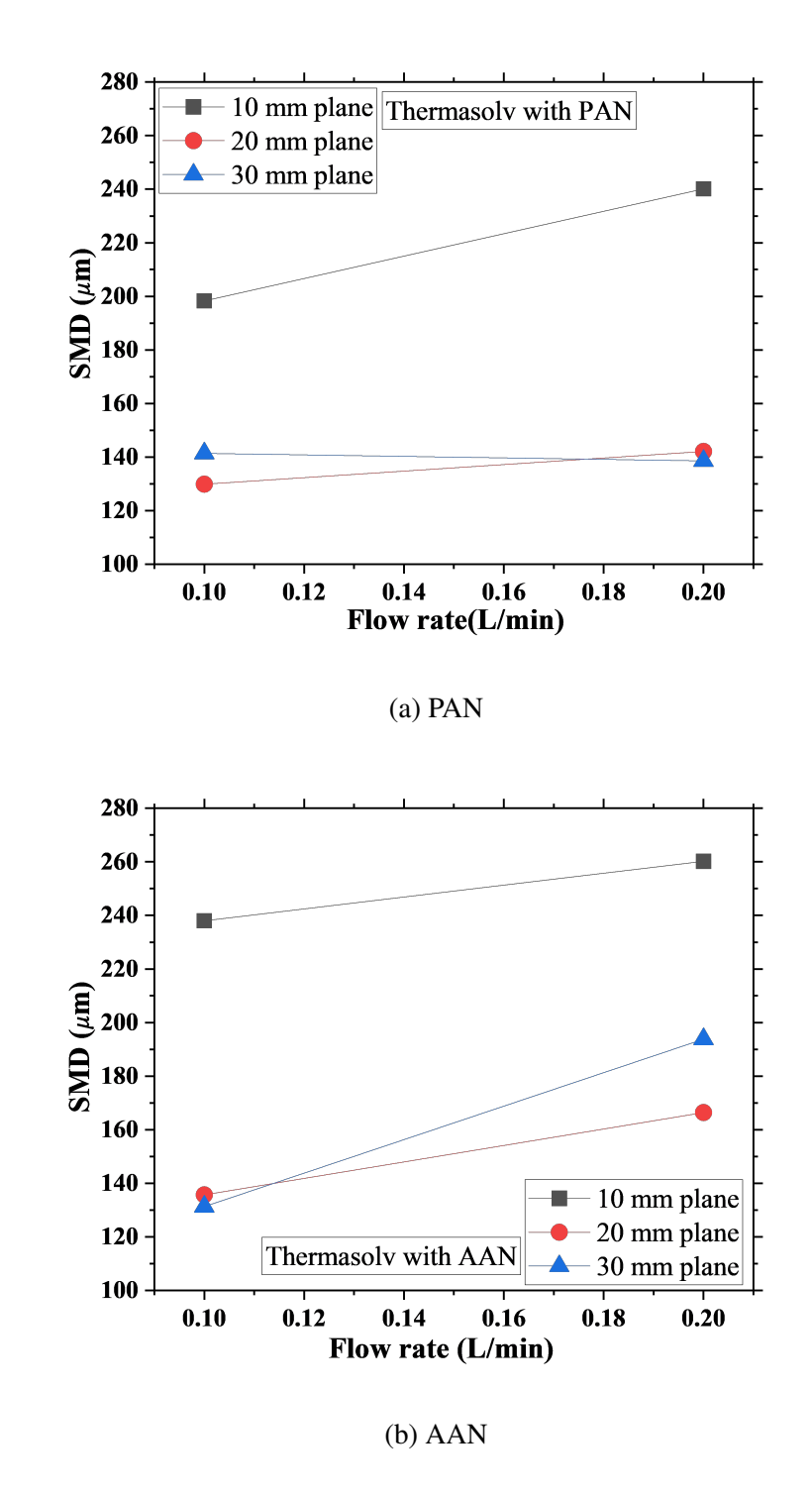


Figure 4.8: Variation of SMD with flow rate at N-SD = 10, 20, and 30 mm for Thermasolv.

average droplet velocity increases steadily with flow rate across all axial planes. This is due to the nature of PAN systems, where higher liquid flow rates generate greater injection pressure, thereby imparting more kinetic energy to the droplets. As the velocity

rises, droplets strike the heated surface with increased momentum, promoting stronger impingement, thinner liquid films, and improved surface wetting conditions that enhance convective heat transfer and support localized evaporative cooling. In contrast, the air atomized nozzle (AAN) exhibits an opposite trend, where the average droplet velocity decreases as the liquid flow rate increases. This is primarily because the air-to-liquid mass flow ratio declines when the air supply remains constant while liquid flow increases. As a result, the energy available for aerodynamic shear is spread thinner across a larger volume of fluid, leading to weaker atomization and lower exit velocities. This reduction in droplet velocity translates to diminished momentum and weaker impingement forces, which can compromise liquid film dynamics and delay evaporation. However, at lower flow rates (0.1 L/min), AAN delivers exceptionally high droplet velocities that are up to 20 m/s, helping in intense cooling through rapid droplet spreading and vigorous evaporation. These conditions are ideal for scenarios requiring fast heat removal and uniform surface cooling, especially with a fluid like Thermasoly that favors fine breakup due to its lower viscosity and surface tension.

Overall, this analysis highlights that the choice of atomizer and flow rate must be carefully balanced based on thermal requirements. PAN performs better at higher flow rates due to its pressure-driven mechanism, while AAN is more effective at lower flow rates when high air-to-liquid ratios enable better atomization and droplet momentum. This interplay between droplet velocity and fluid dynamics ultimately governs the cooling potential of the spray system and should be considered in the design of advanced thermal management solutions.

4.3 COMPARATIVE ANALYSIS OF DROPLET SIZE AND VELOCITY USING PDPA AND HIGH SPEED IMAGING(HSI)

The comparative evaluation of Sauter Mean Diameter (SMD) and droplet velocity using both Phase Doppler Particle Analyzer (PDPA) and High-Speed Imaging (HSI) methods, as illustrated in Figure 4.10a and 4.10b, provides critical insights into measurement

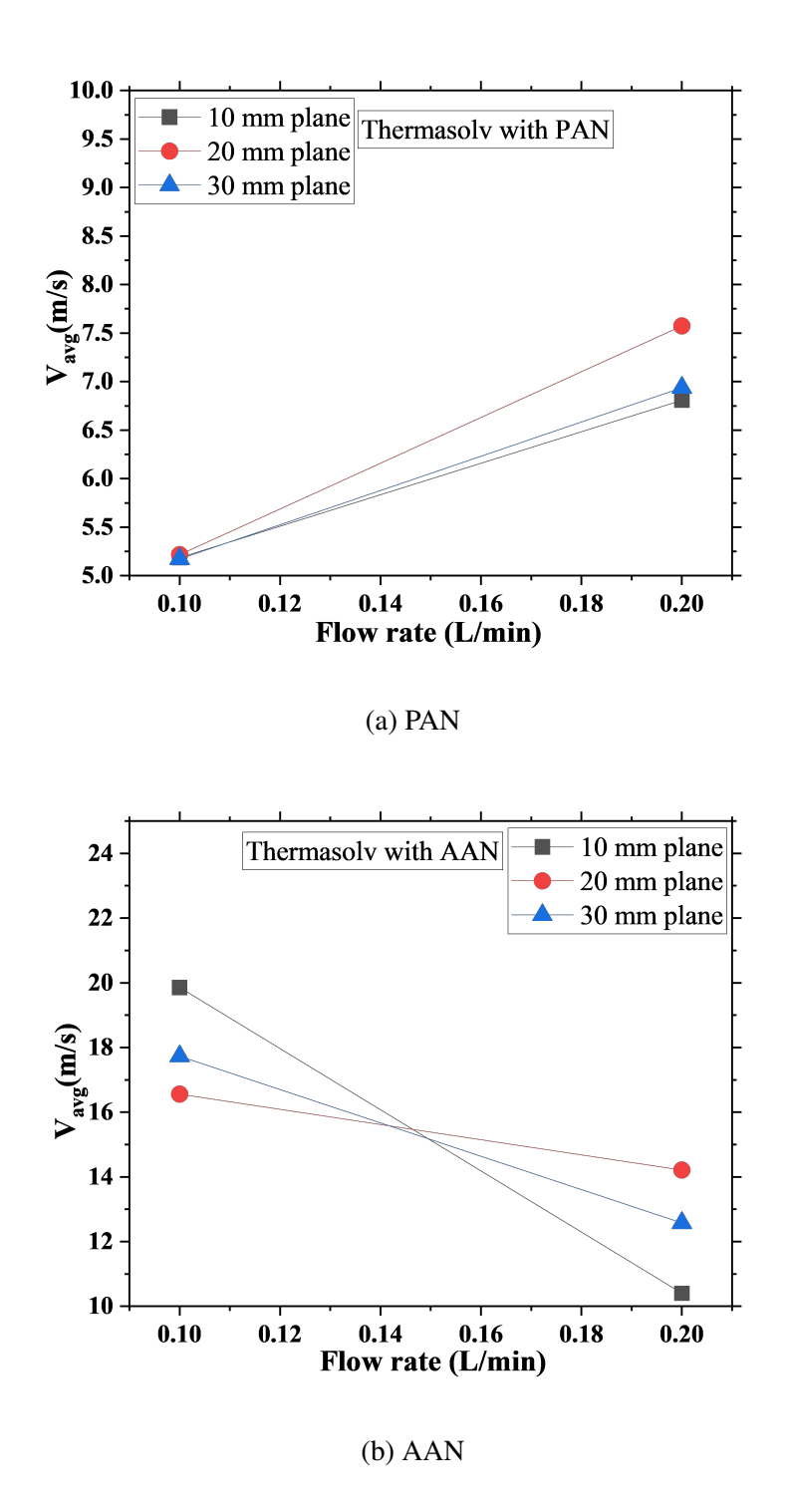
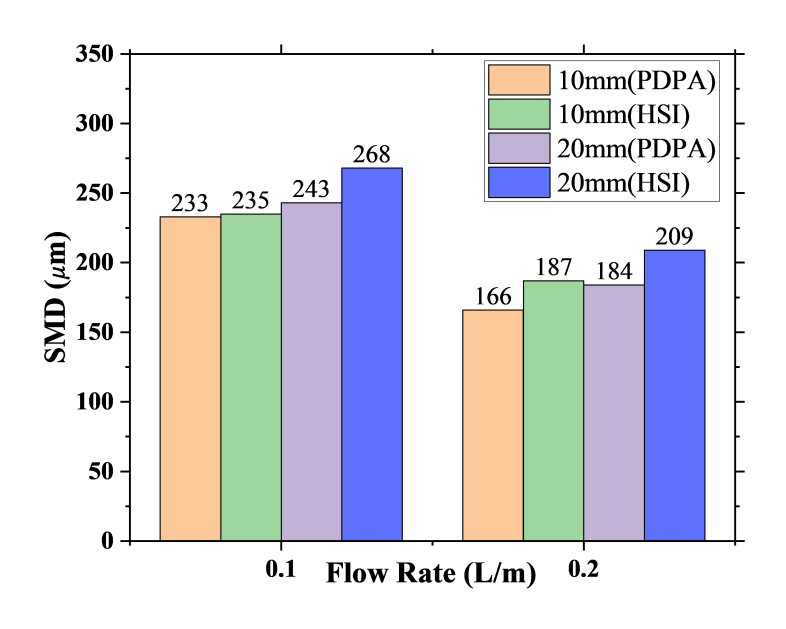


Figure 4.9: Variation of average droplet velocity with flow rate at N-SD = 10, 20, and 30 mm for Thermasolv.

reliability and the physical behavior of DI water sprays under varying flow conditions. In Figure 4.9(a), the SMD values obtained through both techniques exhibit good agreement,

with only slight deviations. PDPA consistently records slightly smaller droplet sizes than HSI, primarily because PDPA's laser-based technique is inherently more responsive to finer droplets. HSI, in contrast, relies on optical resolution and thresholding, which can lead to marginally higher SMD estimates, especially when large ligaments or overlapping droplets are present in the frame. The most notable SMD difference between the methods is observed at the 20 mm plane for a flow rate of 0.2 L/min, where HSI shows a higher value by approximately 25 µm. Despite these small differences, both techniques affirm the expected trend, i.e, higher flow rates result in finer atomization and thus smaller droplets due to increased jet breakup and turbulence. Figure 4.9(b) provides a velocity comparison, where HSI generally measures higher droplet velocities than PDPA, particularly at the lower flow rate of 0.1 L/min. At the 10 mm plane, HSI reports a 1.7 m/s higher velocity than PDPA, while at the 20 mm plane, the discrepancy is about 1.3 m/s. These differences diminish at 0.2 L/min, suggesting that the flow becomes more uniform and easier to track as atomization improves. The higher velocity readings from HSI may stem from artifacts in image-based tracking—such as misidentifying rapidly moving or overlapping droplets—whereas PDPA's laser-based, point-wise velocity measurement offers more localized and precise results. Despite these methodological differences, the overall velocity trends align well between the two approaches, affirming their validity for droplet characterization in spray cooling studies.

Integrating these results into the broader context of spray cooling research, this dual-method validation enhances confidence in droplet size and velocity data used for heat transfer modeling. Smaller droplets and higher velocities are both conducive to improved thermal performance, as they promote enhanced surface coverage, rapid spreading, and effective convective and evaporative cooling. Thus, understanding the strengths and limitations of each measurement technique is essential for accurately assessing atomization quality and optimizing nozzle design for thermal management systems.



(a) PAN

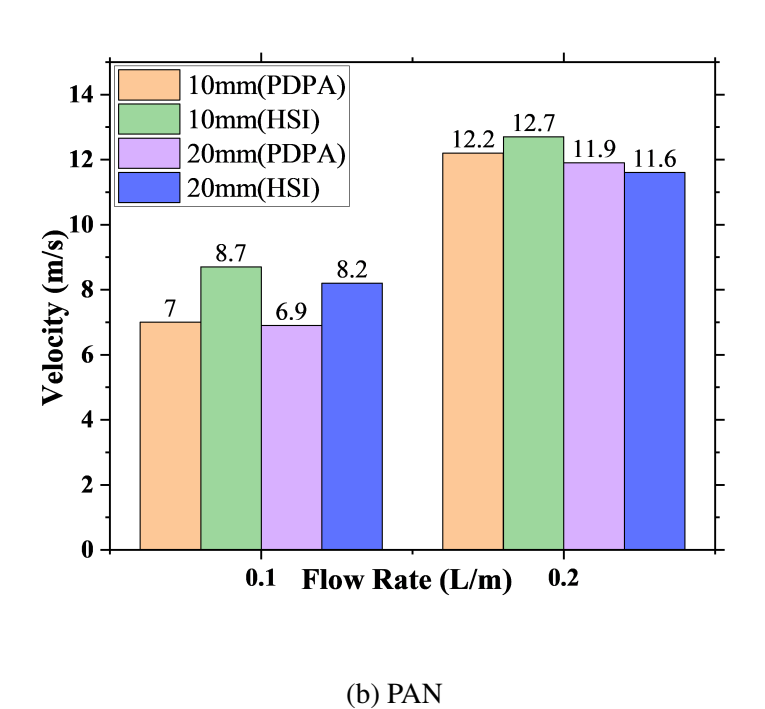


Figure 4.10: Validation of HSI against PDPA for droplet velocity for DI water

CHAPTER 5

RESULTS: HEAT TRANSFER ANALYSIS USING PRESSURE ATOMIZED NOZZLE(PAN)

5.1 SURFACE TEMPERATURE DISTRIBUTION FOR DI WATER AND THERMASOLV

Figure 5.1a and 5.1b illustrates the steady-state foil surface temperature distributions captured using infrared thermography for pressure atomized nozzle (PAN) spray cooling with deionized (DI) water and Thermasolv at two flow rates (0.1 L/min and 0.2 L/min) and two inlet fluid temperatures (25°C and 35°C). These results provide valuable insights into how fluid properties and operating parameters influence cooling behavior on a heated surface maintained at a uniform heat flux of 14.7 W/cm².

The figures 5.1a and 5.1b correspond to the temperature color scale bar used throughout the IR thermography-based surface temperature maps in this study. The scale spans from 25°C to 70°C and employs a continuous color gradient to represent surface temperatures, where blue indicates lower temperatures (near 25°C) and red represents higher temperatures (approaching 70°C). This specific color scale is consistently applied to all contour plots related to Pressure Atomizing Nozzle (PAN) experiments conducted with both DI water and Thermasoly, across both tested flow rates (0.1L/min and 0.2L/min).

To improve clarity and ensure consistency in thermal interpretation, temperature units (°C) have been explicitly labeled adjacent to the scale bar in each applicable figure. Furthermore, a description of this color mapping has been incorporated into the relevant figure captions and the IR methodology section, allowing for accurate interpretation of the spatial surface temperature distributions.

At a lower flow rate of 0.1 L/min, the surface cooled with DI water consistently shows

lower maximum temperatures compared to Thermasolv, attributed to water's higher specific heat capacity and thermal conductivity. These properties enhance its ability to absorb and carry away heat, resulting in more effective convective and evaporative cooling, especially in low mass flux scenarios.

As observed, the highest temperature for Thermasolv occurs at 35°C inlet temperature and 0.1 L/min flow rate (55.4°C), indicating its reduced cooling potential under low subcooling and limited mass flow. On the other hand, water under the same conditions reaches only 48.1°C, reflecting better thermal absorption. This temperature difference arises because Thermasolv, being a dielectric fluid, has inherently lower thermal conductivity and heat capacity compared to water, thus limiting its ability to maintain low surface temperatures under the same thermal load. Interestingly, at the higher flow rate of 0.2 L/min, both fluids show significantly improved performance. The lowest surface temperature (34.5°C) is achieved using water at 25°C, highlighting the combined benefit of increased mass flux and greater subcooling. For Thermasolv, the minimum surface temperature recorded under the same conditions is 39.5°C, again confirming its relatively reduced thermal efficiency.

From a heat transfer perspective, increasing the flow rate enhances convective heat removal by increasing the droplet impingement frequency and liquid film renewal rate. This leads to improved cooling efficiency, particularly in single-phase convection-dominated regimes. Furthermore, the inlet temperature plays a key role in determining subcooling—the temperature difference between the liquid and surface, which directly impacts evaporation rates. Higher subcooling improves evaporative cooling by increasing latent heat absorption, particularly in regions where film evaporation dominates. Additionally, the contours show that Thermasolv maintains more uniform central surface temperatures, possibly due to finer droplet formation and better spray distribution. However, higher corner temperatures suggest less lateral spread, likely caused by higher liquid density and viscosity, which restricts the fluid's ability to reach peripheral areas. These observations emphasize the importance of both fluid

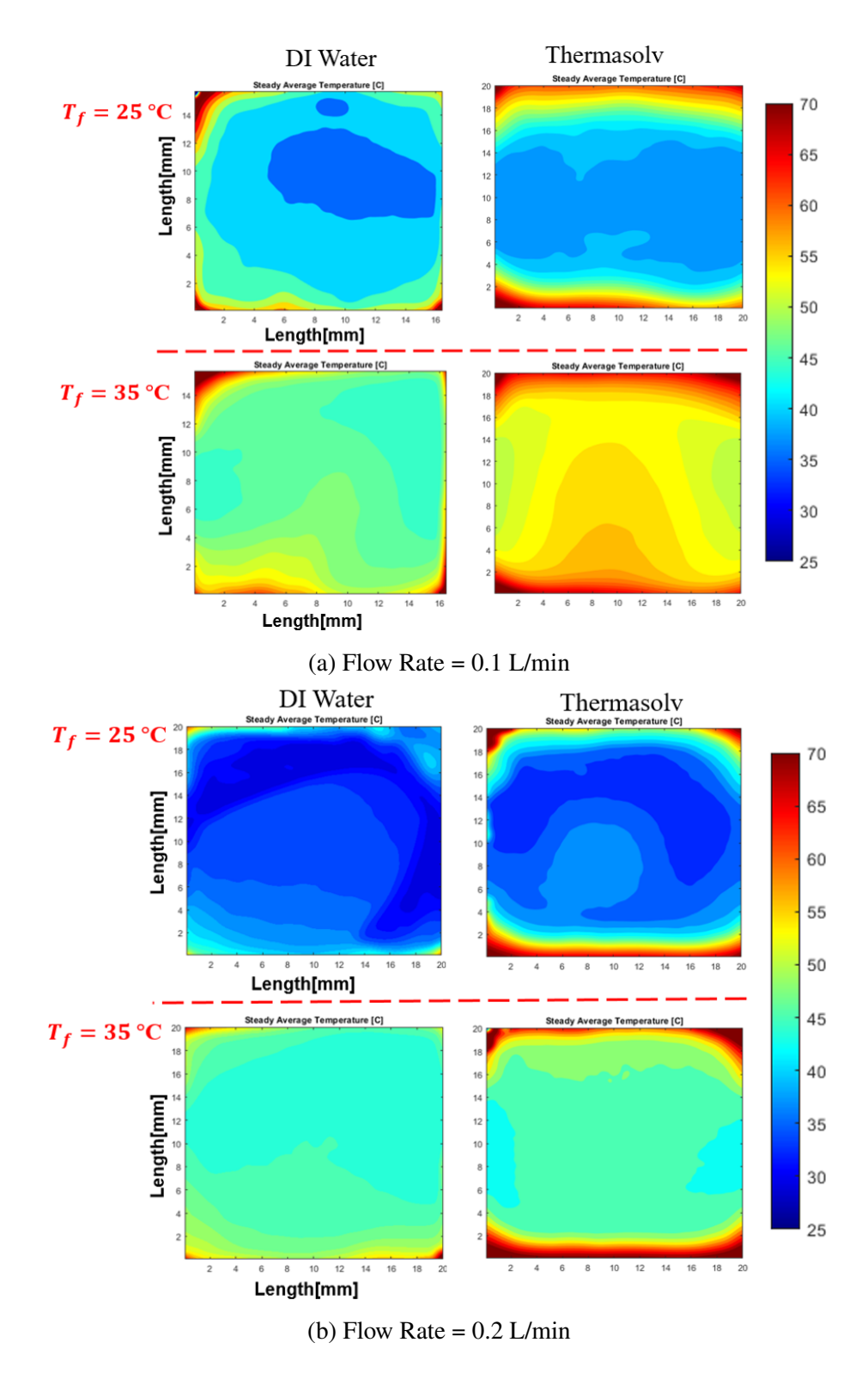


Figure 5.1: Steady Foil Temperature Distribution with IR Camera for PAN

The accompanying scale bar indicates surface temperature in °C.

thermophysical properties and nozzle operating conditions in determining the overall effectiveness and uniformity of spray cooling.

5.2 FOIL TEMPERATURE BEHAVIOR AND UNIFORMITY ANALYSIS WITH VARYING FLUID INLET TEMPERATURES

Average Surface Temperature Estimation(T_{avg}):

In this study, temperature measurement from the IR camera involved a multi-step averaging approach to ensure accurate and smooth thermal profiling during spray cooling. First, the temperature at each pixel was computed using a weighted average across five time frames, assigning greater importance to the current frame. This was followed by a secondary time-averaging step to further smooth transient variations. Finally, to determine the overall steady-state temperature of the heated foil, a spatial average was computed across all 410×410 pixels. This processed average temperature, $T_{\rm avg}$, serves as a reliable indicator of surface cooling effectiveness under different fluid and nozzle configurations.

$$T_{\text{pixel,avg}} = \frac{T_{t-2} + 2T_{t-1} + 3T_t + 2T_{t+1} + T_{t+2}}{9}$$
 (5.1)

$$T_{\text{pixel}}^* = \frac{T_{\text{pixel,avg},t} + T_{\text{pixel,avg},t-1}}{2}$$
 (5.2)

$$T_{\text{avg}} = \frac{1}{410 \times 410} \sum_{i=1}^{410} \sum_{j=1}^{410} T_{\text{pixel}}^*(i, j)$$
 (5.3)

Non-dimensional Temperature Difference (Φ)

$$\Phi = \frac{T_{\text{max}} - T_{\text{min}}}{T_{\text{avg}} - T_{\text{min}}} \tag{5.4}$$

 T_{max} denotes the maximum surface temperature observed on the foil, while T_{min} represents the minimum surface temperature. The term T_{avg} , obtained from equation 5.3, corresponds

to the average surface temperature calculated over the entire measurement area, and is subsequently used in the evaluation of surface temperature uniformity.

Surface temperature uniformity(Φ): Non-dimensional temperature difference was used to assess surface cooling uniformity. A lower non-dimensional temperature difference indicates better temperature uniformity across the surface.

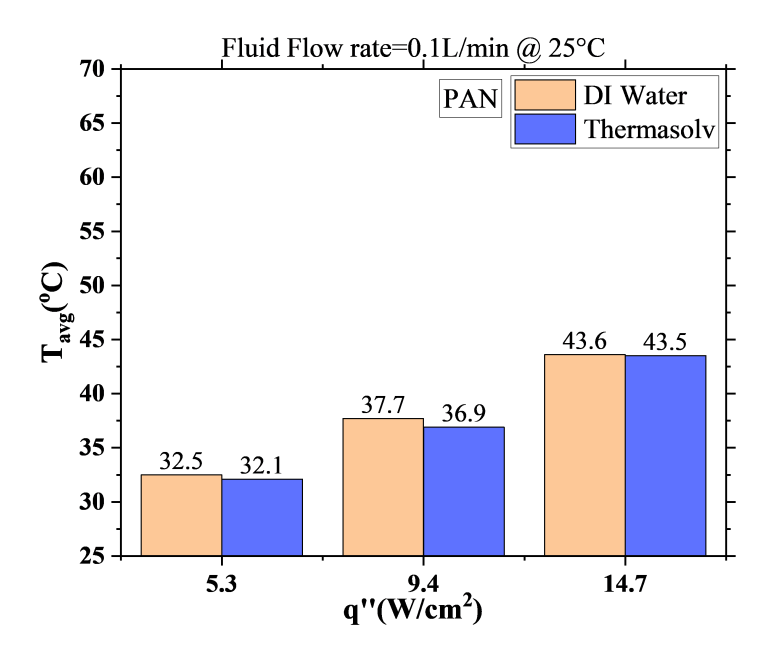
Convective Heat Transfer Coefficient (h):

$$h = \frac{q_{\text{avg}}^{"}}{T_{\text{avg}} - T_{\text{inlet}}} \tag{5.5}$$

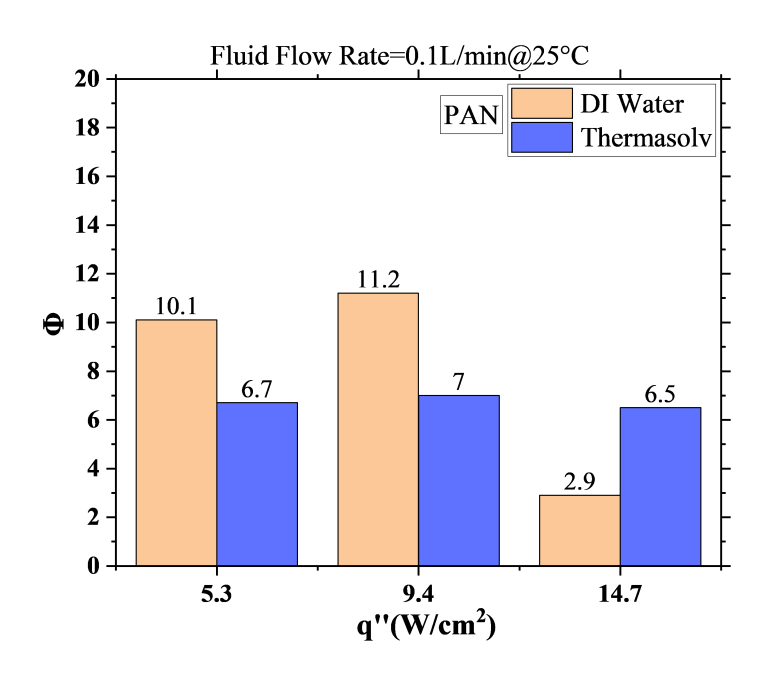
Where $q''_{avg.}$ is the applied heat flux (W/cm²), and $T_{avg.}$ is the Average surface temperature (°C), both obtained from infrared (IR) camera measurements. T_{inlet} is the inlet fluid temperature (°C) obtained from Data logger. The convective heat transfer coefficient (HTC) was calculated using the equation 5.5. Experiments were conducted at three different heat fluxes: 5.6, 9.4, and 14.7 W/cm². Two inlet fluid temperatures, 25°C and 35°C, were used for both water and Thermasolv to investigate the effect of fluid properties and operating conditions.

Figure 5.2a presents a comparison of the average steady foil temperatures for deionized (DI) water and Thermasolv at a flow rate of 0.1 L/min and an inlet temperature of 25°C. As the applied heat flux increases, the steady-state foil surface temperature also rises due to the greater thermal energy input that needs to be dissipated by the cooling spray. At the highest tested heat flux of 14.7 W/cm², the surface temperature reaches 43.6°C for DI water and 43.5°C for Thermasolv.

Although both fluids show similar peak temperatures under these extreme conditions, Thermasolv demonstrates slightly lower temperatures and better thermal uniformity across the surface. This characteristic makes it particularly suitable for electronic cooling applications, where minimizing localized hot spots is crucial to prevent component failure. Figure 5.2b illustrates the surface temperature uniformity for DI



(a) Steady foil average temperature



(b) Surface temperature uniformity

Figure 5.2: Steady foil temperature and uniformity comparison for DI Water and Thermasolv at $\dot{V}=0.1$ L/min (PAN, 25°C).

water and Thermasolv at a flow rate of 0.1 L/min and an inlet temperature of 25°C. An analysis of the non-dimensional temperature difference indicates cooling uniformity.

Water exhibits its highest non-dimensional temperature difference of 11.2 at a heat flux of 9.4 W/cm², while the lowest value of 2.9 occurs at 14.7 W/cm². This decrease in the non-dimensional temperature difference at higher heat flux levels is attributed to enhanced evaporation and more effective cooling across the surface. Thermasolv consistently outperforms water in maintaining a uniform temperature distribution at all heat flux levels, except at the highest level of 14.7 W/cm². This improved performance is likely due to Thermasolv's finer droplet distribution and better spray dispersion, resulting from its lower viscosity and superior atomization characteristics. These factors contribute to more homogeneous surface wetting and heat removal. Despite Thermasolv's relatively lower thermal conductivity and heat capacity compared to water, its atomization behavior ensures more consistent cooling under moderate conditions, which is valuable for thermally sensitive electronic applications. From figure 5.3, at a constant flow rate of 0.1L/min and spray inlet temperature of 25°C, Thermasolv IM6 consistently exhibits a higher heat transfer coefficient (HTC) than DI water across all examined heat fluxes—5, 9.4, and 14.7W/cm²—with respective margins of 411.6, 484.8, and 15W/m²·K.

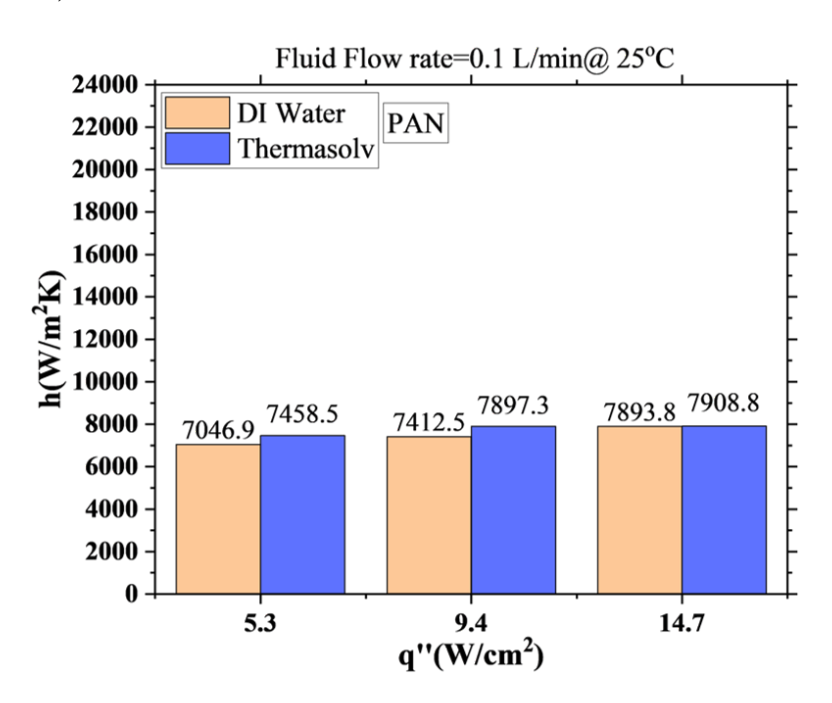
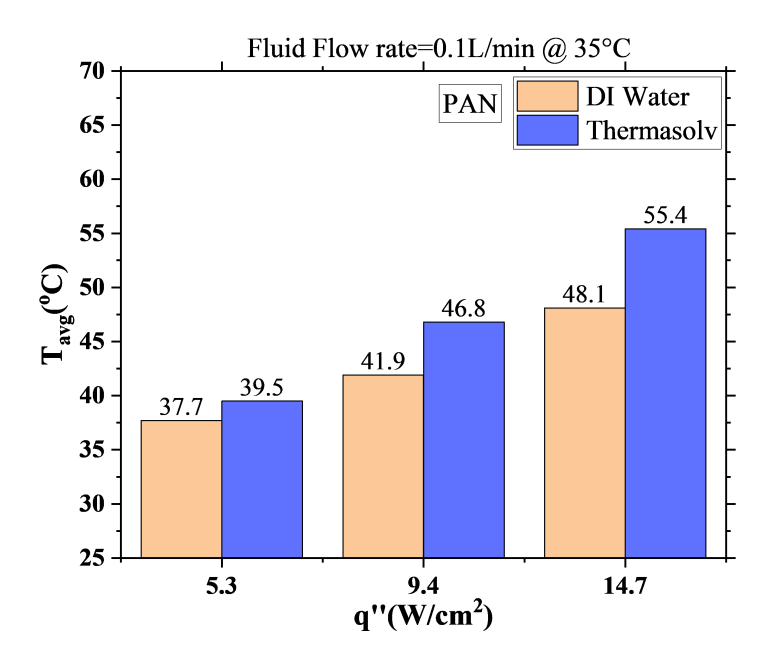


Figure 5.3: Heat Transfer Coefficient Comparison at $\dot{V} = 0.1 \text{ L/min}$ for PAN at 25°C.

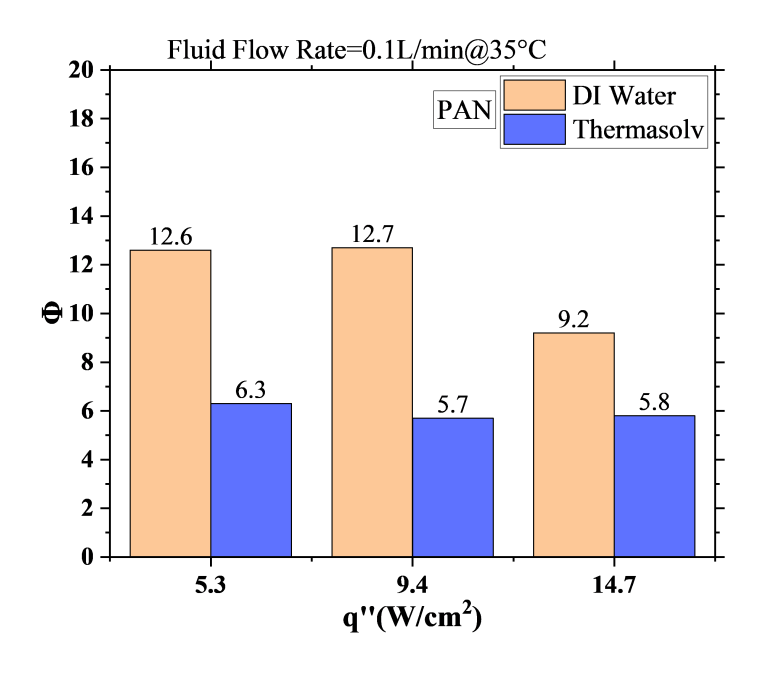
This trend suggests that under lower spray temperatures, Thermasolv may benefit from favorable droplet dynamics such as improved atomization, enhanced surface spreading due to lower surface tension, or higher wettability on the heated surface, leading to more efficient convective heat transfer. Despite water's higher thermal conductivity and specific heat, its relatively higher surface tension and viscosity at 25°C could limit droplet spread and fluid renewal near the surface. As a result, Thermasolv's effective thermal interaction leads to slightly lower steady-state surface temperatures and better cooling performance under single-phase conditions. These findings highlight the potential of Thermasolv as a viable dielectric coolant, particularly when electrical insulation and low global warming potential (GWP) are critical.

Figure 5.4a illustrates the variation in average steady-state foil temperature for DI water and Thermasolv at a constant flow rate of 0.1 L/min, with an inlet fluid temperature of 35°C. At the highest heat flux of 14.7 W/cm², the temperature difference between the two fluids peaks at 7.3°C, with Thermasolv exhibiting the higher temperature. This trend persists across all heat flux levels, indicating that Thermasolv has a comparatively lower heat removal capacity. The smallest temperature difference of 1.8°C is observed at 5 W/cm², where the thermal load is lower and both fluids perform relatively similarly.

Figure 5.4b demonstrates surface temperature uniformity at 35°C. Despite having higher surface temperatures, Thermasolv consistently shows better temperature uniformity across the heater surface. This is evident in the non-dimensional temperature values, where water records significantly higher non-dimensional temperature differences of 12.6, 12.7, and 9.2 for heat fluxes of 5 W/cm², 9.4 W/cm², and 14.7 W/cm², respectively. The superior uniformity of Thermasolv can be attributed to its lower dynamic viscosity, lower specific heat, and improved atomization behavior. These factors lead to finer and more evenly distributed droplets during spray cooling, enhancing the spatial uniformity of liquid film coverage and evaporative cooling. This reduces temperature gradients



(a) Steady foil average temperature



(b) Surface temperature uniformity

Figure 5.4: Steady foil temperature and uniformity comparison for DI Water and Thermasolv at $\dot{V} = 0.1$ L/min (PAN, 35°C).

across the surface. From a physics standpoint, while water benefits from higher thermal conductivity and specific heat, resulting in better absolute cooling, Thermasolv provides

more homogeneous thermal management. This is a critical factor in high-precision electronics, where localized overheating can be detrimental.

Figure 5.5 highlights the dominant heat transfer performance of DI water over Thermasolv IM6 at an elevated spray inlet temperature of 35°C and a fixed flow rate of 0.1L/min, particularly under lower to moderate heat fluxes. The marked difference in heat transfer

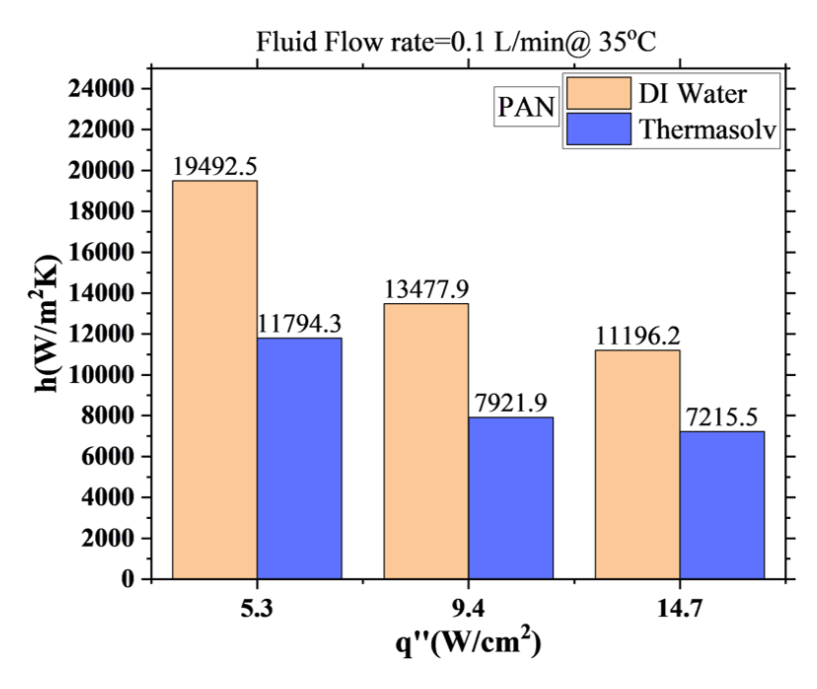


Figure 5.5: Heat Transfer Coefficient Comparison at $\dot{V} = 0.1$ L/min for PAN at 25°C.

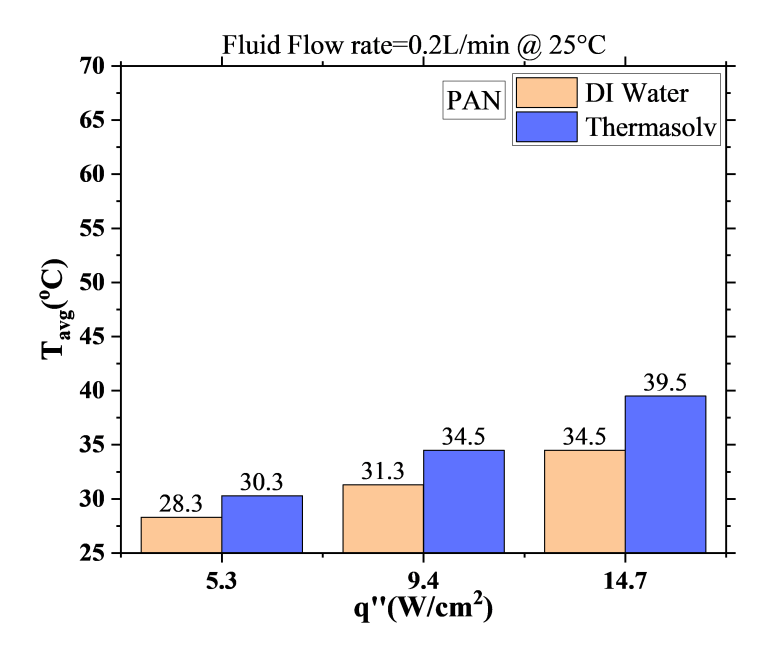
coefficients can be attributed to the reduced thermal resistance between the heated surface and the water droplets, which is further enhanced by improved spreading and thinner liquid film formation at higher fluid temperatures. Elevated spray temperatures lower the viscosity and surface tension of water, promoting faster surface renewal and more uniform wetting, key for efficient convective transport in single-phase spray cooling. Additionally, the higher thermal conductivity and specific heat of water enable greater energy absorption per unit mass, reducing thermal boundary layer thickness and facilitating higher heat flux dissipation. In contrast, Thermasolv, although a dielectric fluid with practical benefits, suffers from relatively poorer thermophysical properties and limited hydrodynamic behavior at this temperature, leading to higher surface temperatures and reduced overall cooling effectiveness.

Figure 5.6a illustrates the steady-state average foil temperature for a flow rate of 0.2 L/min and an inlet fluid temperature of $T_f = 25$ °C, comparing the performance of water and Thermasolv in the PAN configuration. It is clear that water consistently outperforms Thermasolv across all levels of heat flux. According to Particle Dynamic Profile Analysis (PDPA) measurements, water has a higher spray velocity of 12.2 m/s, compared to 7.8 m/s for Thermasolv.

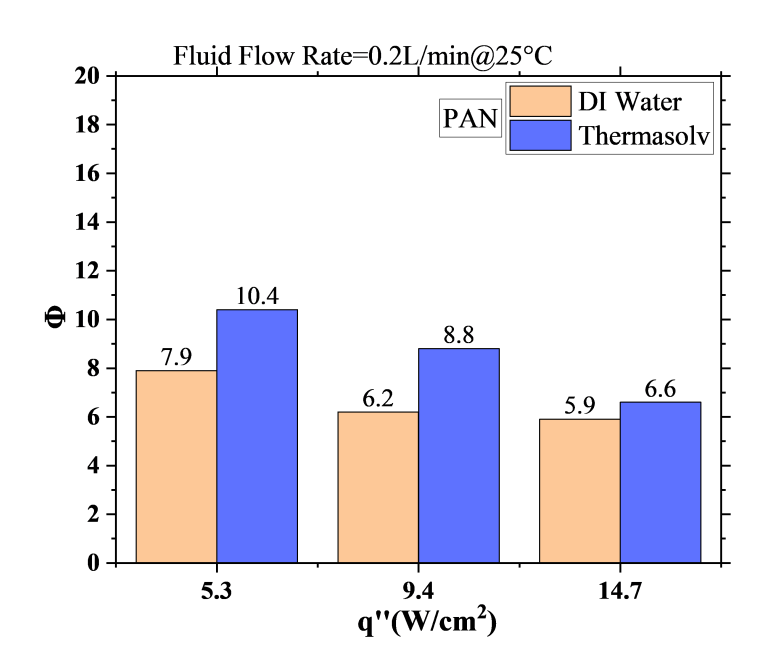
Furthermore, Figure 5.6b shows that water demonstrates better temperature uniformity throughout the range of applied heat fluxes. The best uniformity is observed at a heat flux of 14.7 W/cm², where the non-dimensional temperature difference for water is 5.9, compared to 6.6 for Thermasolv under the same conditions. This improved performance is closely tied to water's exceptional thermal properties, specifically its higher specific heat capacity and thermal conductivity, which enable it to absorb and transfer heat more efficiently during spray impacts and film formation.

Figure 5.8a compares the steady-state average foil temperatures for water and Thermasolv at a flow rate of 0.2 L/min and an inlet fluid temperature of 35 °C in the PAN configuration. Across all tested heat flux levels, water consistently maintains lower average surface temperatures, confirming its superior cooling capacity. This advantage can be attributed to water's higher thermal conductivity and specific heat capacity, which allow for more efficient absorption and dissipation of heat from the surface. However, as the heat flux increases, the performance gap between the two fluids becomes more pronounced. At the highest tested heat flux of 14.7 W/cm², Thermasolv experiences a temperature rise that is approximately 3.7 °C higher than that of water, indicating its reduced ability to manage peak thermal loads under the same flow and temperature conditions.

Figure 5.7 reveals that increasing the flow rate to 0.2L/min at a constant spray inlet temperature of 25°C markedly enhances the heat transfer performance of DI water compared to Thermasolv IM6 across all heat flux levels. The higher mass flux increases the volumetric delivery of cooler fluid to the heated surface, ensuring more frequent



(a) Steady foil average temperature



(b) Surface temperature uniformity

Figure 5.6: Steady foil temperature and uniformity comparison for DI Water and Thermasolv at $\dot{V} = 0.2$ L/min (PAN, 25°C).

surface wetting and quicker replacement of heated liquid layers, thus sustaining strong thermal gradients for convective transport. For water, the combined effects of higher

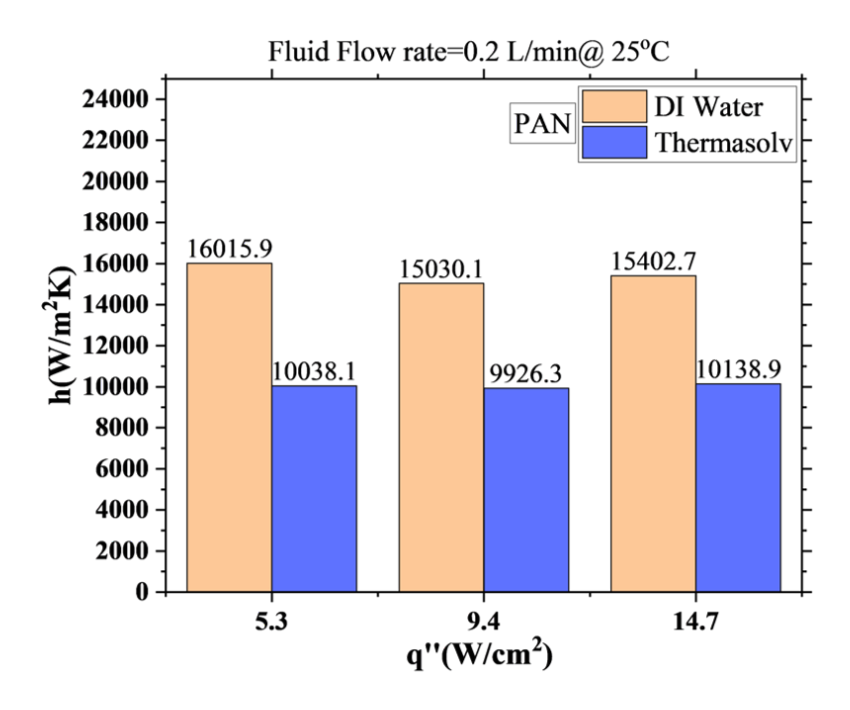
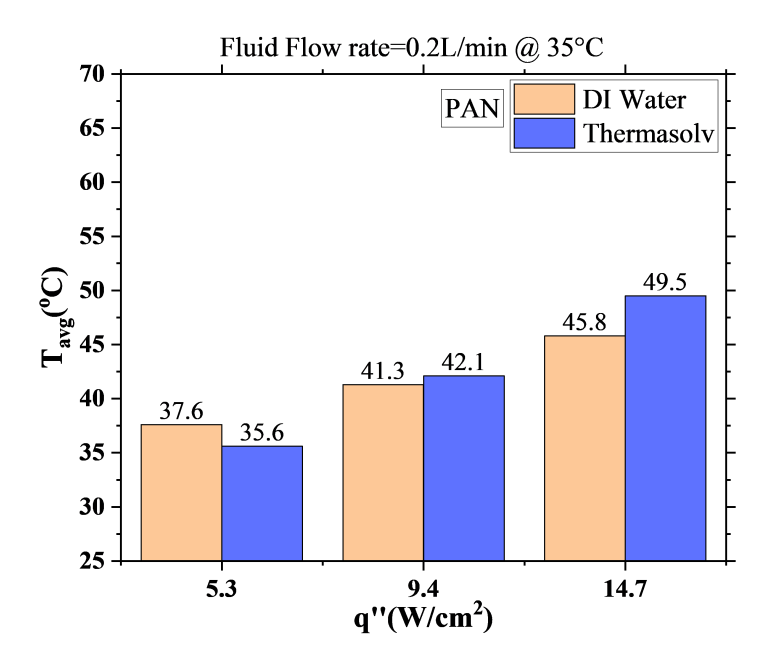


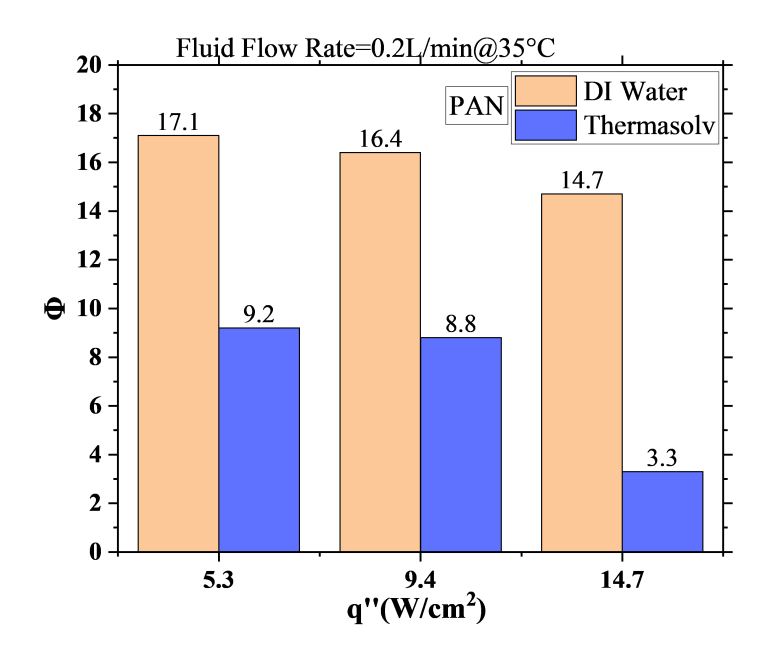
Figure 5.7: Heat Transfer Coefficient Comparison at $\dot{V} = 0.2 \text{ L/min}$ for PAN at 25°C.

thermal conductivity and specific heat at this elevated flow rate amplify its ability to absorb and transport heat efficiently. Furthermore, increased droplet momentum at higher flow rates improves surface penetration and liquid film thinning, promoting rapid heat extraction. Although Thermasolv benefits from higher flow as well, its lower thermophysical properties—especially thermal conductivity—limit its ability to match water's performance. The observed increase in the HTC gap at higher flow confirms that water responds more favorably to flow rate augmentation, reinforcing its dominance as a cooling medium in single-phase spray systems under enhanced hydrodynamic conditions.

Despite its lower cooling efficiency, Thermasolv demonstrates a clear advantage in temperature uniformity, as illustrated in Figure 5.8b. Uniform surface temperature is critical in many thermal management applications to prevent localized overheating or thermal stress. At 14.7 W/cm², the non-dimensional temperature difference (Φ) for Thermasolv is significantly lower at 3.3, compared to 14.7 for water. This smoother temperature gradient suggests that Thermasolv facilitates more consistent heat distribution, likely due to its finer spray structure and reduced premature evaporation at elevated



(a) Steady foil average temperature



(b) Surface temperature uniformity

Figure 5.8: Steady foil temperature and uniformity comparison for DI Water and Thermasolv at $\dot{V}=0.2$ L/min (PAN, 35°C)

fluid temperatures. In applications where uniform cooling is more important than peak heat removal, such as in sensitive electronic devices, this characteristic could offer a significant advantage.

5.3 EVALUATION OF THERMASOLV EVAPORATION USING PAN

5.3.1 Equations

$$\dot{V} \cdot \rho = \dot{m}_{\text{total}} \tag{5.6}$$

Equation 5.6 gives the total mass flow rate of the fluid (\dot{m}_{total}) by multiplying the volumetric flow rate (\dot{V} , in L/min) with the density of the fluid (ρ , in kg/m³). It tells us how much mass is being delivered to the surface per unit time, which is critical to assess how much fluid is available for heat absorption and evaporation.

$$q'' \times \text{Number of Pixels} \times \text{Area of each Pixel} = \dot{m}_{\text{eva}} \cdot h_{\text{fg}}$$
 (5.7)

Equation 5.7 is the energy balance for the evaporated fluid. The left side represents the total thermal power delivered to the evaporating area (W), calculated from surface heat flux (q''), the number of heated pixels, and the physical area each IR pixel covers.

Given that one IR pixel corresponds to an area of $0.04089 \,\mathrm{mm} \times 0.04089 \,\mathrm{mm} = 1.672 \times 10^{-9} \,\mathrm{m}^2$, the total heated area can be calculated. The right side is the thermal energy required to evaporate a certain mass flow rate \dot{m}_{eva} , where h_{fg} is the latent heat of vaporization (J/kg). Solving this equation gives you how much of the supplied energy contributes to evaporation.

Fraction of Evaporated Fluid =
$$\frac{\dot{m}_{\text{eva}}}{\dot{m}_{\text{total}}}$$
 (5.8)

Equation 5.8 calculates what fraction of the total supplied mass flow evaporates. It is a measure of the effectiveness of phase change cooling. Higher values indicate that more fluid is used for latent heat absorption rather than being removed by convective film flow or runoff.

From figure 5.9a, Fluid inlet temperature of 25°C, initiating evaporation requires overcoming a larger thermal gradient between the relatively cool fluid and the heated

surface. At a lower flow rate of 0.1 L/min, droplets spend more time on the surface, which leads to the formation of a thinner liquid film. This enhances surface interaction, promotes localized evaporation, and limits runoff, resulting in an evaporation rate of 5.8% at a heat flux of 14.7 W/cm². However, when the flow rate increases to 0.2 L/min, the thicker liquid film reduces the efficiency of heat transfer to the fluid. This decrease in surface contact favors convective heat removal over phase change, causing the evaporated fraction to drop significantly to only 1.6%, even though the system is operating under the same thermal load. From figure 5.9b, when the fluid enters the spray zone at an elevated inlet temperature of 35°C, it is closer to its boiling point, which requires less energy for a phase change to occur. This thermal advantage significantly enhances the evaporation process, especially at lower flow rates. At a flow rate of 0.1L/min and a heat flux of 14.7W/cm², the evaporation rate increases sharply to 24%, representing a fourfold improvement compared to the evaporation rate at 25°C. This enhancement is due to the combined effects of the preheated fluid and the formation of a thinner film, which allows for more efficient droplet-surface interactions.

In contrast, at a higher flow rate of 0.2L/min, although the inlet temperature is still warmer, the evaporation fraction is limited to just 5.5%. This limitation highlights that a higher flow rate creates a thicker liquid layer, which reduces surface heat absorption and promotes sensible heat transport over latent heat. As a result, this suppresses effective evaporation.

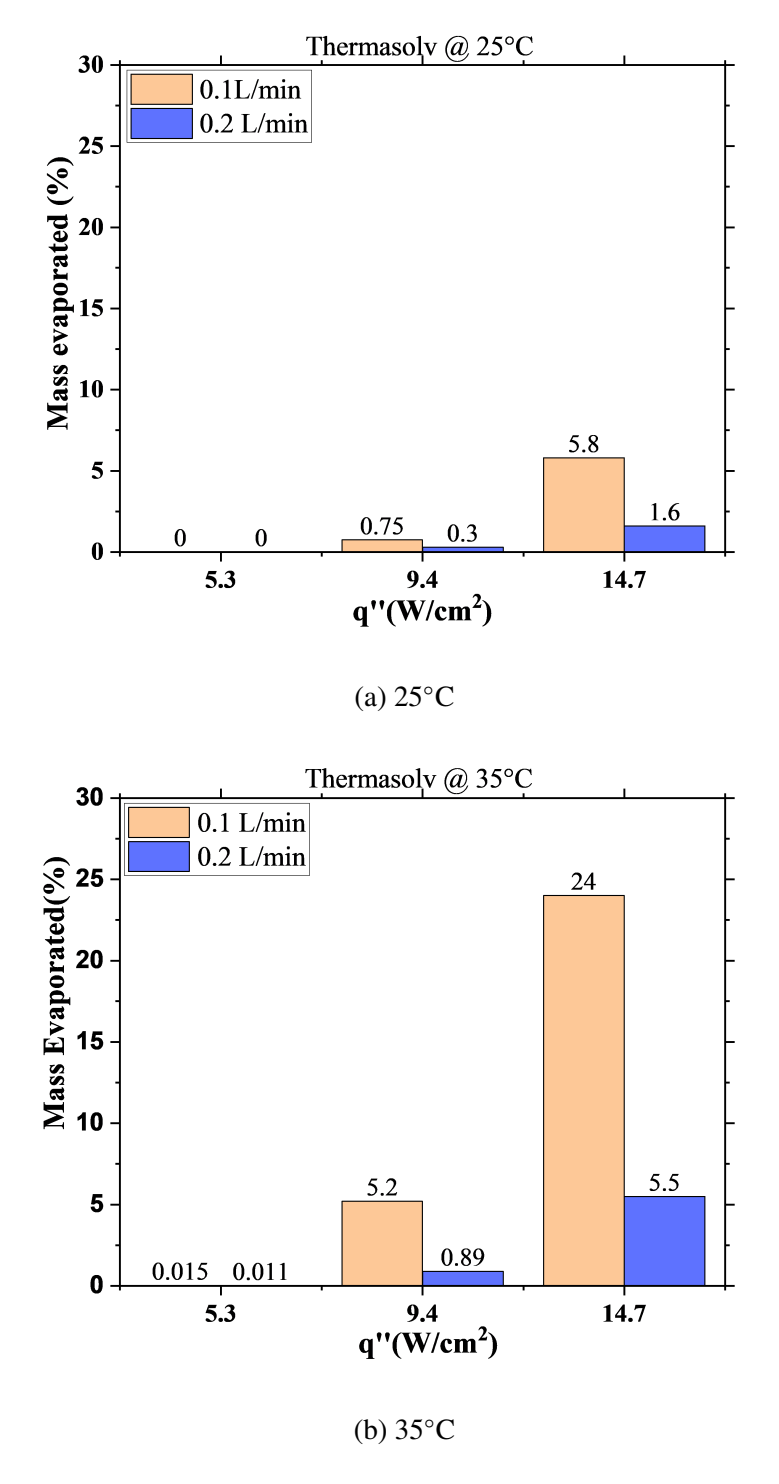


Figure 5.9: Thermasolv mass evaporation (%) on PAN at $\dot{V}=0.1$ and 0.2 L/min

CHAPTER 6

RESULTS: HEAT TRANSFER ANALYSIS USING AIR ATOMIZED NOZZLE(AAN)

6.1 SURFACE TEMPERATURE DISTRIBUTION FOR DI WATER AND THERMASOLV

Figure 6.1a and 6.1b present the steady-state foil surface temperature distributions for air-atomized nozzle (AAN) cooling, captured using infrared thermography at flow rates of 0.1 L/min and 0.2 L/min for both deionized (DI) water and Thermasolv. These experiments were conducted under a uniform heat flux of 14.7 W/cm² and two inlet fluid temperatures (25°C and 35°C). A notable distinction from the pressure atomized nozzle (PAN) configuration is the superior thermal performance of Thermasolv in the AAN setup. The contours indicate that Thermasolv maintains lower and more uniform temperatures across the entire heated surface compared to water.

The temperature scale depicted in figure 6.1a and 6.1b is associated with the infrared (IR) thermography based surface temperature contours obtained from experiments using the Air Atomizing Nozzle (AAN) with both DI water and Thermasolv at flow rates of 0.1L/min and 0.2L/min. This scale ranges from 10°C to 45°C, capturing the broader thermal dynamics specific to AAN-assisted spray cooling. A different scale was intentionally used in this case to accurately represent sub-ambient surface temperatures, which were observed during intense evaporative cooling, particularly with Thermasolv, due to its lower boiling point, high velocity atomization, and fine droplet characteristics.

The color gradient transitions from deep blue (10°C), indicating the coolest regions, to red (45°C) for the warmest areas, enabling detailed visualization of spatial temperature variation. Labels in degrees Celsius (°C) are provided alongside the scale for clarity. This modified temperature range ensures meaningful comparison and interpretation of

cooling performance under aggressive evaporation regimes.

This enhanced cooling capability stems from the synergistic effect of air-assisted atomization, which produces finer droplets with higher velocities, increasing both convective and evaporative heat transfer. For instance, the lowest surface temperature recorded was 18.2°C with Thermasolv at 0.1 L/min and 25°C inlet temperature, significantly outperforming water under the same conditions (33.7°C at 0.2 L/min). Even at elevated inlet temperatures (35°C), Thermasolv demonstrated effective heat removal, maintaining a maximum temperature of just 26.5°C at 0.2 L/min. In contrast, water under similar high-temperature conditions (35°C and 0.1 L/min) reached a surface temperature as high as 44.9°C, highlighting its reduced cooling efficiency in the AAN configuration. This difference is largely due to Thermasolv's more stable droplet distribution and better phase change behavior under forced air conditions. The high velocity imparted by the air stream not only improves droplet breakup and spread but also enhances vapor removal from the surface, enabling continuous rewetting and effective localized cooling.

From a heat transfer perspective, AAN systems benefit from increased droplet surface area and impingement momentum, which significantly boost the convective heat transfer coefficient. Additionally, the evaporative cooling effect becomes more pronounced due to the lower thermal boundary layer resistance and rapid droplet replenishment. The temperature contours further reveal that Thermasolv achieves excellent spatial temperature uniformity, especially at the center of the heated surface, due to its consistent spray distribution and lower Sauter Mean Diameter (SMD). This uniformity is crucial for applications requiring thermal stability, such as electronics and high-precision sensors. Overall, the results affirm that Thermasolv, when used with AAN, offers a highly efficient and uniform thermal management solution, especially at moderate to high subcooling and flow rate conditions.

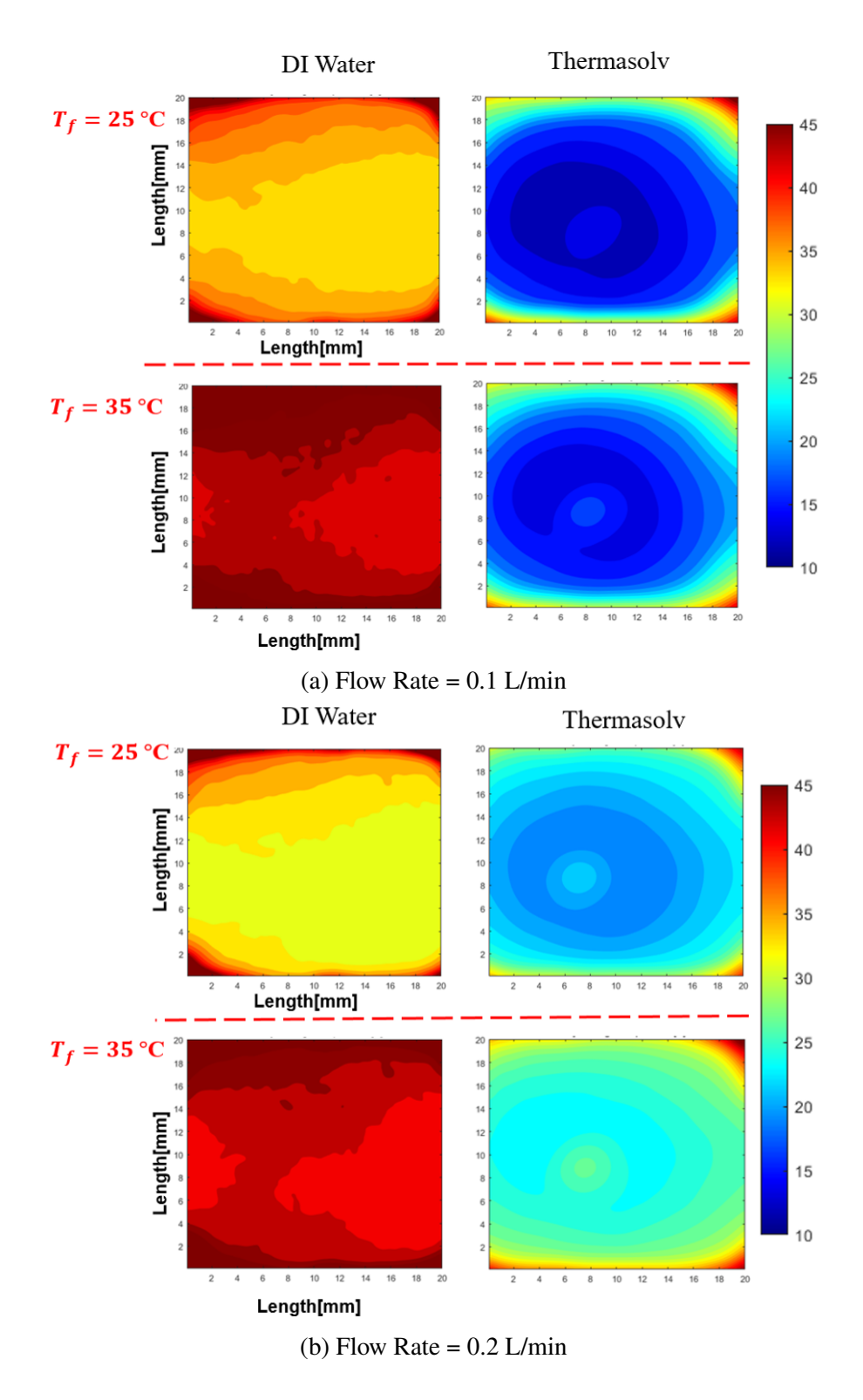


Figure 6.1: Steady Foil Temperature Distribution with IR Camera for AAN The accompanying scale bar indicates surface temperature in °C.

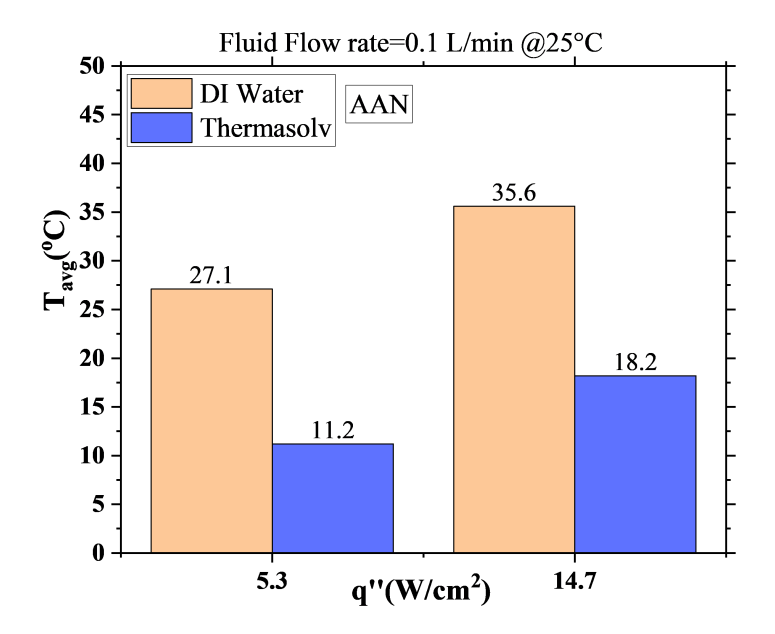
6.2 FOIL TEMPERATURE BEHAVIOR AND UNIFORMITY ANALYSIS WITH VARYING FLUID INLET TEMPERATURES

Figure 6.2a compares the steady-state average temperatures of the foil for Thermasolv and water under AAN spray cooling conditions, with a flow rate of 0.1 L/min and an inlet fluid temperature of 25°C. Thermasolv consistently demonstrates significantly lower surface temperatures than water across all tested heat fluxes. Specifically, at a heat flux of 5.3 W/cm², the foil temperature for Thermasolv is just 11.2°C, notably below the inlet fluid temperature, while the foil temperature for water reaches 27.1°C. At a higher heat flux of 14.7 W/cm², Thermasolv maintains a foil temperature of 18.2°C, compared to 35.6°C for water.

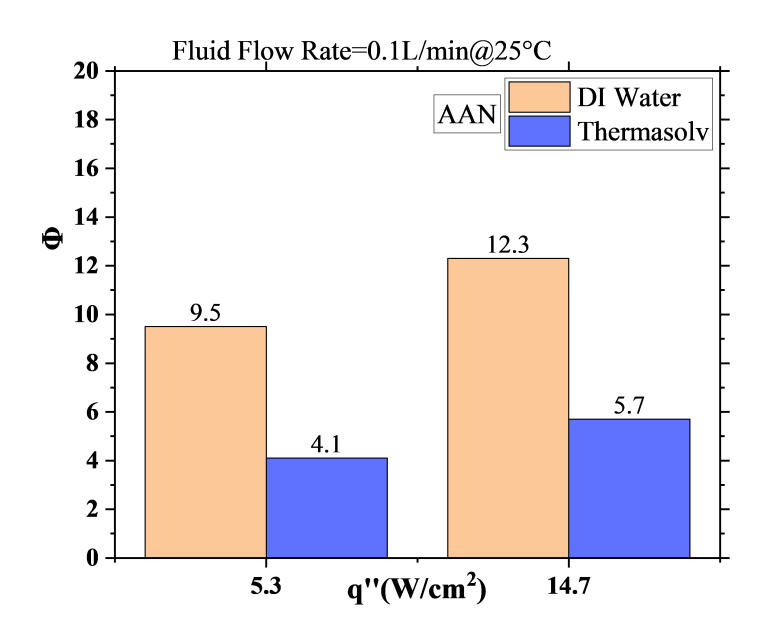
Phase Doppler Particle Analyser (PDPA) measurements indicate that Thermasolv has a higher spray velocity of 16.6 m/s, compared to 13.2 m/s for water. Additionally, the Sauter Mean Diameter (SMD) is somewhat smaller for Thermasolv at 135.7 μ m, while water shows an SMD of 151.1 μ m.

The enhanced cooling performance of Thermasolv under AAN conditions is attributed to its favorable thermo-physical properties and spray dynamics. Compared to water, Thermasolv has a lower boiling point, lower viscosity, and higher spray velocity, as confirmed by PDPA measurements. These characteristics facilitate rapid liquid spreading and the formation of a thin, uniform film over the heated surface, which enhances local evaporation. The increased evaporation rate enables more effective absorption of latent heat, which is the primary mechanism for spray cooling. Furthermore, Thermasolv's lower specific heat capacity means it requires less energy to reach its boiling point, allowing for a quicker transition to the evaporative phase. This reduces the energy retained as sensible heat and increases the energy available for the phase change, further improving the cooling capability.

The high-velocity spray also contributes to better surface wetting and reduced thermal resistance, resulting in lower steady-state surface temperatures. In addition to the average temperature performance, Figure 6.2b shows that temperature uniformity across the



(a) Steady foil average temperature



(b) Surface temperature uniformity

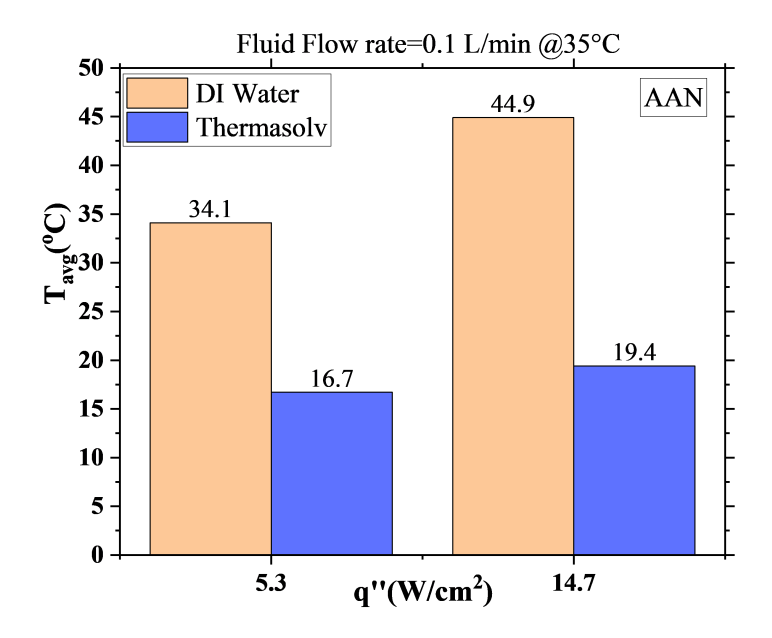
Figure 6.2: Steady foil temperature and uniformity comparison for DI Water and Thermasolv at $\dot{V} = 0.1$ L/min (AAN, 25°C).

surface is significantly better with Thermasolv. The uniformity metric values are 4.1 and 5.7 at 5.3 and 14.7 W/cm², respectively, compared to 9.5 and 12.3 for water. Lower values

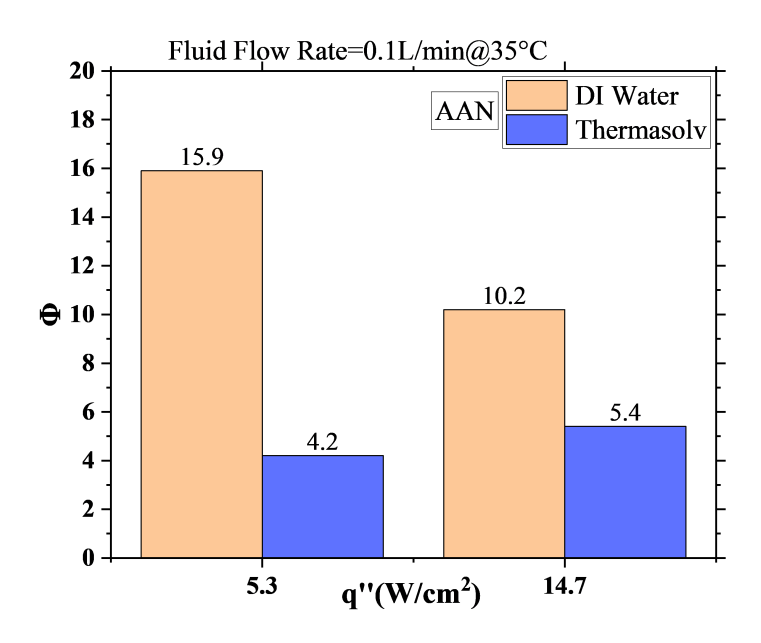
represent more uniform cooling, which is critical for sensitive electronics or materials that require thermal homogeneity. This uniformity is likely enhanced by Thermasolv's consistent evaporation-driven cooling mechanism, which operates efficiently regardless of minor local variations in heat flux or surface temperature.

Importantly, these findings suggest that Thermasolv is particularly well-suited for applications involving ambient temperature fluid supply, providing uniform and efficient cooling without the need for elevated inlet temperatures.

Figure 6.3 presents a comparative analysis of the steady-state thermal performance and uniformity of deionized water and Thermasolv at an elevated fluid inlet temperature of 35 °C, utilizing air-assisted nozzle (AAN) spray cooling at a fixed flow rate of 0.1 L/min. As shown in Figure 6.3a, Thermasolv significantly outperforms water in terms of surface temperature across both examined heat fluxes. At a heat flux of 5.3 W/cm², Thermasolv achieves an average foil temperature of 16.7 °C, compared to the much higher temperature of 34.1 °C recorded for water. Likewise, at 14.7 W/cm², the foil temperature for Thermasolv is 19.4 °C—25.5 °C lower than the 44.9 °C observed for water. This substantial thermal difference highlights Thermasolv's enhanced cooling capacity, attributed to its higher evaporation potential at elevated inlet temperatures. At 35 °C, Thermasolv requires less energy to reach the phase-change threshold, allowing a greater portion of the input heat to be utilized for evaporation. This latent heat-driven mechanism enhances local cooling intensity and accelerates temperature reduction across the heated surface. Beyond average temperature performance, Fig. 6.3b illustrates Thermasoly's superiority in maintaining thermal uniformity. The non-dimensional temperature difference (Φ) for Thermasolv is 4.2 and 5.4 at heat fluxes of 5.3 and 14.7 W/cm², respectively. Both are significantly lower than the values for water, which are 15.9 and 10.2. A lower Φ value indicates a more even temperature distribution, which is crucial for applications involving thermally sensitive electronics or components with low tolerance for spatial temperature gradients. The improved uniformity with Thermasolv is due to finer atomization, higher spray velocity, and greater evaporation coverage,



(a) Steady foil average temperature



(b) Surface temperature uniformity

Figure 6.3: foil temperature and uniformity comparison for DI Water and Thermasolv at $\dot{V}=0.1$ L/min (AAN, 35°C).

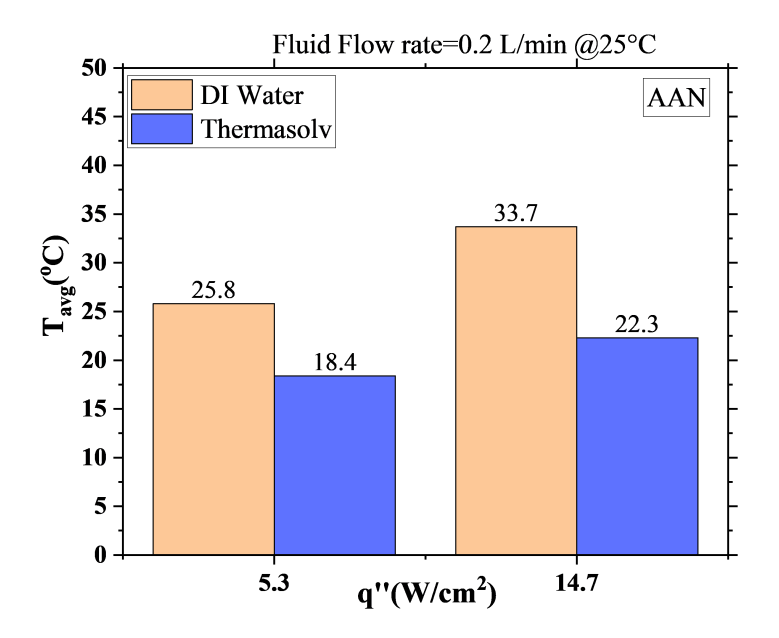
enabling consistent heat removal across the surface. Furthermore, the lower specific heat of Thermasolv allows for quicker thermal saturation and more active evaporation,

thereby reducing thermal gradients. These combined advantages underscore the efficacy of Thermasolv in high-performance spray cooling systems that operate with preheated fluids, ensuring both efficient cooling and temperature uniformity.

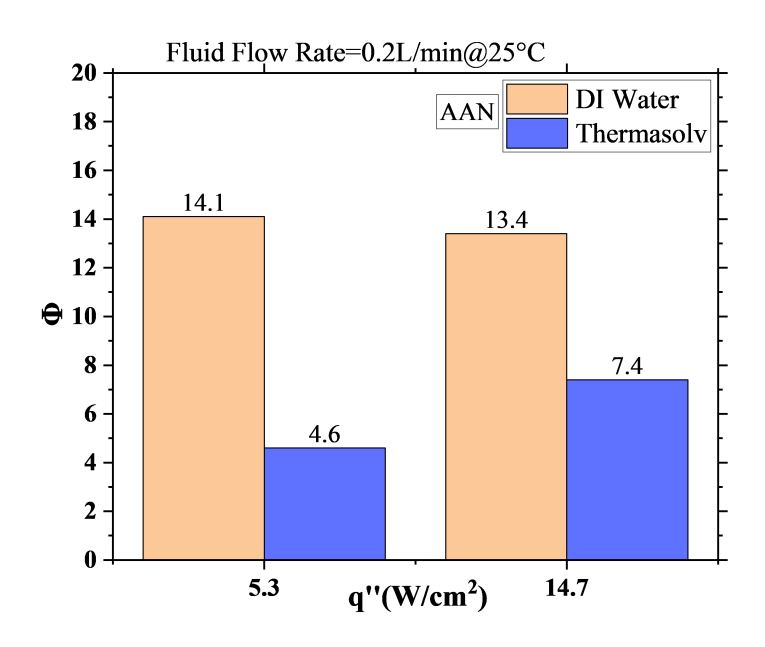
Figure 6.4 offers valuable insights into the spray cooling performance of Thermasolv compared to DI water under air-assisted atomization (AAN). The tests were conducted at a flow rate of 0.2 L/min and an inlet fluid temperature of 25 °C. As shown in Figure 6.4a, Thermasolv consistently achieves lower average surface temperatures across both heat flux levels. Specifically, at heat fluxes of 5.3 W/cm² and 14.7 W/cm², the foil temperatures with Thermasolv are 18.4 °C and 22.3 °C, respectively—significantly lower than the corresponding temperatures for water, which are 25.8 °C and 33.7 °C.

The distinct spray cooling behaviors of DI water and Thermasolv under AAN conditions are effectively illustrated through PDPA data and temperature uniformity plots. For DI water, the presence of small droplets and high velocity—indicated by a mean droplet diameter (SMD) of 116.6 µm and a velocity of 18.97 m/s—creates a high surface area-to-volume ratio, which facilitates rapid heat absorption via sensible heating. Additionally, the higher velocity enhances droplet momentum, improving convective interaction with the heated surface. However, these smaller droplets are more susceptible to lateral deflection by the air stream in AAN, leading to inconsistent surface wetting. This results in localized regions experiencing either stronger or weaker convective cooling, causing non-uniform temperature distributions across the foil. Consequently, despite the strong sensible cooling capacity of water, thermal maps reveal greater non-dimensional temperature differences, particularly at higher heat fluxes, indicating uneven heat removal and patchy temperature profiles.

Furthermore, Figure 6.4b illustrates the non-dimensional temperature difference (Φ), which reflects the uniformity of surface cooling. Thermasolv demonstrates superior uniformity with Φ values of 4.6 and 7.4 at the two respective heat flux levels. In contrast,



(a) Steady foil average temperature



(b) Surface temperature uniformity

Figure 6.4: foil temperature and uniformity comparison for DI Water and Thermasolv at $\dot{V}=0.2$ L/min (AAN, 25°C).

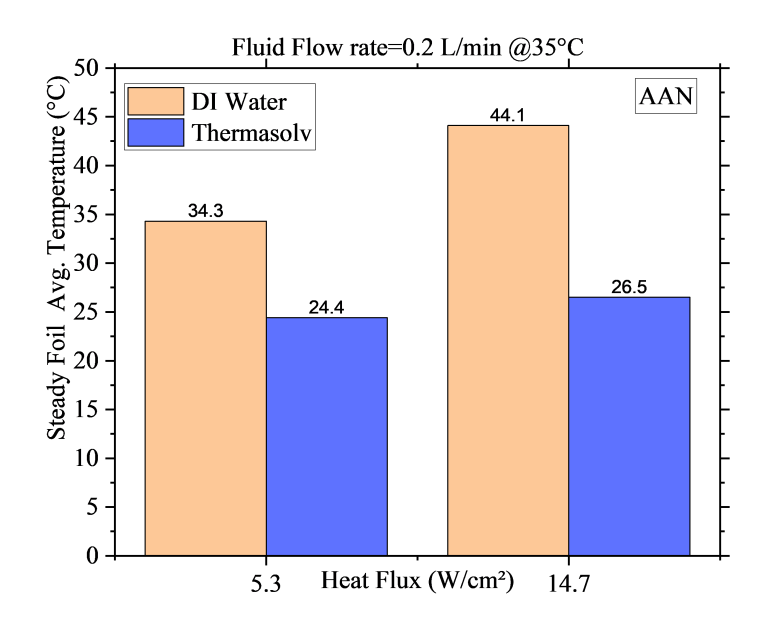
water shows significantly higher Φ values of 14.1 and 13.4.

In contrast, Thermasolv exhibits an optimized balance of droplet size and velocity, with an SMD of approximately 166.2 µm and a velocity of about 14.2 m/s. This configuration provides improved resistance to air shear and promotes more stable surface impingement. The slightly larger droplet size enhances directional stability, allowing for more uniform coverage across the heated surface. Furthermore, Thermasolv benefits from both sensible and latent heat transfer mechanisms. Its lower boiling point and increased volatility enable effective phase change cooling, which reduces foil temperatures more efficiently. Importantly, the air assist in AAN not only facilitates atomization but also removes vapor near the surface, allowing for continuous surface renewal and consistent heat removal. This synergy results in more homogeneous cooling, as indicated by lower and tighter non-dimensional temperature variations across all tested heat fluxes. The improved spreading, coupled with enhanced evaporative cooling and reduced thermal resistance, positions Thermasolv as a superior coolant in AAN configurations. The physics-based advantage is evident in both IR thermographic data and PDPA results, confirming that Thermasolv achieves lower and more uniform foil temperatures, making it highly suitable for high-precision thermal management applications.

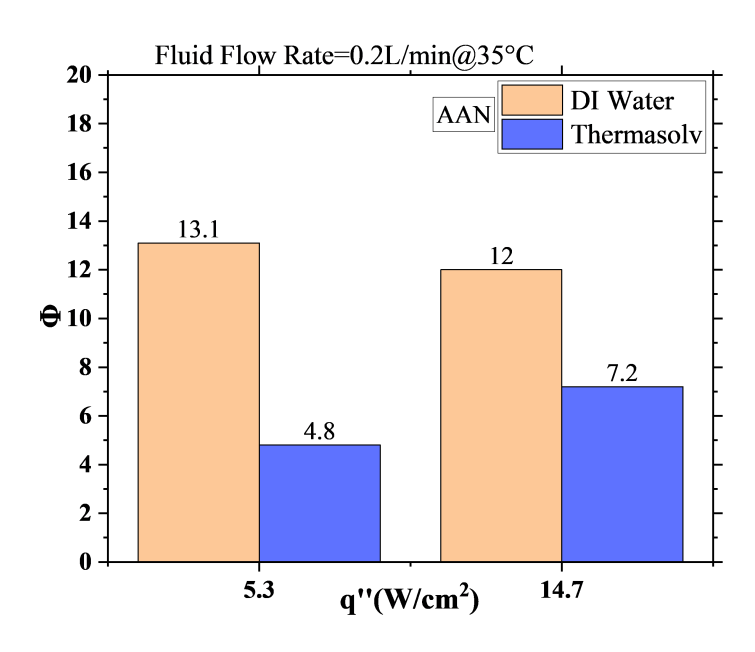
Figure 6.5 presents a comparative evaluation of steady-state foil temperature and thermal uniformity for deionized (DI) water and Thermasolv at a flow rate of 0.2 L/min and an inlet fluid temperature of 35°C under AAN spray cooling. As shown in Figure 6.5a, Thermasolv achieves significantly lower average foil temperatures of 24.4°C and 26.5°C at heat fluxes of 5.3 W/cm² and 14.7 W/cm², respectively. These temperatures are substantially lower than those recorded with water, which are 34.3°C and 44.1°C, revealing temperature differences of 9.9°C and 17.6°C in favor of Thermasolv.

In terms of spatial uniformity from Figure 6.5b, Thermasolv also demonstrates superior performance, maintaining non-dimensional temperature differences of 4.8 and 7.2, while water shows larger values of 13.1 and 12 at the corresponding heat fluxes. This behavior, although counterintuitive given Thermasolv's lower thermal conductivity (0.07–0.1

W/m·K) compared to that of water (0.6 W/m·K), can be explained by its favorable thermophysical and dynamic spray characteristics. Thermasolv's lower dynamic viscosity



(a) Steady foil average temperature



(b) Surface temperature uniformity

Figure 6.5: foil temperature and uniformity comparison for DI Water and Thermasolv at $\dot{V} = 0.2$ L/min (AAN, 35°C).

enhances its surface spreading behavior, allowing for the formation of a thinner, more continuous liquid film. This improvement promotes better surface contact and minimizes the presence of dry zones. In contrast, water's higher viscosity and surface tension at 35°C contribute to droplet splashing and film instability, which leads to uneven wetting and reduced heat transfer efficiency. Furthermore, although water has a higher specific heat capacity (4.18 kJ/kg·K), the effectiveness of cooling in spray systems depends more critically on surface interaction and evaporation dynamics rather than solely on bulk heat storage.

The PDPA data further supports these results, indicating that Thermasolv droplets, though larger (SMD=166.4 μ m) and slightly slower, exhibit significantly higher momentum than water droplets (SMD=116 μ m). This increased momentum allows the droplets to resist air deflection, penetrate closer to the foil, and maintain longer residence times, thereby facilitating efficient heat removal.

6.3 SPRAY COOLING BEHAVIOR BASED ON NON-DIMENSIONAL NUMBERS

1. **Nusselt Number (Nu)**: Higher Nu indicates enhanced convective heat transfer relative to conduction.

$$Nu = \frac{\text{Convective heat transfer}}{\text{Conductive heat transfer}} = \frac{hL}{k} = \frac{\dot{Q}L}{k\Delta T}$$
 (6.1)

where L is the characteristic length, taken as the spray width (20 mm), and k is the thermal conductivity of the fluid(W/m·K).

2. **Weber Number (We)**: Governs droplet breakup, spray formation, and surface impingement behavior.

We =
$$\frac{\text{Inertia forces}}{\text{Surface tension force}} = \frac{\rho V^2 D}{\sigma}$$
 (6.2)

3. Capillary Number (Ca): Ratio of viscous to surface tension forces.

$$Ca = \frac{\text{Viscous force}}{\text{Surface tension force}} = \frac{\mu V}{\sigma}$$
 (6.3)

The comparison of capillary numbers and average Nusselt numbers across different spray configurations (PAN and AAN) and working fluids (DI water and Thermasolv) provides important insights into the physics of spray cooling performance.

From figure 6.6a, it is observed that for DI water under the PAN configuration, a lower capillary number corresponds to a lower average Nusselt number. This suggests weaker liquid spreading and less effective convective and evaporative cooling. At a flow rate of 0.1 L/min, the capillary number is 0.077, resulting in an average Nusselt number of 369.5. In contrast, at a higher flow rate of 0.2 L/min, the capillary number increases to 0.1327, and the average Nusselt number rises to 526.9. This trend confirms that a higher flow rate enhances liquid film spreading (higher Ca) and convective transport (higher Nu).

In contrast, the AAN configuration significantly improves performance with the same DI water. At a flow rate of 0.1 L/min, the capillary number exceeds 0.07165, leading to a corresponding Nusselt number greater than 992.7. When the flow rate increases to 0.2 L/min, the capillary number rises to 0.708, while the Nusselt number surges by 3275.3. This indicates a substantial enhancement in heat transfer due to finer atomization and forced vapor removal by the air stream.

Figure 6.6b shows that the Weber number, which indicates the ratio of inertial to surface tension forces, increases with flow rate. The AAN configuration demonstrates significantly higher Weber numbers than the PAN configuration at both flow rates, supporting improved droplet breakup and surface wetting in AAN.

In Figure 6.7a, we observe that with Thermasolv under PAN conditions, both the capillary number and the Nusselt number increase significantly with flow rate. The capillary number rises from 0.2636 to 0.3827, while the Nusselt number jumps from 1442.4 to

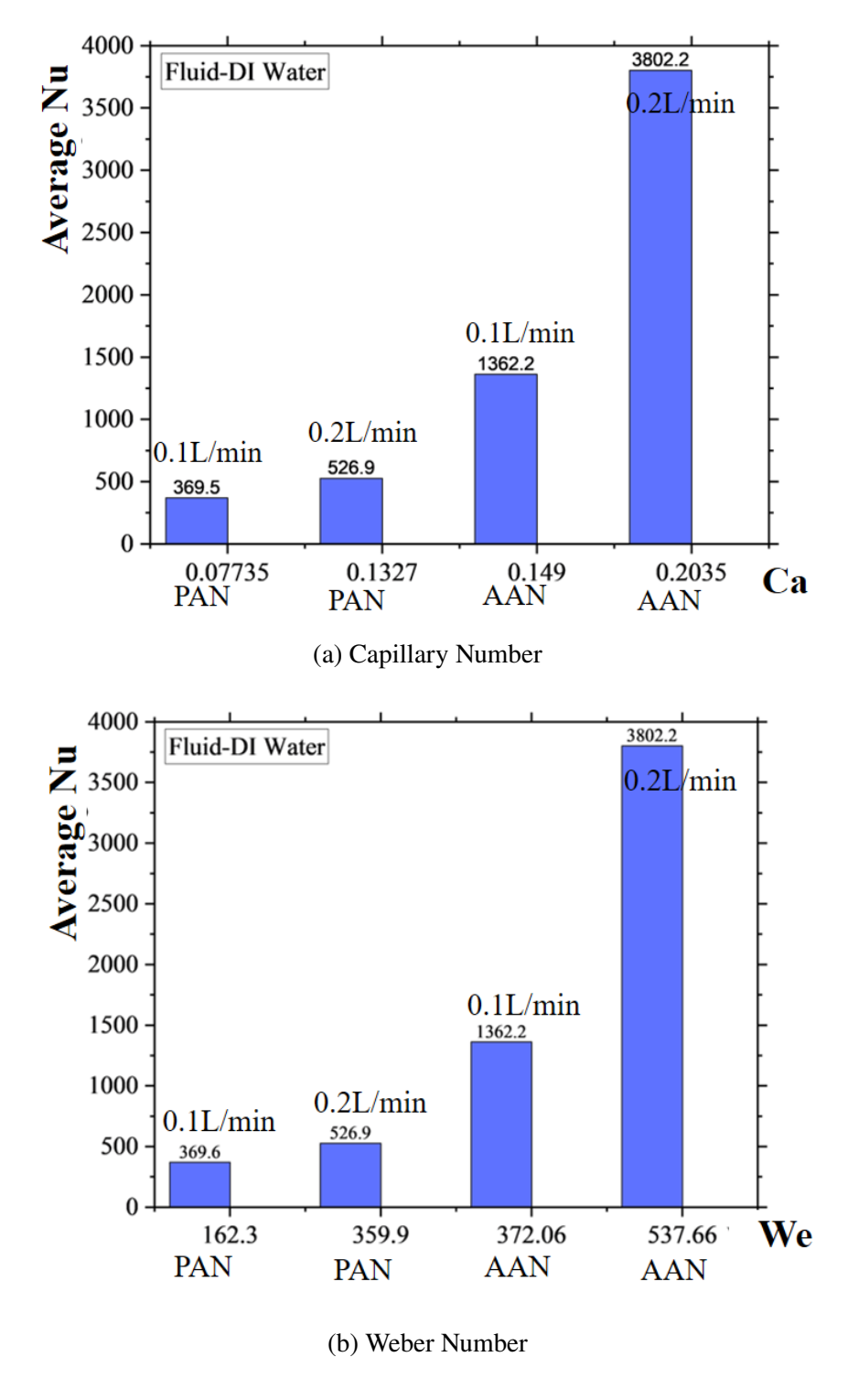


Figure 6.6: Average Nusselt number for DI water with PAN and AAN

4199.6. This substantial increase highlights the favorable thermophysical properties of Thermasolv, such as its lower surface tension and viscosity. These properties, combined

with improved spreading (higher Capillary number), enhance both convective and evaporative cooling, even without the assistance of air.

Furthermore, figure 6.7b shows that the Weber number increases by 647.9 when the flow rate is doubled, indicating stronger atomization forces. When we correlate these trends with Particle Differential Phase Analysis (PDPA) results, we see that for deionized (DI) water, increasing the flow rate under PAN and AAN conditions results in a decreased Sauter Mean Diameter (SMD) and increased droplet velocity. This supports the idea of enhanced atomization and faster droplet delivery, leading to better cooling performance. However, for Thermasolv under PAN conditions, both the SMD and droplet velocity increase with a higher flow rate.

Despite this, the higher boiling potential and superior spreading behavior of Thermasolv effectively compensate for these increases, resulting in improved heat transfer (higher Nusselt number). This trend aligns with the increases observed in the capillary and Weber numbers. Therefore, for Thermasolv, even larger droplets can still provide strong cooling performance due to their better wetting and evaporation efficiency.

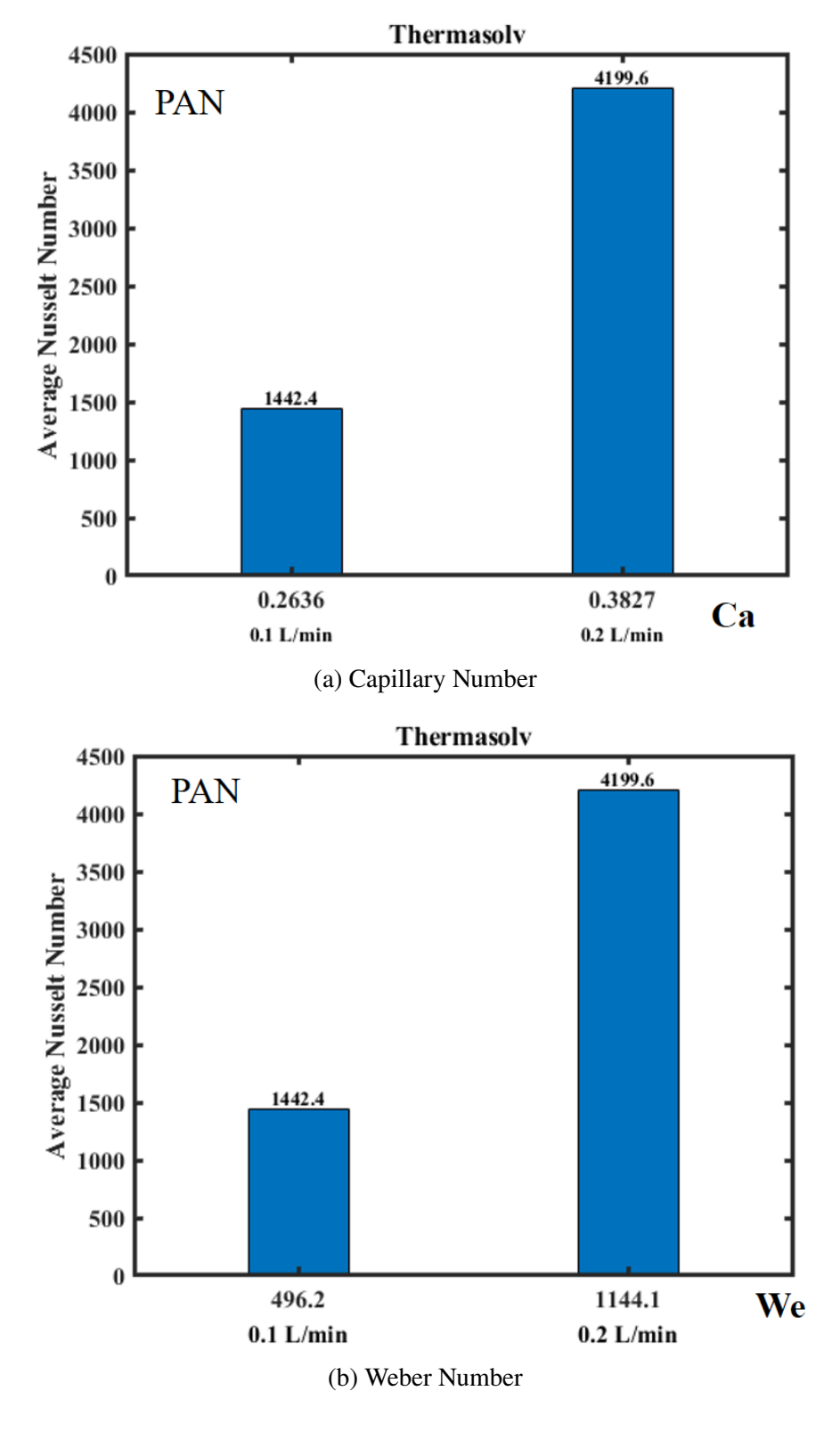


Figure 6.7: Average Nusselt number for Thermosolv with PAN and AAN

CHAPTER 7

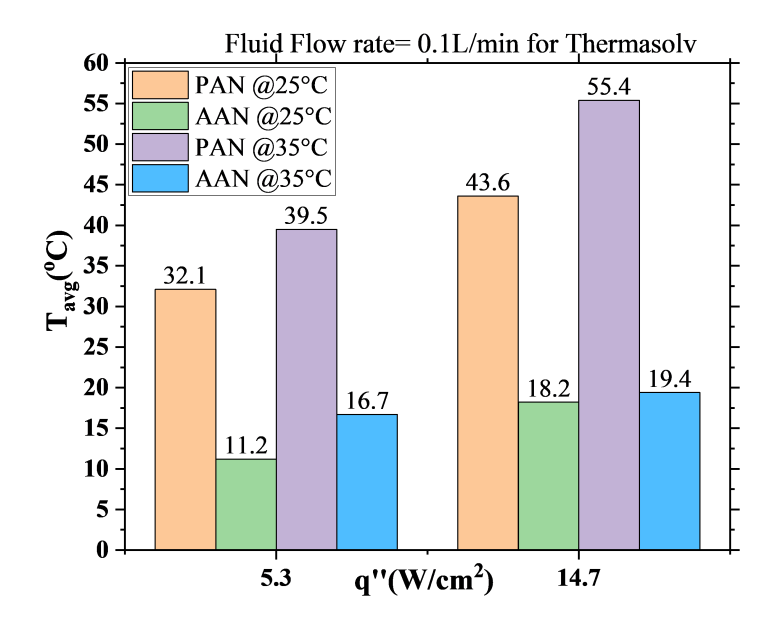
CONCLUSIONS AND FUTURE SCOPE

7.1 CONCLUSIONS

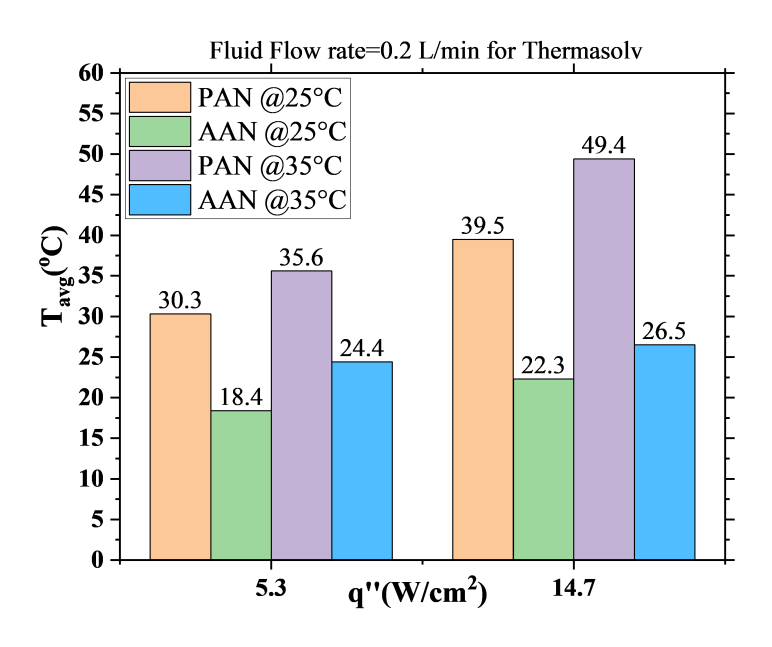
The comparative performance of pressure atomized nozzles (PAN) and air-assisted atomized nozzles (AAN) is illustrated in Figure 7.1, which clearly shows that AAN outperforms PAN in maintaining lower steady-state foil temperatures across all tested flow rates and heat fluxes when using Thermasolv. This advantage is fundamentally tied to the spray characteristics, specifically droplet size and velocity obtained from PDPA measurements.

At a flow rate of 0.1 L/min and a heat flux of 5.3 W/cm² in figure 7.1a, AAN reduces the average foil temperature by 20.9°C (at a 25°C inlet) and 22.8°C (at a 35°C inlet) compared to PAN. This benefit is even more pronounced at a heat flux of 14.7 W/cm², where AAN surpasses PAN by 25.4°C and 36.0°C at 25°C and 35°C, respectively. This significant improvement is attributed to the higher droplet velocity and favorable atomization dynamics offered by AAN. According to PDPA data, the spray velocity under AAN at 0.1 L/min is 16.55 m/s, more than triple the 5.2 m/s observed with PAN. While the Sauter mean diameter (SMD) is marginally larger (135.7 μm vs. 130 μm), the increased velocity enhances momentum transfer. This ensures better droplet penetration, improved impingement on the heated surface, and faster surface film renewal, all of which intensify both sensible and evaporative heat transfer.

At a flow rate of 0.2 L/min in figure 7.1b, the differences between PAN and AAN become less dramatic due to the overall increase in fluid supply, but AAN still shows clear advantages. At this flow rate, AAN achieves foil temperature reductions of 11.9°C and 11.2°C at 5.3 W/cm² for the 25°C and 35°C inlet temperatures, respectively. At



(a) $\dot{V} = 0.1 \,\text{L/min}$



(b) $\dot{V} = 0.2 \text{ L/min}$

Figure 7.1: Foil temperature variation with PAN and AAN at \dot{V} = 0.1 and 0.2 L/min, and $T_{\rm f,inlet}$ = 25°C and 35°C.

14.7 W/cm², AAN improves cooling by 17.2°C and 22.9°C compared to PAN. This performance can be attributed to the more favorable spray behavior of AAN, even at

higher flow rates. PDPA data indicates that, while the droplet velocity in AAN slightly decreases to 14.2 m/s at 0.2 L/min, it remains significantly higher than PAN's 7.5 m/s. Additionally, although the SMD increases to 166.4 μ m in AAN (compared to 142 μ m in PAN), the enhanced inertia of larger droplets helps maintain directional stability and better surface contact, which is critical for uniform and effective cooling at higher heat flux.

From a thermophysical perspective, Thermasolv has lower surface tension and viscosity compared to water, which contributes to its favorable breakup and spreading behavior, especially in AAN. The larger, high-momentum droplets resist deflection from the assistive air stream and maintain longer residence times on the surface, promoting both sensible and phase change heat transfer. Furthermore, the air in AAN helps clear vapor films and boundary layers, further reducing thermal resistance and enhancing cooling uniformity.

- 1. This study establishes, for the first time, a direct correlation between spray dynamics—characterized using Phase Doppler Particle Anemometry (PDPA) and high-speed imaging—and surface heat transfer behavior, which was visualized through infrared (IR) thermography. The dual-technique approach was applied to two working fluids (deionized water and Thermasolv IM6) and two atomization methods (pressure nozzle atomization and air-assisted nozzle atomization). This comprehensive analysis provides a clear understanding of how droplet size and velocity influence thermal performance under varying spray conditions.
- 2. Superior Atomization with AAN: The Air-Assisted Nozzle (AAN) consistently produces finer droplets with smaller Sauter Mean Diameter (SMD) compared to the Pressure Atomized Nozzle (PAN). This finer atomization enhances spray dispersion, improves surface wetting, and allows for rapid evaporation upon contact. As a result, AAN significantly improves cooling effectiveness through a combination of convective and latent heat transfer mechanisms, particularly under high heat flux conditions.
- 3. Inlet Temperature Sensitivity: Even at a high inlet temperature of 35°C, the AAN

configuration effectively maintains below ambient surface cooling. This performance shows that the effectiveness of heat removal in the AAN system is primarily influenced by droplet dynamics such as velocity, dispersion, and impingement behavior, as well as the uniformity of spray coverage, rather than just the fluid's initial temperature. This demonstrates the robustness of AAN-driven cooling in thermally challenging conditions, which requires uniformity in surface temperature for electronics.

- 4. Evaporative Advantage of AAN with Thermasolv: While AAN offers only a modest improvement over PAN when using deionized (DI) water, mainly due to enhanced convective effects, the combination of AAN with Thermasolv at a low flow rate of 0.1 L/min significantly enhances cooling performance. This improvement is attributed to rapid evaporation caused by high droplet velocity and the favorable thermophysical properties of Thermasolv. This process allows surface temperatures to drop well below ambient levels, thanks to rapid phase changes and effective vapor removal with the help of Air used in the atomizing process, resulting in both intense temperature reduction and superior thermal uniformity.
- 5. Efficient High Heat Flux Management with Thermasolv: Under High heat flux conditions of 100 W/cm² with a fluid inlet temperature of 25 °C, Thermasolv effectively manages thermal management, achieving an extrapolated average foil temperature of approximately 81 °C. This efficient cooling is primarily due to Thermasolv's low boiling point, which facilitates the early phase change behavior, along with its lower viscosity, which enhances surface spreading and promotes the formation of a uniform liquid film. Together, these properties support sustained and efficient heat removal through evaporation.

In summary, the Air-Assisted Nozzle (AAN) exhibits markedly superior heat transfer performance compared to the Pressure Atomizing Nozzle (PAN), particularly under conditions of high heat flux and low flow rates. This enhanced thermal performance is attributed to improved atomization characteristics, as substantiated by Phase Doppler

Particle Anemometry (PDPA) measurements, along with the advantageous thermophysical properties of Thermasolv. The combined effects of elevated droplet velocity, optimal droplet sizing, improved surface wetting, and efficient air-assisted vapor evacuation position AAN as a highly effective solution for advanced spray cooling scenarios requiring uniform and efficient heat dissipation.

Final Remark on Applicability: These results underscore the potential of integrating AAN technology with Thermasolv IM6, a low-global warming potential (GWP) dielectric fluid, as a forward-looking strategy for sustainable and high-performance spray cooling. The dual benefits of superior atomization and environmentally responsible fluid selection affirm the system's suitability for thermal management in next-generation high-power electronic devices, where compactness and energy efficiency are critical.

7.2 FUTURE SCOPE

Transient Heat Flux Response: This study emphasizes steady-state behavior. Expanding the experiments to include transient thermal loads like those found in pulsed electronics or power cycling. It would enhance understanding of the dynamic responses of various spray cooling configurations and fluids.

Investigation of Intermittent Spray Cooling Dynamics: A custom-designed intermittent spray cooling setup can be developed, allowing for precise control over the characteristics of the spray pulse, including frequency of spray, duty cycle, and durations of idle and spray phases. Future studies using this system can examine how pulsed fluid injection affects droplet impact dynamics, surface wetting, uniformity, and evaporation rates. This method has the potential to significantly reduce fluid consumption while maintaining effective thermal regulation, making it highly relevant for energy-efficient cooling in transient or adaptive electronic environments.

Further research can focus on the application of spray cooling techniques to compact electronic modules or localized hotspots, such as chip-level cooling, where uniform temperature distribution and localized control are essential. Microfabricated test sections could be used to replicate the heat distribution found in real devices.

CFD and Spray Modeling Validation: The development of computational fluid dynamics (CFD) models using experimental Phase Doppler Particle Analyzer (PDPA) and infrared (IR) data can enhance the prediction of droplet behavior, film formation, and heat transfer. This approach helps to make these predictions more efficient and reduces the need for extensive experimental trials/work.

Surface Modification for Enhanced Heat Transfer: The current study used a plain SS-304 foil as the target surface. However, future research could explore the use of micro-structured or nano-textured surfaces to study their effects on droplet interactions, nucleation behavior, and boiling phenomena at high heat fluxes. These surface enhancements could significantly improve liquid spreading, delay dry-out, and promote controlled phase changes, thereby increasing thermal effectiveness for electronic devices operating under extreme heat loads within the working temperature.

APPENDIX A

GENERAL NOTES

The equipment and materials utilized for the experiments are listed below.

Table A.1: Equipment and materials utilized for the experiments.

Equipment	Make	Purpose		
Infrared camera	FLIR X6900sc MWIR	To acquire temperature field during pool boiling		
Infrared lens	FLIR MWIR4214995	Microscopic lens used for infrared camera		
Optical camera	Phantom VEO 340	To visualize bubble dynamics during pool boiling		
Optical lens	NAvitar Zoom 6000	Lens used for the optical camera		
DC power supply (high current)	TDK Lambda GEN 120-12.5	To heat thin foil		
DC power supply (high voltage)	TDK Lambda GEN 5-300	To operate the LED Light		
Gear Pump	(SHENCHEN, labGM	To supply the Liquid for Spraying		
Temperature bath	Sub-zero Technologies	To supply water at constant temperature		
Nozzle	TG-0.3 and SU22B Spraying System co.	To Atomize the Liquid		
LED Light	300 watt, Wipro	Lighting Arrangement for HSI		
Data Logger	keysight Keysight DAQ970A	To measure the accurate fluid inlet temperature		
Coriolis Flow Meter	Emerson Micro Motion F-Series	To accurate measurement of fluid mass flow rate		
Plate Heat Exchanger	Alfa LAval	To precise control of Liquid Temperature		
Liquid Filter	Swagelok	to prevent the clogging of nozzles		
Condenser	-	To condense the Dielectric Vapour		

APPENDIX B

CALIBRATION OF INFRARED CAMERA

B.1 Calibration Procedure of Infrared Camera

The section presents the procedure for the pixel-wise in-situ calibration of the infrared camera used to acquire temperature fields. The infrared camera is calibrated before performing pool boiling experiments to convert the radiation intensity into temperature. The infrared camera is calibrated by following the references (Schweizer (2010)), (Voglar et al. (2019)) available in the literature. The infrared camera is calibrated in increments of 5 °C over the range of 5 to 80 °C. The schematic of the experimental setup used for calibrating the infrared camera is shown in Figure B.1. The calibration is performed under a controlled environmental setting with a 1 mm thick copper sample plate mounted to a copper heater block equipped with a temperature control mechanism. The bottom surface of the copper sample used for calibration is painted black with high-temperature-resistant matte black paint to increase emissivity and reduce reflection and glare. The emissivity, thickness, and thermal conductivity of black paint are 0.92, 10 μ m, and 1.45 W/mK, respectively. Four micro thermocouples of bead diameter 0.2 mm are embedded in the copper sample at a distance of 0.15 mm from the bottom surface, which is visualized by the infrared camera. The copper heater block with cartridge heater and PID controller is used to maintain the copper sample at the required constant temperature. A layer of thermal grease is applied between the heater block and the sample to eliminate air gaps. The copper sample and copper heater block are used to maintain a uniform temperature on the bottom surface of the copper sample. The spatial variation in the surface temperature of the copper sample is less than 0.1 °C. The radiation intensity field given by the infrared camera is spatially averaged, and the corresponding average temperature from micro thermocouples is noted. The same procedure is repeated for temperatures over the range

of 5 to 80 °C in 5 °C increments.

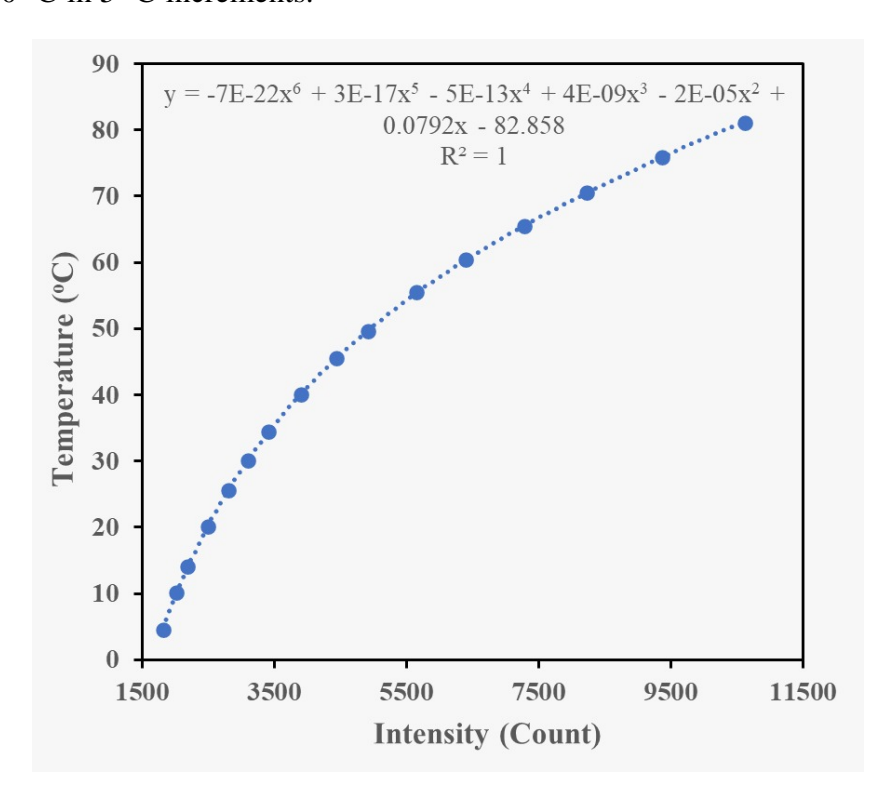


Figure B1: Curve fitting for converting intensity to temperature.

$$T = -7 \times 10^{-22} I^6 + 3 \times 10^{-17} I^5 - 5 \times 10^{-13} I^4 + 4 \times 10^{-9} I^3 - 2 \times 10^{-5} I^2 + 0.0792 I - 82.858$$
(B.1)

$$R^2 = 1$$

where T is the temperature in °C and I is the radiation intensity given in counts by the infrared camera. The corresponding temperature and radiation intensity are plotted in Figure B.1. Finally, the relation between temperature and intensity is determined by fitting a Sixth-order polynomial curve. The Sixth-order polynomial, as given in Equation B.1, fits very well and has a R^2 value of 1. Equation B.1 is used to convert the intensity field given by the infrared camera into temperature fields during Spray Cooling experiments.

REFERENCES

- 1. **Benther, J., J. Pelaez-Restrepo, C. Stanley**, and **G. Rosengarten** (2021). Heat transfer during multiple droplet impingement and spray cooling: Review and prospects for enhanced surfaces. *International Journal of Heat and Mass Transfer*, **178**, 121587. ISSN 0017-9310. URL https://www.sciencedirect.com/science/article/pii/S0017931021006906.
- 2. **Bostanci, H., V. V. R. Yata**, and **S. Kaluvan** (2021). Flow-controlled spray cooling approaches for dynamic thermal management. *Journal of Electronic Packaging*, **143**(3), 031004. ISSN 1043-7398. URL https://doi.org/10.1115/1.4049174.
- 3. **Chen, R.-H., L. C. Chow**, and **J. E. Navedo** (2002). Effects of spray characteristics on critical heat flux in subcooled water spray cooling. *International Journal of Heat and Mass Transfer*, **45**(19), 4033–4043. ISSN 0017-9310. URL https://www.sciencedirect.com/science/article/pii/S0017931002001138.
- 4. Chen, R.-H., L. C. Chow, and J. E. Navedo (2004). Optimal spray characteristics in water spray cooling. *International Journal of Heat and Mass Transfer*, 47(23), 5095–5099. ISSN 0017-9310. URL https://www.sciencedirect.com/science/article/pii/S0017931004002364.
- **Q.-N. Liu**, and **H.-L. Fan** (2011). 5. Cheng, W.-L., F.-Y. Han, Spray characteristics and cooling heat transfer in the non-boiling spray 3399-3405. regime. **36**(5), **ISSN** 0360-5442. URL Energy, https://www.sciencedirect.com/science/article/pii/S0360544211002064.
- 6. **Elliott, J. W.** and **A. J. Robinson** (2025). Optimized liquid impinging jet arrays for cooling cpu packages. *IEEE Transactions on Components, Packaging and Manufacturing Technology*, **15**(3), 488–505.
- 7. GaneshKumar, P., V. Sivalingam, V. Vigneswaran, V. Ramalingam, K. Seong Cheol, and R. Vanaraj (2024). Spray cooling for hydrogen vehicle, electronic devices, solar and building (low temperature) applications: A state-of-art review. Renewable and Sustainable Energy Reviews, 189, 113931. ISSN 1364-0321. URL https://www.sciencedirect.com/science/article/pii/S136403212300789X.
- 8. **Gao, X.** and **R. Li** (2017). Effects of nozzle positioning on single-phase spray cooling. *International Journal of Heat and Mass Transfer*, **115**, 1247–1257. ISSN 0017-9310. URL https://www.sciencedirect.com/science/article/pii/S0017931017327862.
- 9. Ghodbane, M. J. Holman (1991).and **Experimental** study of spray cooling with freon-113. *International* **Journal** of Heat Transfer, **34**(4), 1163-1174. ISSN 0017-9310. URL and Mass https://www.sciencedirect.com/science/article/pii/001793109190025A.

- 10. **Guggilla, G., R. Narayanaswamy**, and **A. Pattamatta** (2020). An experimental investigation into the spread and heat transfer dynamics of a train of two concentric impinging droplets over a heated surface. *Experimental Thermal and Fluid Science*, **110**, 109916.
- 11. **He, Z.**, **Y. Yan**, and **Z. Zhang** (2021). Thermal management and temperature uniformity enhancement of electronic devices by micro heat sinks: A review. *Energy*, **216**, 119223. ISSN 0360-5442. URL https://www.sciencedirect.com/science/article/pii/S0360544220323306.
- 12. **Hu, Y., Y. Lei, X. Liu**, and **R. Yang** (2025). Record-high heat transfer performance of spray cooling on 3d-printed hierarchical micro/nano-structured surface. *Science Bulletin*, **70**(2), 223–231. ISSN 2095-9273. URL https://www.sciencedirect.com/science/article/pii/S2095927324007722.
- A. 13. Kheirabadi, C. and D. Groulx (2016).Cooling server technology. electronics: design review A of existing Applied **ISSN** Engineering, 105. 622-638. 1359-4311. **URL** Thermal https://www.sciencedirect.com/science/article/pii/S1359431116303490.
- 14. **Kim, J.** (2007). Spray cooling heat transfer: The state of the art. *International Journal of Heat and Fluid Flow*, **28**(4), 753–767.
- 15. **Kumar, M.**, **V. Dusane**, **A. Pattamatta**, and **M. Marengo** (). Spray and thermal analysis of pressure and air atomized nozzles for electronic cooling.
- 16. **Labergue**, **A.**, **M. Gradeck**, and **F. Lemoine** (2015). Comparative study of the cooling of a hot temperature surface using sprays and liquid jets. *International Journal of Heat and Mass Transfer*, **81**, 889–900. ISSN 0017-9310. URL https://www.sciencedirect.com/science/article/pii/S0017931014009909.
- 17. **Liang, G.** and **I. Mudawar** (2017*a*). Review of spray cooling part 1: Single-phase and nucleate boiling regimes, and critical heat flux. *International Journal of Heat and Mass Transfer*, **115**, 1174–1205. ISSN 0017-9310. URL https://www.sciencedirect.com/science/article/pii/S0017931017302946.
- 18. **Liang, G.** and **I. Mudawar** (2017*b*). Review of spray cooling part 2: High temperature boiling regimes and quenching applications. *International Journal of Heat and Mass Transfer*, **115**, 1206–1222. ISSN 0017-9310. URL https://www.sciencedirect.com/science/article/pii/S0017931017302958.
- 19. **Lin, Y.-K.**, **Z.-F. Zhou**, **Y. Fang**, **H.-L. Tang**, and **B. Chen** (2019). Heat transfer performance and optimization of a close-loop r410a flash evaporation spray cooling. *Applied Thermal Engineering*, **159**, 113966. ISSN 1359-4311. URL https://www.sciencedirect.com/science/article/pii/S1359431118376725.

- 20. **Liu, L., X. Wang, M. Ge**, and **Y. Zhao** (2021). Experimental study on heat transfer and power consumption of low-pressure spray cooling. *Applied Thermal Engineering*, **184**, 116253. ISSN 1359-4311. URL https://www.sciencedirect.com/science/article/pii/S1359431120337327.
- 21. **Liu, P., R. Kandasamy, J. Y. Ho, T. N. Wong**, and **K. C. Toh** (2023). Dynamic performance analysis and thermal modelling of a novel two-phase spray cooled rack system for data center cooling. *Energy*, **269**, 126835. ISSN 0360-5442. URL https://www.sciencedirect.com/science/article/pii/S0360544223002293.
- 22. **Mudawar, I.** (2013). Recent advances in high-flux, two-phase thermal management. *Journal of Thermal Science and Engineering Applications*, **5**(2), 021012.
- 23. **Mudawar, I., D. Bharathan, K. Kelly**, and **S. Narumanchi** (2009). Two-phase spray cooling of hybrid vehicle electronics. *IEEE Transactions on Components and Packaging Technologies*, **32**(2), 501–512.
- 24. **Pautsch, A. G.** and **T. A. Shedd** (2005). Spray impingement cooling with single-and multiple-nozzle arrays. part i: Heat transfer data using fc-72. *International Journal of Heat and Mass Transfer*, **48**(15), 3167–3175.
- 25. **Sadique, H., Q. Murtaza**, and **Samsher** (2022). Heat transfer augmentation in microchannel heat sink using secondary flows: A review. *International Journal of Heat and Mass Transfer*, **194**, 123063. ISSN 0017-9310. URL https://www.sciencedirect.com/science/article/pii/S0017931022005361.
- 26. Salman, A. S., N. M. Abdulrazzaq, S. K. Oudah, A. Tikadar, N. Anumbe, T. C. Paul, and J. A. Khan (2019). Experimental investigation of the impact of geometrical surface modification on spray cooling heat transfer performance in the non-boiling regime. *International Journal of Heat and Mass Transfer*, 133, 330–340. ISSN 0017-9310. URL https://www.sciencedirect.com/science/article/pii/S0017931018338055.
- 27. **Salman, A. S.** and **J. A. Khan**, The effects of spraying parameters on spray cooling heat transfer performance in the non-boiling regime. *In ASME International Mechanical Engineering Congress and Exposition*, volume 58431. American Society of Mechanical Engineers, 2017.
- 28. **Salman, A. S., T. C. Paul**, and **J. A. Khan**, The effects of coverage area on the spray cooling heat transfer performance. *In ASTFE Digital Library*. Begel House Inc., 2018.
- 29. **Schmidt, J., F. Tenzer, C. Tropea, J. Hussong**, and **I. Roisman** (2023). Modelling of drop and spray impact in the transitional boiling regime. *International Journal of Heat and Mass Transfer*, **217**, 124586. ISSN 0017-9310. URL https://www.sciencedirect.com/science/article/pii/S0017931023007317.
- 30. Schweizer, N. (2010). Multi-scale investigation of nucleate boiling phenomena in

- microgravity. Ph.D. thesis, Technische Universität Darmstadt.
- 31. **Sielaff, A., J. Dietl, S. Herbert**, and **P. Stephan** (2014). The influence of system pressure on bubble coalescence in nucleate boiling. *Heat Transfer Engineering*, **35**(5), 420–429.
- 32. **Sijs, R., S. Kooij, H. Holterman, J. Van De Zande**, and **D. Bonn** (2021). Drop size measurement techniques for sprays: Comparison of image analysis, phase doppler particle analysis, and laser diffraction. *AIP advances*, **11**(1).
- 33. **Smakulski, P.** and **S. Pietrowicz** (2016). A review of the capabilities of high heat flux removal by porous materials, microchannels and spray cooling techniques. *Applied Thermal Engineering*, **104**, 636–646. ISSN 1359-4311. URL https://www.sciencedirect.com/science/article/pii/S1359431116307530.
- 34. **Tao, Y., X. Huai**, **L. Wang**, and **Z. Guo** (2011). Experimental characterization of heat transfer in non-boiling spray cooling with two nozzles. *Applied Thermal Engineering*, **31**(10), 1790–1797. ISSN 1359-4311. URL https://www.sciencedirect.com/science/article/pii/S1359431111001050.
- 35. **Visaria, M.** and **I. Mudawar** (2009). Application of two-phase spray cooling for thermal management of electronic devices. *IEEE Transactions on Components and Packaging Technologies*, **32**(4), 784–793.
- 36. **Voglar, J., M. Zupančič, A. Peperko, P. Birbarah, N. Miljkovic**, and **I. Golobič** (2019). Analysis of heater-wall temperature distributions during the saturated pool boiling of water. *Experimental Thermal and Fluid Science*, **102**, 205–214.
- 37. Wang, J.-X., Y.-Z. Li, J.-X. Li, C. Li, Y. Zhang, and X.-W. Ning (2019). A gas-atomized spray cooling system integrated with an ejector loop: Ejector modeling and thermal performance analysis. *Energy Conversion and Management*, 180, 106–118. ISSN 0196-8904. URL https://www.sciencedirect.com/science/article/pii/S0196890418312238.
- 38. Wang, J.-X., Y.-Z. Li, X.-K. Yu, G.-C. Li, and X.-Y. Ji (2018). Investigation of heat transfer mechanism of low environmental pressure large-space spray cooling for near-space flight systems. *International Journal of Heat and Mass Transfer*, 119, 496–507. ISSN 0017-9310. URL https://www.sciencedirect.com/science/article/pii/S001793101731918X.
- 39. **Xie, J., Z. Gan, T. Wong, F. Duan, S. Yu**, and **Y. Wu** (2014). Thermal effects on a pressure swirl nozzle in spray cooling. *International Journal of Heat and Mass Transfer*, **73**, 130–140.
- 40. **Xu, R., G. Wang**, and **P. Jiang** (2021*a*). Spray cooling on enhanced surfaces: A review of the progress and mechanisms. *Journal of Electronic Packaging*, **144**(1), 010802. ISSN 1043-7398. URL https://doi.org/10.1115/1.4050046.

- 41. **Xu, R.**, **G. Wang**, and **P. Jiang** (2021*b*). Spray cooling on enhanced surfaces: A review of the progress and mechanisms. *Journal of Electronic Packaging*, **144**(1), 010802. ISSN 1043-7398. URL https://doi.org/10.1115/1.4050046.
- 42. Yan, Z., K. Toh, F. Duan, T. Wong, K. Choo, P. Chan, and Y. Chua (2010). Experimental study of impingement spray cooling for high power devices. *Applied Thermal Engineering*, **30**(10), 1225–1230. ISSN 1359-4311. URL https://www.sciencedirect.com/science/article/pii/S1359431110000621.
- 43. **Zeng, R.**, **H. Kang**, **M. Umar**, **X. Liang**, and **Y. nan Zhao** (2025). Design and thermal management study of fuel cell spray cooling system. *Applied Thermal Engineering*, **270**, 126271. ISSN 1359-4311. URL https://www.sciencedirect.com/science/article/pii/S1359431125008634.
- 44. **Zhang, L., Q. Duan, X. Meng, K. Jin, J. Xu, J. Sun**, and **Q. Wang** (2022*a*). Experimental investigation on intermittent spray cooling and toxic hazards of lithium-ion battery thermal runaway. *Energy Conversion and Management*, **252**, 115091. ISSN 0196-8904. URL https://www.sciencedirect.com/science/article/pii/S019689042101267X.
- 45. **Zhang, T., Z. Mo, X. Xu, X. Liu, H. Chen, Z. Han, Y. Yan**, and **Y. Jin** (2022*b*). Advanced study of spray cooling: From theories to applications. *Energies*, **15**(23). ISSN 1996-1073. URL https://www.mdpi.com/1996-1073/15/23/9219.
- 46. **Zhao, Y., S. Gong, Q. Yang, Z. Xuan, W. Li, L. Xie, L. Liu,** and **M. Ge** (2024). Experimental investigation of heat transfer performance in gas-atomized spray cooling. *International Journal of Heat and Mass Transfer*, **218**, 124768. ISSN 0017-9310. URL https://www.sciencedirect.com/science/article/pii/S0017931023009134.
- 47. **Zhou, N., F. Chen, Y. Cao, M. Chen**, and **Y. Wang** (2017). Experimental investigation on the performance of a water spray cooling system. *Applied Thermal Engineering*, **112**, 1117–1128. ISSN 1359-4311. URL https://www.sciencedirect.com/science/article/pii/S1359431116328873.
- 48. **Zhou, Z.-F.**, **Y.-K. Lin**, **H.-L. Tang**, **Y. Fang**, **B. Chen**, and **Y.-C. Wang** (2019). Heat transfer enhancement due to surface modification in the close-loop r410a flash evaporation spray cooling. *International Journal of Heat and Mass Transfer*, **139**, 1047–1055. ISSN 0017-9310. URL https://www.sciencedirect.com/science/article/pii/S0017931019301784.

CURRICULUM VITAE

NAME MONU KUMAR

*ME*22*S*032

DATE OF BIRTH 03 August 1997

EDUCATION QUALIFICATIONS

2019 Bachelor of Technology

Institution M.I.T Muzaffarpur Bihar

Specialization Mechanical Engineering

Master in Science

Institution IIT MADRAS

Specialization Thermal Engineering

Registration Date 10 july 2022

GENERAL TEST COMMITTEE

Chairperson Prof. Chakravarthy Balaji

Department of Mechanical Engineering Indian Institute of Technology, Madras.

Guide(s) Prof. Arvind Pattamatta

Department of Mechanical Engineering Indian Institute of Technology, Madras.

Prof. Marco Marengo

Department of Civil Engineering and Architecture

University of Pavia, Italy

Member(s) Prof. Pijush Ghosh

Department of Applied Mechanics Indian Institute of Technology Madras

Prof. Srinivasan K

Department of Mechanical Engineering Indian Institute of Technology, Madras.